A NON-LINEAR DYNAMICAL MODEL OF TUMOUR-HEALTHY-IMMUNE CELL INTERACTIONS UNDER THERAPEUTIC INTERVENTION

NICHOLAS MURIMI WAITHEGA

A Thesis Submitted to the Graduate School in Partial Fulfilment of the Requirements for the Award of the Degree of Master of Science in Applied Mathematics of Tharaka University.

THARAKA UNIVERSITY
NOVEMBER 2025

DECLARATION AND RECOMMENDATION

Declaration

This thesis is my original work and has not been submitted for the award of a diploma or the conferment of a degree at any other university

Signature:..... Date: 14/11/2025

Nicholas Murimi Waitheega
SMT12/10033/23

Recommendation

This thesis has been examined, passed and submitted with our approval as University supervisors.

Signature:..... Date: 14/11/2025

Dr. Jimrise Ochwach., Ph.D.,
Mama Ngina University College.

Signature:..... Date: 14/11/2025

Dr. Daniel Mwangi., Ph.D.,
Tharaka University.

Signature:..... Date: 14/11/2025

Dr. Alex Muthengi., Ph.D.,
Tharaka University.

THARAKA UNIVERSITY
DIRECTOR BOARD OF POST GRADUATE STUDIES
14 NOV 2025
RECEIVED
P. O. Box 193-60215
MARIMANTI, KENYA

DEDICATION

I commit this endeavour to my parents, my brothers (William, Geoffrey, and Bernard) who have motivated me to pursue excellence, and to my fiancee, Purity, for her unwavering support and continuous prayers.

ACKNOWLEDGEMENTS

This study owes its completion first and foremost, to the grace of God, who provided me with the strength, knowledge, and perseverance to see it through. I am profoundly grateful to the many individuals whose support and guidance were essential throughout this research journey.

I would like to sincerely thank my supervisors, Dr. Alex Muthengi of Tharaka University, Dr. Daniel Mwangi of Tharaka University, and Dr. Jimrise Ochwach of Mama Ngina University College. Their knowledgeable advice, unwavering availability, and priceless insights were essential to this work's successful conclusion. Despite their hectic schedules, I am very appreciative of their commitment.

For their support and academic direction, I would also like to express my sincere gratitude to the entire Faculty of Science, Engineering, and Technology, with a special thanks to the Department of Physical Sciences. I would especially like to thank the faculty-level examiners and panelists who attended my first defense for their helpful criticism and support, which inspired me to keep going. The academic members have continuously been helpful and eager to provide guidance and support on my study.

I am also indebted to my classmates, particularly Alex Ngatia, for his assistance with editing, his late-night feedback sessions, and his unwavering moral support throughout this journey.

A special mention goes to my parents, William and Judith for instilling in me from an early age the values of hard work, resilience, and a commitment to excellence. Lastly, my deepest gratitude is reserved for my family. To my beloved Purity, her constant support, even in the most challenging moments, have been invaluable. To my children, you are my greatest source of inspiration and strength. I am profoundly thankful for your love and support.

May God richly bless all those who have stood by me throughout this research journey.

ABSTRACT

Cancer therapy remains a major biomedical challenge due to the coexistence of healthy, tumour, quiescent, and immune cells that interact in complex and often unpredictable ways. This thesis presents a mathematical model of tumour-host interactions under radiotherapy and chemotherapy. The limited understanding of how radiotherapy and chemotherapy when applied singly or in combination, influences tumour-immune dynamics and long-term treatment efficacy is the problem to be addressed. The model incorporates four compartments: healthy cells, tumour cells, quiescent tumour cells, and immune cells. The system of non-linear ordinary differential equations is analysed for positivity, boundedness, invariant regions, and equilibria. The basic reproduction number R_0 is derived, and stability analysis establishes conditions for tumour persistence or eradication. Sensitivity analysis identifies the parameters most influential to treatment outcomes. Numerical simulations, conducted using biologically consistent parameter values, reveal key dynamics. In the absence of therapy, tumour and quiescent populations expand while healthy cells decline, corresponding to $R_0 > 1$. Radiotherapy efficacy ε exerts a threshold effect: low values slow tumour growth without elimination, while sufficiently high values reduce R_0 below one, driving eradication. Chemotherapy schedules show similar behavior. In both modalities, continuous administration consistently outperforms pulsed or fractionated delivery. Combination therapy achieves the most rapid and sustained suppression, highlighting non-linear synergy between the two interventions. Timing is also decisive: early treatment stabilizes the system and prevents resurgence, whereas late initiation produces larger oscillations and slower recovery. These findings demonstrate the value of mathematical modelling in oncology by showing how efficacy, scheduling, and timing jointly determine long-term therapeutic success. The results provide quantitative insights that may guide clinical decision-making and the design of optimized cancer treatment strategies.

TABLE OF CONTENTS

LIST OF TABLES

LIST OF FIGURES

ABBREVIATION AND ACRONYMS

ABMS	Agent-Based Models .
DFE	Disease-Free Equilibrium.
DNA	Deoxyribonucleic Acid.
KNH	Kenyatta National Hospital.
MATRAB	Matrix Laboratory.
MRI	Magnetic Resonance Imaging.
NACOSTI	National Commission for Science, Technology and Innovation.
N	Nodes.
ODE	Ordinary Differential Equation.
R_O	Reproduction number.
ROS	Reactive Oxygen Spaces.
SA	Sensitivity Analysis.
TNM	Tumour , Lymph Node , Metastasis.
WHO	World Health Organisation.

CHAPTER ONE

INTRODUCTION

1.1 Background Information

Cancer remains a leading cause of death worldwide, accounting for nearly 10 million deaths in 2020 according to the (World Health Organization [WHO], 2021). Due to delayed diagnosis, restricted access to treatment, and rising risk factor prevalence, the incidence is rapidly increasing in sub-Saharan Africa (Bray et al., 2018). After cardiovascular and infectious diseases, cancer is currently the third most common cause of death in Kenya (Kenya Ministry of Health, 2020). The ability to systematically describe tumour growth, investigate tumour–immune interactions, and assess the expected effects of medicines without immediate reliance on clinical trials has made mathematical modelling a crucial tool in oncology (Baykara & Onur, 2015; Kareva, 2011). Tumour–host dynamics, immune surveillance, and treatment responses have all been captured by compartmental and nonlinear ordinary differential equation (ODE) models (de Pillis & Radunskaya, 2003; Kuznetsov et al., 1994). Through stability, sensitivity, and bifurcation analysis, these models elucidate the circumstances in which tumours endure or are eliminated, and emphasize the significance of therapeutic timing and dosage (Kirschner and Panetta, 1998). Many existing formulations consistently neglect or oversimplify the effects of treatment and the nonlinear interactions among immune effector, active tumour, quiescent tumour, and healthy cells (Hahnfeldt et al., 1999; Eftimie et al., 2011). These shortcomings reduce the models' ability to provide reliable insights into treatment optimization, particularly for combination therapeutic strategies.

Researchers can better comprehend the evolution of cancer and develop treatment plans by using mathematical models of tumour growth. (Garner *et al*., 2006) formulated a simple cell population model equation 1.1.1 to study the long-term behavior of quiescent and proliferating cells.

$$\begin{aligned} \frac{dP}{dt} &= k_{pp} - k_{pq} - k_{pd}P + k_{qp}Q \\ \frac{dQ}{dt} &= k_{PQ}P - k_{qp}Q + Kqp + KqdQ \\ \frac{dD}{dt} &= k_{pd}P + k_{qd}Q - \lambda D \end{aligned} \tag{1.1.1}$$

The initial conditions are ; $P(0) = p_o, Q(0) = q_o, D(0) = d_o$

Where ; P,Q,D are the densities of proliferating cells, Quiescent cells and dead cells respectively , $k_(pq)P$ transition from proliferating to quiescent cell, $-k_(qp)Q$ Quiescent cells becoming proliferating, $-k_(qd)$ Q Quiescent cells dying ,$-\lambda D$ decay of dead cells and p_o,q_o,d_o are their initial conditions. Although these functional models neglect the spatial effects, they provide insight into the overall growth dynamics of solid tumours. The model does not explicitly account for cell death (apoptosis) or differentiation into other cell types. The simplest model of tumour growth assumes that cells proliferate at a constant rate, leading to exponential expansion equation 1.1.2 over time (Laird *et al*.,1965).

$$N(t) = N_0 e^{rt} \tag{1.1.2}$$

Where $N(t)$ is the tumour size at time t, N_0 is the initial size, and r is the growth rate. The model does not account for nutrient depletion, oxygen limitations, or immune responses that slow down growth over time.The tumour is treated as a homogeneous entity, ignoring spatial factors like angiogenesis (formation of new blood vessels). The effects of the surrounding tissue, immune system interactions, and mechanical constraints are not included. In reality, tumour growth follows a sigmoidal pattern (Gompertzian growth) rather than pure exponential growth. Classical mathematical models, such as the Gompertz and logistic growth models, have been instrumental in shaping our understanding of tumour behaviour over time. Tumour growth is more accurately depicted by the Gompertz model, which takes into account the fact that tumours grow quickly at first but slow down once they reach a limiting size because of resource limitations, the immune system, and other biological variables (Laird *et al*., 1965). Empirical discoveries that tumour growth does not exhibit simple exponential behavior over time led to the development of the Gompertz model. Growth may seem exponential in the early stages of tumour development, but as the tumour gets bigger, its rate of growth drastically slows down because of constraints on oxygen, nutrients and available space. The Gompertz equation was proposed as a more physiologically plausible substitute to represent this sigmoidal growth pattern. In order to account for the inhibitory effects that intensify as the tumour approaches its carrying capacity, the exponential growth law is modified to incorporate a logarithmic deceleration term. The Gompertz model, for example, describes the growth of tumours as a function of time, accounting for the slowing growth rate as the tumour reaches a certain size (Anderson & May, 1991). The Gompertz equa-

tion is ;

$$\frac{dN}{dt} = rN \ln \frac{K}{N} \tag{1.1.3}$$

Where : N(t) is the tumour size (number of cells) at time t, r is the growth rate constant,K is the carrying capacity, or the maximum tumour size the environment can sustain. ln (K/N) accounts for the decreasing growth rate as N approaches K.

However, these traditional models often fall short in capturing the intricate interactions between healthy and tumour cells, particularly in the context of radiotherapy, where timing and dosage can significantly influence treatment outcomes (Wang *et al*., 2020). The equations of the Lotka-Volterra type are used to describe the competition for nutrients between cancer cells,normal cells and activated immune cells. These cells will be denoted as C, N, and T respectively. The population of each of the cells will depend upon time t. Considering that the cells can't spread to other parts of the body, for example metastasis is not present. The following set of equations is supported by the arguments made by Liu and Yang 2014. Using the Lotka-Volterra equations to examine the interaction between cancer cells and healthy cells is the most straightforward mathematical method for describing the dynamics of cancer. It outline the process for identifying the crucial points in this straightforward model, and use the outcome to ascertain its stability. The Lotka-Volterra equations provide the most basic model of the interaction between malignant and healthy cells in the absence of a therapy phase and additional immune responses. The equations for this straightforward scenario are;

$$\frac{dC}{dt} = kC(1 - C) - aCN \tag{1.1.4}$$

$$\frac{dN}{dt} = cN(1 - N) - dCN \tag{1.1.5}$$

Where a is the inhibitory effect of normal cells on tumour cell growth, c is the intrinsic growth rate of normal cells and d is the negative effect of tumour cells on the proliferation of normal cells.

The first equation indicates that the growth of tumour cells is a logistical growth whereas the rate of loss results from the competition between the cancer cells and the normal cells according to the numerical value of the coefficient a. The second equation indicates that a normal cell is also determined from a logistical growth with a growth rate given by the

coefficient c and the coefficient d represents the rate that the tumour cells are activated by the normal cells. From this system, we observe that for the cancer cells that increase in the first equation, the coefficients must satisfy the requirement that $a < k$. For the case that $d > c$, the cancer cells are predominant over the normal cells. The model does not include immune system interactions, which play a crucial role in controlling tumour growth. The model assumes no medical intervention (chemotherapy, radiation, immunotherapy). Cancer can best be described as a disease of the cells characterized by uncontrolled growth and invasion, driven by underlying genetic abnormalities. This definition captures the essence of cancer as a collection of related disorders, rather than a single disease. The term, ”cancer” refers to the presence of a set of characteristics commonly associated with tumours.

Despite notable advancements in treatment modalities, including surgery, chemotherapy and radiotherapy, the intricate dynamics of tumour behaviour continue to pose substantial challenges for effective management (Pucci *et al* ., 2019). Age is another critical factor in cancer risk; most patients are over 55 years old, with lifetime probabilities of developing cancer estimated at 1 in 2 for males and 1 in 3 for females (Nawrocki *et al*., 2015). According to WHO statistics from 2020, there were approximately 19.3 million new cancer cases globally alongside nearly 9.9 million deaths (Sung *et al*., 2021).

In Kenya, a striking 60% of cancer patients are under the age of 70, with breast cancer (34 per 100,000) and cervical cancer (25 per 100,000) being the most prevalent among women (Danaei *et al*.,2005). In men, prostate cancer (17 per 100,000) and esophageal cancer (9 per 100,000) dominate the statistics. Unfortunately, many cases are diagnosed at advanced stages due to lack of awareness, inadequate diagnostic facilities, high treatment costs and a significant poverty index (Korir *et al*.,2016). Notably, 15% of all cancer therapy referrals to Kenyatta National Hospital (KNH) in Nairobi originate from Meru County. The factors contributing to the high incidence of cancer in this region remain poorly documented.

In Meru County specifically, brain and lung cancers are particularly prevalent in areas such as Igembe and parts of Tigania. This trend may be linked to lifestyle choices including high consumption of miraa and heavy smoking (Mutiso *et al*., 2023). Additionally, data from local hospitals indicate a concerning prevalence of throat and brain cancers

potentially exacerbated by excessive alcohol consumption (Mutiso *et al*., 2023). Additionally, inadequate post-harvest management methods have been largely blamed for the increase in cancer cases in Meru County. The growth of aflatoxin, an environmental toxin that poses major health concerns, is caused by farmers' hasty harvesting of crops with high moisture content during the rainy season (Mutiso *et al*., 2023). This toxin can be ingested by humans through contaminated grains or through the consumption of meat from animals fed with such grains. Furthermore, the region's cool temperatures facilitate the growth of weeds and pests, prompting farmers to use unregulated agrochemicals at excessive concentrations (Mutiso *et al*., 2023). Consequently, individuals consuming these contaminated foods may be exposed to heavy metals that increase their cancer risk. Poor dietary habits further compound the risk of lifestyle diseases among the population (Hamilton *et al*., 2010).

Cancer encompasses more than 100 distinct diseases, each varying significantly in origin, progression and treatment options. However, they all share a common characteristic: unregulated growth and dissemination of abnormal cells resulting from failures in biological control mechanisms governing cell division (Vieira *et al*., 2023). The hallmark of cancer is the uncontrolled proliferation of aberrant cells that can invade surrounding tissues. Tumours can be classified as benign or malignant; while benign tumours are generally well-controlled and non-invasive, malignant tumours exhibit rapid growth and metastasis.

The complexity inherent in cancer necessitates prompt detection and intervention to improve patient outcomes. Current treatment strategies include chemotherapy, radiotherapy, immunotherapy, surgery and hyperthermia; often requiring combinations thereof for optimal efficacy. However, these treatments frequently produce significant side effects without guaranteeing a definitive cure (Datta *et al*., 2015).

Recent advancements have focused on immunotherapy as a promising avenue for enhancing patient outcomes by stimulating the immune system's ability to target cancer cells more effectively while minimizing adverse effects (De Mello *et al*., 2021). The challenge remains to develop optimal control strategies that maximize therapeutic efficacy while minimizing harm.

Yorke *et al*. (1993) credited with developing the first mathematical model of prostate cancer progression. The study created a basic kinetic model based on Gompertzian growth in order to explain how prostate cancer spreads, how it metastasizes, and how local treatments (such as radiation and surgery) are impacted by the metastasis process. Yorke and colleagues proposed that local relapse is linked to more aggressive cancer morphologies by contrasting their model simulations with the patient survival data in (Fuk *et al*., 1991).

They also propose that local control (such as the total removal of the main tumour and lymph node metastases) can greatly increase the disease-free survival and metastasis-free survival time because of the aggressive cancer phenotypes seen in local relapse.But once the cancer has spread, conventional therapies produce encouraging first outcomes but are unable to prevent tumour recurrence. Jackson, T.L.(2003). Prostate cancer has long been thought to be composed of distinct cell subpopulations, each with varying degrees of reliance on extracellular testosterone, which explains the return that occurs after favourable responses to hormonal castration. Jackson used mathematical modelling to illustrate this idea for the first time in 2001. Jackson created a set of partial differential equations for androgen deprivation therapy in prostate cancer by balancing the fluxes of two cell types, death, and proliferation under radial symmetry, as shown by equation (1.1.6)

$$\frac{dR}{dt} = u(R(t), t) \tag{1.1.6}$$

In this model, the tumour radius is denoted by R(t), the volume fractions of androgen dependent (AD) and androgen independent (AI) prostate cancer cells are denoted by p (R, t), q (R, t), and the net rate of collective cellular motion is denoted by $u(R(t), t)$. The model states that a high level of androgen stimulates the growth of cells that require it, but has no influence on the growth of cells that do not. On the other hand, a low dose of androgen causes a decrease in the apoptosis rate of androgen dependent cells and an increase in the death rate of androgen independent cells.These presumptions allowed the models to accurately represent the qualitative dynamics seen in the experimental data of LuCaP 23 in mice (Ellis *et al*., 1996). Therefore, Jackson comes to the conclusion that the model supports the idea that cancer relapse happens because AI cells have a lower apoptosis rate instead of a higher proliferation rate. This finding is in line with some

experimental evidence (Liu *et al*., 1996). This finding is consistent with the theory that prostate cancer cells incur expenses to develop treatment resistance, making them less competitive with AD cells in the absence of treatment (Zhang *et al*., 2017). Additionally, Jackson T.L.(2003). showed that androgen deprivation therapy is only effective for a small region of parameter which agrees with clinical data showing that androgen deprivation therapy is not curative, even in early stage disease. As with all models, Jackson's modelling effort has certain limitations. First, the assumption of spherical symmetry in the model formulation limits the application of the model to the early stage, where the cancer can be approximated with a sphere. Secondly, the assumption that increasing the level of androgen increases the apoptosis rate of androgen independent cells is arguable because androgen independent cells may still be dependent on AI ,which is known as the outlaw pathway to resistance (Feldman *et al*., 2001,Kuang *et al*., 2018, Heinlein *et al*., 2004). Regardless, Jackson's work has paved the way for future modelling studies.

Recent advancements in mathematical modelling have sought to address these limitations by incorporating more complex interactions within the tumour micro-environment. For instance, models that integrate the effects of immune response, nutrient availability and cellular signalling pathways provide a more comprehensive understanding of tumour dynamics (Ferlay *et al*., 2015). Additionally, the use of Ordinary Differential Equations (ODEs) allows for the simulation of various treatment scenarios, enabling researchers to explore the potential impacts of different radiotherapy protocols on tumour and healthy cell populations.

This thesis develops and analyses a non-linear ODE dynamics model that explicitly depicts immune cells, active tumour cells, quiescent tumour cells, and healthy tissue under time-dependent therapeutic interventions such as chemotherapy, immunotherapy, and radiation therapy. The analysis focuses on establishing the system's biologically significant properties (boundedness and positivity), determining threshold conditions for tumour control, identifying influential parameters through sensitivity analysis, and analysing the impact of treatment timing and dosing schedules through numerical simulations. Collectively, these contributions provide mathematical and computational evidence to support the design of more effective, less toxic, and sustainable cancer therapies.

However, despite mathematical progress in oncology, there remains a need for models that integrate therapeutic effects with healthy-tumour-immune cell dynamics under realistic treatment schedules.This gap motivates the present study.

1.2 Statement of the Problem

Treatment outcomes in cancer therapy are still quite unpredictable despite advancements in cancer therapy due to tumour heterogeneity, treatment toxicity, and intricate relationships between immune response, healthy tissue, and tumour cells. Clinicians frequently use empirically developed treatment plans, but there are currently few systematic tools available to forecast the combined effects of immunotherapy, chemotherapy, and radiotherapy.Although useful for comprehending tumour dynamics, existing mathematical models often oversimplify biological processes by neglecting quiescent tumour states, reducing non-linear interactions with immune cells, or portraying therapy as having constant effects rather than time-dependent ones (de Pillis & Radunskaya, 2003; Hahnfeldt et al., 1999; Eftimie et al., 2011). Their ability to direct individualized treatment plans or contribute to evidence-based cancer care policy is limited by these simplifications. There is therefore a critical need for robust non-linear models that intergrate therapy effects with the dynamics of tumours, immune cells, and healthy tissue, while capturing biologically plausible mechanisms and enable methodical evaluation of stability, sensitivity, and treatment timing. Addressing this gap will help develop more sustainable, less harmful, and more successful treatment strategies. In light of this challenge, the current study develops and analyses a non-linear healthy-tumour-immune therapy model as outlined in the following objectives.

1.3 Objectives of the Study

1.3.1 Main Objective

To develop and analyse a non-linear dynamical model of interactions between tumour-healthy-immune cells under therapeutic interventions.

1.3.2 Specific Objective

i. To develop a non-linear mathematical model that involves the dynamics of interactions between healthy-tumour-immune cells under therapeutic interventions.

ii. To perform stability analysis of the model in order to determine how therapy efficacy influences tumour persistence or eradication.

iii. To conduct sensitivity analysis to evaluate the impact of key parameters on tumour dynamics and treatment outcomes.

iv. To perform numerical simulation to investigate the effects of radiotherapy, chemotherapy, and combined therapies with emphasis on dosage and timing on the proliferation and survival rates of healthy cells ,and tumour cells within the mathematical framework.

1.4 Significance of the Study

This study is significant because it advances mathematical oncology by integrating healthy-tumour-immune cells within a single non-linear dynamical model under therapeutic interventions. By incorporating therapy efficacy, stability conditions, and parameter sensitivity, the research contributes to the theoretical insights of tumour–immune dynamics and extends the prior knowledge in cancer modelling.

Additionally, it has a practical importance. Stability and sensitivity analysis provide a rigorous basis for identifying the most influential treatment parameters, thereby guiding the design of optimal therapeutic strategies. Numerical simulations exploring therapy dosage and timing offer understanding in improving treatment effectiveness while minimising toxicity, which are critical factors in enhancing patient quality of life.

Beyond its theoretical and practical contributions, the study has policy relevance, particularly in resource-limited settings such as sub-Saharan Africa where access to treatment is restricted. By offering a systematic framework for assessing treatment outcomes and exploring sustainable cancer therapies, the findings can support evidence-based decision-making among policymakers, clinicians, and researchers.

1.5 Operational Definition of Terms

1.5.1 Tumour

A tumour refers to an abnormal mass or growth of tissue in the body, resulting from uncontrolled cell division. Tumours can form in virtually any part of the body and can vary widely in size, shape, and nature. Although the term ”tumour” is often associated

with cancer, not all tumours are cancerous. Tumours can be classified into benign and malignant categories, depending on their characteristics and potential to cause harm (Reich *et al*., 2024)

1.5.2 Sensitivity Analysis (SA)

Sensitivity Analysis is a fundamental scientific framework for comprehending the impact of model parameter variability on system outputs. The study of how various sources of uncertainty in a mathematical model's inputs might be allocated to the model's output uncertainty. When it comes to radiotherapy-induced tumour-healthy cell interaction models, sensitivity analysis offers a methodical approach to determine which biological or treatment related factors such as tumour suppression, preservation of healthy tissue, or time to remission have the most impact on treatment results. (Saltelli *et al*., 2008). Sensitivity analysis comes in two main varieties: local and global. Local SA uses partial derivatives to analyse the impact of minor changes in parameters around a baseline. This method may overlook interactions in non-linear systems, yet it is helpful for comprehending system behavior close to a nominal point. (Saltelli *et al*., 2008), global SA takes into account interactions between factors and examines their effects over their whole feasible ranges. Because of this, complex biological models where parameter dependency is likely to occur are particularly well-suited for global SA.

1.5.3 Mathematical Modelling in Oncology

The use of equations and simulations to predict tumour growth, response to treatment, and potential therapeutic outcomes (Preziosi *et al*., 2003).

1.5.4 Stability Analysis

A mathematical examination of whether small changes in system variables (such as tumour cell population) lead to predictable, bounded outcomes or drastic changes over time (Hirsch *et al*., 2013).

1.5.5 Tumour-Healthy Cell Interactions

The biological and physiological interactions between cancerous (tumour) cells and normal (healthy) cells in a given environment (Atkinson and Sophie 2010).

1.5.6 Non-linear Dynamical Model

A mathematical framework for describing the time dependent development of a system with non-linear governing equations in the state variables is called a non-linear dynamical model. Small changes in beginning conditions can result in drastically divergent trajectories, and the notion of superposition does not apply as it does in linear models. These models can capture complicated behaviours including bifurcations, limit cycles, and chaotic dynamics. They are usually stated as discrete time mappings or systems of non-linear ordinary or partial differential equations . Variable interactions, feedback systems or inherent characteristics of the system's constituent parts are the sources of the nonlinearity (Strogatz and Steven H 2024).

1.5.7 Senescence

Senescence refers to a state of permanent loss of cell proliferative capacity. Although they are still alive, senescent cells do not divide, stop producing DNA, and expand, flatten, and become more granular. Senescence has been observed in cancer cells after they have undergone substantial cellular stress due to radiation treatment-induced DNA damage (Roninson *et al*., 2003, Schmitt *et al*., 2007) and thereafter die primarily through apoptosis.

1.5.8 Apoptosis

The induction of apoptosis in cancer cells is crucial to the effectiveness of radiation therapy (Eriksson *et al*., 2010). Programmed cell death, also known as apoptosis, is a major mechanism of cell death involved in cancer therapy and radiation therapy in particular (Cragg *et al*., 2009). Apoptosis is characterized by cell shrinkage and the formation of apoptotic bodies; mitochondria play a major role for the apoptotic cell death (Fogg *et al*., 2011). Blebbing of cell membrane is frequently observed with condensed chromatin with nuclear margination and DNA fragmentation

1.5.9 Radiation Therapy

Radiation therapy is a therapeutic treatment approach that reduces tumor size and kills cancer cells by administering high doses of ionizing radiation. Although it effectively eliminates malignant tissues, it may also inadvertently damage neighbouring healthy cells, particularly those that are adjacent to the tumour bulk (Saini *et al*., 2020).

1.5.10 Lyapunov Function

Finding the stability, instability, or asymptotic stability of an equilibrium point without explicitly solving the system is a basic issue in the study of dynamical systems. The Lyapunov function, named for the Russian mathematician Aleksandr Lyapunov, is an effective instrument made for this use. Constructed to mimic the idea of ”energy” in a physical system, it is a scalar function V(x) that is ordinarily continuously differentiable. To determine the qualitative behavior of solutions in the vicinity of an equilibrium point, this function is utilized. It is used mathematically to evaluate a dynamical system's stability (Khalil *et al*., 2002).

1.5.11 Chemotherapy

Chemotherapy is a form of cancer treatment that involves a standardized schedule of one or more anti-cancer (cytotoxic) medications. By focusing on fast dividing cells a feature that many cancer cells share it prevents the growth and multiplication of cancer cells. The kind and stage of cancer will determine whether chemotherapy is administered alone or in conjunction with other treatments like immunotherapy, radiation therapy, or surgery (DeVita Jr *et al*.,2008).

1.5.12 Immunotherapy

Immunotherapy is a biological treatment that makes the body's immune system more capable of identifying and getting rid of unhealthy or aberrant cells, including cancerous ones. In contrast to traditional therapies like chemotherapy or radiation therapy, which directly target the tumour, immunotherapy makes use of the immune system's innate capacity to recognize and react to infections or cancers. Immune checkpoint inhibitors, monoclonal antibodies, cancer vaccines, cytokine treatments and adoptive cell transfer are among the various forms of immunotherapy that aim to improve or restore immune function in various ways (Sharma and Allison, 2015).

CHAPTER TWO
LITERATURE REVIEW

2.1 Overview of Cancer

Cancer is a complex and heterogeneous disease characterized by abnormal and uncontrolled cell proliferation, the ability to evade regulatory mechanisms, invasion of surrounding tissues, and the potential to metastasize to distant organs (Hanahan & Weinberg, 2011; Abalde et al., 2021). Globally, cancer remains one of the leading causes of death, accounting for nearly 10 million deaths in 2020, which represents approximately one in six deaths worldwide (WHO, 2021). Epidemiological studies further estimate that approximately one in three individuals will be diagnosed with cancer during their lifetime (Barrett et al., 2020). The multifaceted nature of cancer including its ability to evolve resistance mechanisms and present with variable biological subtypes poses significant challenges in both treatment and management.

The burden of cancer is disproportionately high in sub-Saharan Africa, where delayed diagnosis, inadequate infrastructure, and restricted access to advanced therapies exacerbate outcomes (Bray et al., 2018). In Kenya, cancer ranks as the third leading cause of mortality after infectious and cardiovascular diseases (Kenya Ministry of Health, 2020). Breast and cervical cancers dominate among women, while prostate and esophageal cancers are most common in men (Korir et al., 2016). In Meru County, lifestyle related factors such as heavy smoking, high consumption of miraa, and alcohol abuse have been linked to increased incidence of throat, brain, and lung cancers (Mutiso et al., 2023). Environmental exposures such as aflatoxin contamination due to poor post-harvest practices and overuse of unregulated agrochemicals further increase risks, reflecting the interplay between genetics, lifestyle, and environment in cancer development (Hamilton et al., 2010).

Despite advances in treatment including surgery, radiotherapy, chemotherapy, immunotherapy, and targeted therapies clinical outcomes remain unpredictable. Tumour heterogeneity, treatment toxicity, and therapy resistance often limit success, while variability in patient responses highlights the inadequacy of one size fits all approaches (Smith et al., 2020; Pucci et al., 2019). For instance, glioblastomas remain among the most aggressive primary brain tumours, with median survival of approximately one year even after extensive surgery, radiotherapy, and chemotherapy (Meaney et al., 2019). Al-

though radiotherapy provides precise local tumour control by targeting malignant cells (Nelson et al., 2003), recurrence and resistance remain common.

These limitations have spurred interest in more systematic frameworks for understanding cancer progression and guiding therapeutic design. Mathematical and systems biology models have been employed to capture tumour dynamics, immune interactions, and treatment responses. Some models emphasize patient-specific parameterization to account for heterogeneity (Poleszczuk et al., 2018; Powathil et al., 2015; Rockne et al., 2010), while others incorporate advanced techniques such as fractional derivatives for more realistic dynamics (Arfan et al., 2021). In prostate cancer research, system-based approaches have demonstrated how combining androgen deprivation therapy (ADT) with immunotherapy can enhance treatment efficacy (Aragon-Ching et al., 2007; Tang et al., 2012). The FDA-approved Provenge (sipuleucel-T) immunotherapy illustrates such innovations, though validation of these complex models remains a challenge due to limited clinical data (Fontana et al., 2023).

Taken together, the unpredictability of treatment outcomes, coupled with the growing cancer burden in resource-constrained regions, highlights the need for novel approaches that can integrate biological complexity, patient heterogeneity, and therapeutic interventions. Mathematical modelling provides a promising framework for this integration, enabling systematic analysis of tumour–host–therapy dynamics and informing evidence-based strategies for more effective, less toxic, and sustainable cancer management (Baykara & Onur, 2015; Kareva, 2011).

2.2 Mathematical Models of Tumours

The dynamical process of cancer cell growth has been better understood through the development of mathematical models. It has been a common practice to describe tumour growth using deterministic models of exponential, logistic, Gompertz, and Bertalanffy morphology. In order to forecast the rate at which the tumor volume would vary over time, the model was created. A typical trend among exponential models is shared by the Bertalanffy, Gompertz, and logistic models (Tabassum *et al*., 2019). The exponential model naturally illustrates how cancer develops in its early stages. The exponential model states that every cancer cell in the afflicted region divides into two daughter cells at a steady rate (Murphy *et al*., 2016). The population of the tumour, not specific

cells, is the focus of this concept. The growth in individuals, however, is negligible in comparison to the total population when it is very high. The growth rate decreases linearly with size until it approaches zero at carrying capacity, according to the logistic equation, which was initially proposed by (Verhulst,P.- F, 1838) . According to the Bertalanffy model, tumour volume rises in relation to surface area and falls with cell death. Nevertheless, the Bertalanffy model is not appropriate for forecasting how cancer would spread .In order to understand human mortality curves and calculate the worth of life insurance policies, Benjamin Gompertz developed the Gompertz model in 1825. A logistic model with an asymmetric curve and inflection points is generalized by the Gompertz model. With its S-curve, it was eventually used to simulate the scale of cell development in whole organisms.

2.2.1 Deterministic Model

Many deterministic models, including logistic, Gomperzt, exponential, and Bertalanffy models, have been used to simulate the proliferation of cancer cells. The four models that have been used to explain the process of cancer cell proliferation are reviewed in this section. The models are developed to forecast how quickly the tumour's volume will change in relation to variations in time, t. This section begins with a discussion of the exponential model of tumour growth because the logistic, Gompertz, and Bertalanffy models all follow the same exponential model pattern (Anwar *et al*, 2016). Exponential model is the natural description of early stages of cancer growth (Ishak & Anuar, 2010). In exponential model , each cancer cell split into two daughter cells in the affected area at the rate of constant, a. The exponential model is given by

$$dv(t) = av(t) \tag{2.2.1}$$

where,a is the kinetic parameter , $v(t)$ is the volume of the cancer cells and d is the derivative notation. The cancer cell growth in exponential model is proportional to the population of the cancer (Ishak & Anuar, 2010). The maximum tumour growth volume at doubling time is estimated by the exponential model. Nevertheless, the simple exponential growth model does not capture the effects of nutrient depletion and the onset of angiogenesis as tumours transition from the avascular to vascular stage. Therefore, it is necessary to extend the exponential model to incorporate nutrient-limited

and vascular-dependent tumour growth dynamics (Greenspan, 1972; Byrne & Chaplain, 1996; Mantzaris, Webb, & Othmer, 2004; Husain et al., 2017).

2.2.2 Logistic Model

The long-term growth rate of cancer cell proliferation cannot be accurately predicted by the exponential model. To overcome these issues, a logistic model was developed to describe how cancer cells grow and proliferate (Chamkha *et al*., 2015). The logistic model's general equation was first presented by Pierre Francois Verhulst in 1883. In order to determine the components of an organic population, the model was put out, focusing on the intrinsic development rate a, whose total size is constrained by the carrying capacity of b. According to the logistic model equation, cell growth increases linearly with size until it reaches the carrying capacity, b. The S-shape curve for the volume of cancer cells is produced via a logistic equation (Bataller *et al*., 2008). According to Roşca *et al*. (2014), this model has been used to model cancer cells and can explain the competition between cells. The general logistic formula is

$$\frac{dv}{dt} = a(1 - \frac{v}{b}) \tag{2.2.2}$$

Where a and b are intrinsic proliferation rate and carrying capacity respectively. Numerous biological processes, including bacterial populations and tumour formation, have been successfully represented by this model.

2.2.3 Gompertz Model

This model is an extension of the logistic model, consisting of an asymmetric curve with an inflection point. This model can show the latent stages of a cancer tumour. The magnitude of the cell proliferation for the entire organism was eventually modelled using its sigmoidal curve. According to research, it has the best prediction quality for the occurrence of breast and lung cancer. Other researchers utilized this model, which Gompertz first developed in 1825 to explain the human death curve, to fit and describe the tumour development data.The model's mathematical formula is,

$$\frac{dv}{dt} = aV \ln \frac{b}{v + c} \tag{2.2.3}$$

where a, b and c are parameters that can be adjusted to describe a particular data set. V is the volume of tumour and t is function of time.

$$\frac{dv}{dt} \tag{2.2.4}$$

is directly proportional to the number of cells in tumour . This model is popular for modelling the tumour growth as it slows down the process of tumour growth as the size of tumour increases.

2.2.4 Bertalanffy Models

In 1838, Von Bertalantfy presented this model as an organism growth model. According to this concept, the tumour's volume rises in proportion to its surface area and falls with cell death. (Benzekry *et al*., 2014) claims that this model forecasts sufficient growth of human tumours. The equation of this model is

$$\frac{dv}{dt} = aV2/3 - bv \tag{2.2.5}$$

where, a is the intrinsic growth rate, b is the growth rate declaration factor of antiangiogenic process, v is the descriptive variable for total tumour volume and t is time . The growth pattern of breast cancer is described by equation (2.5), which is also in line with clinical evidence. This model suggests the best fits to the experimental data for the early growth of tumours. Nevertheless, it would be difficult to anticipate how cancer will develop using the Bertalanffy model. The Gompertz model has been demonstrated to provide the best fits to the experimental and clinical data, explaining the growth of the breast and lung cancer data adequately.

In reality, there is no deterministic pattern to the growth and proliferation of cancer cells; instead, they are influenced by uncontrollable elements such as cellular metabolism, energy needs, hormone fluctuations, respiration, and personal traits like body mass index, genes, smoking, and stress (Mohamed *et al*., 2014). None of the models discussed above can forecast the long-term tumour growth rate, and they are all limited in their ability to forecast the last stages of cancer development. Therefore, deterministic models such as logistic, Gomperzt, exponential, and Bertalanffy cannot accurately capture the actual behavior of the cancer progression. These models must be extended to their stochas-

tic counterpart. The increasing popularity of mathematical modelling is not surprising, given that current research is arguably characterized by quantitative proof. Due to insignificant part to the dramatic growth in the availability of biological data produced by contemporary medical technologies, the application of mathematical modelling in oncology has grown rapidly over the past few decades (Stepien *et al*., 2020). Biologists and physicians, who have traditionally been slow to accept significant advances in their profession, have begun to adopt modelling more widely as a result of this increase. These days, research involving mathematicians and experimentalists is typical, with many experiments created especially to be verified by mathematical analyses that go along with them.

Mathematical modelling has become an essential component in the study of tumour dynamics, providing insights into the complex interactions between tumour cells and their micro-environment. These models serve as a framework for simulating tumour growth, predicting treatment responses, and optimizing therapeutic strategies (Gatenby & Gawlinski, 1996). The application of mathematical models in oncology has evolved significantly, with various approaches being developed to address the intricacies of cancer biology.

Samedi et al. (2021) in his study on mathematical models and their application in cancer growth highlighted two models which include, Malthusian and Logistic Model: Malthusian model assumes that the rate of increase of a population is proportional to its size at any given time. However, it is noted to have limitations, particularly in modelling long-term growth of malignant tumours, as it does not account for factors that lead to regression in growth over time. Gompertzian Model : Named after mathematician Benjamin Gompertz, this model describes the growth and decay rates of bio-organisms, including cancer cells. The basic Gompertz curves function is ;

$$V(t) = V_0 e^{\frac{\alpha}{\beta}(1-e^{-\beta t})} \tag{2.2.6}$$

Where V(t) is the tumour volume at time t , v_0 the volume at time t = 0 , α is the intrinsic (initial) tumour growth rate constant , β is the deceleration constant and $\frac{\alpha}{\beta}$ is the asymptotic tumour volume. It is recognized for its ability to model tumour growth more accurately over longer periods, as it captures the sigmoidal growth pattern typical

of many tumours. He also mentions the use of other mathematical methods, such as partial differential equations, for solving tumour growth problems.The study enhances conventional mathematical frameworks by using this model, which gives a more realistic depiction of tumour growth dynamics and how it interacts with healthy cells during radiation therapy.

This study's stability and sensitivity analysis provides insights for improving therapeutic approaches by enabling a more thorough investigation of tumour response to therapy. Additional characteristics, such as immunological response, pharmacological effects, or radiation impact, can be added to the Gompertzian model to assist clinical decision-making and further refine predictions.As a result, the Gompertzian model is a useful tool for academics and clinicians alike because its incorporation into this research framework not only improves its theoretical underpinnings but also increases its application in actual oncological treatments.

In addition to ODEs, agent-based models (ABMs) have gained prominence in cancer research. ABMs simulate individual cell behaviours and interactions within the tumour micro-environment, providing a more detailed understanding of spatial dynamics and heterogeneity (Gong *et al*., 2017). These models are particularly valuable for investigating the effects of immune cell infiltration and the spatial distribution of tumour cells, which can significantly influence treatment outcomes.

2.2.5 Applications and Implications of Mathematical Tumour Models

The integration of mathematical models into clinical oncology has profound implications for treatment optimization. By incorporating patient-specific data, these models can facilitate personalized medicine approaches, tailoring treatment regimens to individual tumour characteristics and patient responses (Park *et al*., 2008). For example, mathematical models can predict the efficacy of combination therapies, helping clinicians identify optimal dosing strategies that maximize tumour eradication while minimizing damage to healthy tissues.

Moreover, mathematical modelling has been instrumental in advancing our understanding of tumour evolution and resistance mechanisms. By simulating various treatment scenarios, researchers can identify critical factors that influence treatment efficacy and

develop strategies to overcome resistance (Hatzikirou *et al*., 2015). This predictive capability underscores the importance of mathematical models in guiding clinical decision-making and improving patient outcomes.

Poleszczuk et al. (2016) modelled the activation and movement of activated effector T cells within and between distinct metastases following an unspecified local therapy. The growth dynamics of individual sites are governed by logistic growth with immune predation, as in (Kuznetsov *et al*., 2017) tumour regrowth model . Here, the immune compartment is extended to include the probability that T cells that are activated at one anatomical site arrive at a tumour in a different location after extravasation out of the circulatory system, dependent on the blood flow fraction to the different organs and tissues. These models can be spatially explicit, accounting for the spatial distribution of cells within a tumour and their interactions with surrounding tissue. The advantage of mathematical models is providing insight into disease growth, treatment response, and ultimately building the framework for precision medicine (Olson *et al*., 2017). In conclusion, mathematical models of tumours represent a vital intersection of mathematics and cancer biology, offering valuable insights that enhance our understanding of tumour dynamics and inform clinical practice. Continued research in this area is essential for developing more effective and personalized cancer treatment strategies.

2.3 Stability and Sensitivity Analysis

2.3.1 Stability Analysis

Stability analysis refer to examination of a system's behaviour in response to perturbation or change. It involves assessing equilibrium state of a system and analysing its ability to recover from disturbances, maintaining stability over time. The main aim is to determine the condition under which a system remain stable or transition into instability. Stability analysis predict the system behaviour and take preventive measure to avoid undesirable outcome. It provide insight into the resilience of system.

Van den Driessche et al. (2002) defined the local stability of an equilibrium point as the point in a system at which the system returns to the equilibrium point after being disturbed. Additionally, they reported that a Disease-Free Equilibrium (DFE) is locally stable if all epidemiological situations evolve to the equilibrium point in such a way that a small perturbation of the system returns the system to the DFE.

Nenya et al. (2019) investigated the local and global stability conditions of discrete-time dynamics model equilibrium points with and without the Allee effect. Local asymptotic stability conditions for the equilibrium points were investigated in the study, and then the global stability of the model's equilibrium points was evaluated and compared. The study concluded that the Allee effect reduces the local and global stability of the population dynamic model's equilibrium points.

Gao et al. (2018) defined the global stability of a system's equilibrium point as the inevitable outcome of an epidemic process regardless of its origin. Globally stable disease free equilibrium exists when the disease cannot persist in the population regardless of the magnitude of the perturbation to the system. They reported that global stability for endemic equilibrium is typically a difficult mathematical problem due to disease models' complexity and high dimension. Additionally, they stated that the Lyapunov function method could be used to determine the global stability of an epidemiological model.

Shuai et al. (2013) used Lyapunov functions to investigate the global stability of infectious disease models. The study provided instructions for developing Lyapunov functions for generic infectious disease models and their global dynamics. The global stability of the disease-free equilibrium was established using a matrix-theoretic method based on Kirchhoff's matrix tree theorem and two new combinatorial identities. The global stability of the endemic equilibrium was established using a graph-theoretic method based on Kirchhoff's matrix tree theorem and two new combinatorial identities. The study discovered that these two methods completely established the sharp thresholds property, demonstrating that the basic reproduction number was the sharp threshold property. However, they reported that the sharp threshold property did not hold in some models when backward bifurcation occurred.

Ak Gümüş (2014) defined the global stability of a system's equilibrium point as the inevitable outcome of an epidemic process regardless of its origin. A globally stable, disease-free equilibrium exists when the disease cannot persist in the population regardless of the magnitude of the perturbation to the system. They reported that global stability for endemic equilibrium is typically a difficult mathematical problem due to disease models' complexity and high dimension. Additionally, they stated that the Lyapunov

function method could be used to determine the global stability of an epidemiological model.

2.3.2 Sensitivity Analysis

The rise of systems biology, sensitivity analysis methods have been widely used to study metabolic networks, signalling pathways, and genetic circuits. An analysis of model inputs and outputs' sensitivity can reveal the robustness of biological responses to changes in biological parameters (Zi, 2011; Charzyńska *et al*., 2012). Sensitivity analysis can also help design experiments,reduce models, and estimate parameters. Local and global sensitivity analyses are commonly used in systems biology. Local sensitivity analysis is a well-known method for assessing the impact of small changes on model outputs. Global sensitivity analysis techniques were used to determine how large variations in model input parameters affect model outputs. Zi (2011) introduced the basic concepts of sensitivity analysis applied to systems biology models. Aspects of sensitivity analysis for systems biology models are also discussed, as are the limitations of interpreting sensitivity analysis results.

Local sensitivity analysis, as defined by Zhou *et al*., (2014) is the process of determining the local impact of input factor variation on the model response by focusing on the sensitivity in the vicinity of a set of factor values. Such sensitivity is frequently evaluated using gradients or partial derivatives of the output functions at these factor values, like when studying the local sensitivity of an input factor, the values of other input factors are held constant.

Shah et al. (2017) also developed a model of Optimum control for spread of pollutants through forest resource used the same approach where the normalised sensitivity index of the parameters. The study found that the model parameter and some parameters had positive effects on R_0 which means they are helping us save forest resource and other parameter have negative impact on model.

2.4 Effect of Radiation on Tumour Cells

Radiation therapy is a cornerstone of cancer treatment, utilized to target and eradicate tumour cells while sparing healthy tissue. The effectiveness of radiation in tumour control is influenced by various biological factors, including the intrinsic characteristics of

tumour cells, the micro-environment, and the timing and dosage of radiation exposure (Baskar *et al*., 2012). Understanding the effects of radiation on tumour cells is crucial for optimizing treatment protocols and improving patient outcomes.

2.4.1 Mechanisms of Radiation Action

The primary mechanism by which radiation exerts its effects on tumour cells is through the induction of DNA damage. Ionizing radiation generates Reactive Oxygen Species (ROS) that lead to single-strand and double-strand breaks in DNA, ultimately triggering cellular responses such as apoptosis, senescence, or repair (Hall & Giaccia, 2012). The ability of tumour cells to repair DNA damage plays a significant role in their sensitivity to radiation. Cells with proficient DNA repair mechanisms may survive radiation exposure, leading to treatment resistance and tumour recurrence (Stefanou *et al*., 2021).

In addition to direct DNA damage, radiation can also affect the tumour micro-environment. The exposure of tumour cells to radiation can induce changes in the surrounding stromal cells, immune cells, and vasculature, which may either enhance or mitigate the therapeutic effects of radiation (Arnold *et al*., 2018). For instance, radiation can stimulate the release of pro-inflammatory cytokines and chemokines, promoting immune cell infiltration and potentially enhancing anti-tumour immunity (Dewan *et al*., 2009). Conversely, radiation-induced changes in the tumour vasculature can lead to hypoxia, which may reduce the efficacy of subsequent treatments (Huang *et al*., 2013).

2.4.2 Clinical Implications and Treatment Optimization

The interplay between radiation and tumour biology underscores the importance of personalized treatment approaches. By understanding the specific responses of tumour cells to radiation, clinicians can tailor treatment regimens to maximize therapeutic efficacy while minimizing adverse effects. For example, the timing of radiation in relation to other therapies, such as chemotherapy or immunotherapy, can significantly influence treatment outcomes (Baskar et al., 2012).

Recent advancements in mathematical modelling have facilitated the exploration of optimal radiation schedules and dosages. These models can simulate the dynamic interactions between tumour cells and their micro-environment, providing insights into how variations in treatment parameters affect tumour response (Montaseri *et al*., 2020). Such

modelling efforts are essential for developing evidence-based guidelines that enhance the effectiveness of radiation therapy in clinical practice.

Bekker et al. (2022) developed a mathematical model of radiotherapy and its impact on tumour interaction with immune system. The study emphasizes the importance of mathematical models in predicting tumour responses to various radiotherapy schedules. These models have been calibrated with experimental data, leading to the identification of optimal treatment schedules that outperform standard regimens. It was found that proliferating cells within tumours are more radiosensitive than quiescent cells. This insight is crucial for understanding how different cell populations within a tumour respond to radiation, influencing treatment outcomes. The study discusses the potential of radiotherapy to have immune-sparing effects, particularly when combined with immunotherapies. This combination may enhance the overall therapeutic benefit for patients. The study suggests conducting more clinical trials to validate the mathematical model predictions and to explore the timing and dosing strategies that maximize the immunomodulatory effects of radiotherapy.

2.5 Optimization of Tumour Models

The optimization of tumour models is a critical area of research that aims to enhance the predictive accuracy of mathematical models in oncology. These models serve as essential tools for understanding tumour dynamics, treatment responses, and the complex interactions between tumour cells and their micro-environment (Baker *et al*., 2018). By refining model parameters and assumptions, researchers can improve the utility of these models in guiding clinical decision-making and personalizing treatment strategies.

2.5.1 Methodologies for Optimization

Various methodologies are employed to optimize tumour models, including parameter estimation techniques and sensitivity analysis. Parameter estimation involves fitting mathematical models to clinical data, allowing for the calibration of model parameters to reflect real-world tumour behavior (Ghaffari *et al*., 2020). This process is crucial for validating model predictions and ensuring that they accurately represent the biological processes underlying tumour growth and response to treatment. Sensitivity analysis further enhances model optimization by exploring how variations in model parameters influence outcomes. This analysis identifies critical factors that impact treatment effi-

cacy, enabling researchers to focus on the most influential parameters when developing treatment strategies (Copas *et al*., 2019). For instance, understanding how changes in tumour growth rates or treatment dosages affect overall survival can inform the design of more effective therapeutic regimens.

2.5.2 Integration with Clinical Data

The integration of mathematical models with clinical data is paramount for advancing personalized medicine approaches. By tailoring treatment regimens based on patient-specific characteristics and tumour biology, clinicians can optimize therapeutic outcomes while minimizing side effects (Baker *et al*., 2018). This personalized approach is particularly relevant in the context of combination therapies, where the interactions between different treatment modalities can be complex and variable. Recent studies have demonstrated the potential of optimized tumour models to predict treatment responses and guide clinical decision-making. For example, models that incorporate patient-specific data have been shown to identify optimal treatment schedules that outperform standard regimens, leading to improved patient outcomes (Montaseri et al., 2020). These findings underscore the importance of continued research in this area to refine existing models and develop new optimization strategies. The optimization of tumour models, therefore, is essential for enhancing the predictive capabilities of mathematical frameworks in oncology. By employing robust methodologies for parameter estimation and sensitivity analysis, researchers can develop models that accurately reflect tumour dynamics and inform clinical decision-making. The integration of these models with clinical data paves the way for personalized treatment approaches, ultimately improving patient outcomes in cancer therapy.

2.5.3 Numerical Simulation Approaches in Tumour–immune Models

Mathematical models of tumour–immune interactions are commonly analysed using a combination of analytical methods (existence, positivity, stability, and reproduction numbers) and numerical simulation to explore transient behaviour, bifurcations, and treatment protocols.

Early and influential ODE studies (Kuznetsov et al., 1994; de Pillis & Radunskaya, 2003; van den Driessche & Watmough, 2002) employed fixed–step Runge-Kutta methods to examine tumour-immune dynamics. More recent investigations (Montaseri et al., 2020; Poleszczuk et al., 2018) have adopted adaptive stiff or nonstiff solvers such as LSODA and BDF, available in standard scientific libraries, to handle stiffness arising from immune-kill terms and rapid therapy pulses.

Best practice in modern mathematical oncology combines the following elements:

i. A primary, widely used solver (LSODA via `odeint` or `solve_ivp`);

ii. Verification using a high–order fixed–step method (RK4) with step–size refinement; and

iii. Explicit reporting of solver settings (`rtol`/`atol`) and parameter provenance (de Pillis et al., 2005; Murphy et al., 2016), together with archiving of simulation scripts and random seeds to ensure reproducibility (Poleszczuk et al., 2018).

The literature also emphasizes clear visual and numerical diagnostics, including semilog time-series for multi-scale variables, eigenvalue spectra of the Jacobian at equilibria, sensitivity indices for threshold quantities such as R_0, and convergence or solver-comparison checks to demonstrate numerical robustness (Shuai & van den Driessche, 2013; Saltelli et al., 2008).

In summary, recent studies converge on the use of adaptive stiff solvers complemented by fixed-step verification and complete disclosure of solver parameters practices adopted in this thesis and described in detail in Chapter 3.

CHAPTER THREE
METHODOLOGY

3.1 Model Formulation and Description

3.1.1 Model Formulation

In this study, a compartmental model involving healthy cells $H(t)$, tumour cells $T(t)$, quiescent tumour cells $Q(t)$, and immune cells $I(t)$ will be developed. The model will incorporates biological processes such as proliferation, transformation, immune response, and treatment effects without introducing new compartments for control mechanisms. The treatments such as radiotherapy, chemotherapy, and immunotherapy are represented as time-dependent external influences.

3.1.2 A non-linear Model Assumptions

The following assumptions underlie the model:

i. Healthy cells grow logistically with growth rate r_H and carrying capacity K_H.

ii. A fraction of healthy cells transforms into tumour cells at rate α_1.

iii. Tumour cells proliferate logistically with rate r_T and carrying capacity K_T.

iv. Tumour cells can enter a quiescent (dormant) state at rate β, and revert to active state at rate γ, especially under favourable conditions.

v. Immune cells attack tumour and quiescent cells with saturating (Michaelis-Menten) kinetics.

vi. Tumour cells stimulate immune cell recruitment. Immune cells decay naturally at rate d_I.

vii. Radiotherapy and chemotherapy damage tumour and quiescent cells and also affect healthy cells.

viii. Radiotherapy effectiveness decays with repeated application due to resistance development.

ix. Immunotherapy enhances immune activity without affecting healthy cells.

3.1.3 Model Flow Chart

The research proposed model flow chart that is intended to visually depict the key processes and interactions within the healthy cells, tumour cells, quiescent cells and immune cells focussing particularly on the impact of therapeutic intervention. The flow chart illustrate the movement of individuals between various compartments of the model as shown in Figure 3.1:

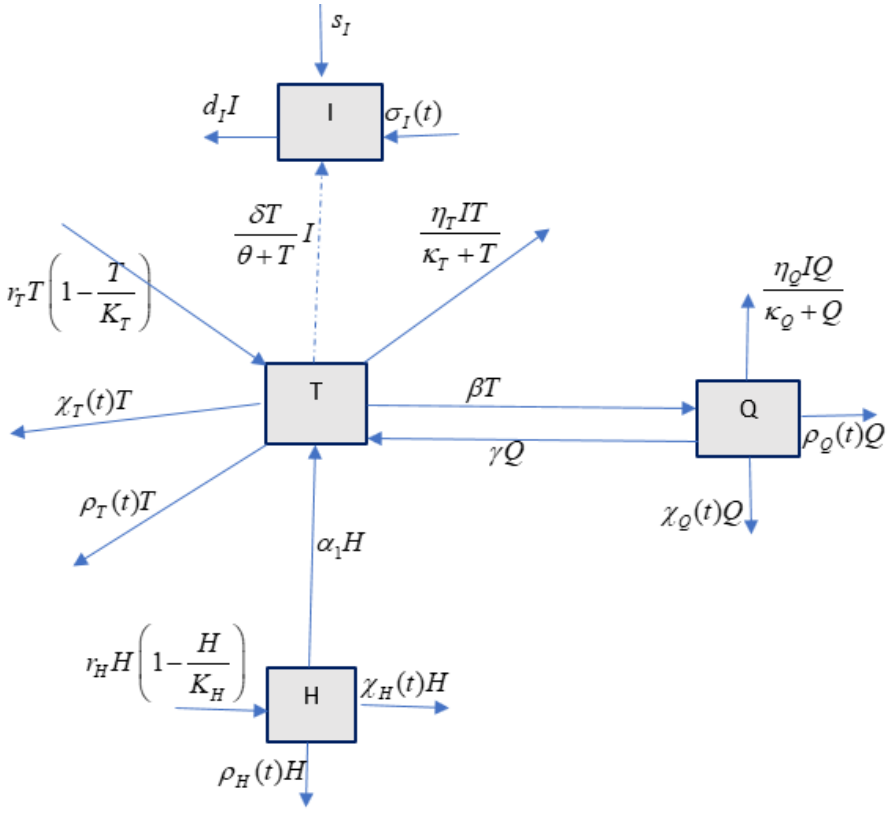

Figure 3.1: A non-linear model flow chart

3.1.4 Model Description

The population of healthy cells exhibits logistic growth, characterized by a natural proliferation rate r_H and constrained by a carrying capacity K_H, reflecting the finite availability of resources such as nutrients and space. The logistic growth term $r_H H(1-\frac{H}{K_H})$ ensures that the healthy cell population stabilizes as it nears the environment's capacity. However, healthy cells can transform into tumour cells due to genetic mutations or environmental insults, represented by the term $\alpha_1 H$, where α_1 is the transformation rate from healthy to tumour cells. In addition, treatment modalities such as radiotherapy and chemotherapy can directly damage healthy tissue. This is incorporated into the model

by including the radiotherapy-induced death term $\rho_H(t)H$, where $\rho_H(t)$ is the time-dependent rate of radiotherapy damage to healthy cells, and the chemotherapy-induced death term $\chi_H(t)H$, with $\chi_H(t)$ representing the time-dependent toxicity of chemotherapy to healthy cells. These considerations lead to the formulation of the healthy cell dynamics as shown in equation 3.1.1. Similar approaches to modelling healthy-tumour interactions under treatment have been discussed by Kim, Lee, and Levy (2014) in the context of optimal therapy strategies.

$$\frac{dH}{dt} = r_H H \left(1 - \frac{H}{K_H}\right) - \alpha_1 H - \rho_H(t)H - \chi_H(t)H \tag{3.1.1}$$

The tumour cell population increases through two main processes: transformation from healthy cells at a rate α_1, and intrinsic proliferation modelled by logistic growth with proliferation rate r_T and carrying capacity K_T. Tumour cells also receive additional input from the reactivation of quiescent tumour cells at rate γ, which accounts for cells that re-enter the active cycle under favourable conditions such as hypoxia recovery or nutrient availability. Losses in the tumour population occur due to several mechanisms. Natural tumour cell death is modelled by the parameter β. Immune response contributes to tumour reduction through a saturating cytotoxic effect represented by the Michaelis-Menten-like term $\frac{\eta_T IT}{\kappa_T + T}$, where η_T is the immune killing rate and κ_T is the half-saturation constant. Additionally, tumour cells are targeted by radiotherapy and chemotherapy. The time-dependent killing terms $\rho_T(t)$ and $\chi_T(t)$ represent the rates of tumour cell death due to radiotherapy and chemotherapy, respectively. Altogether, these processes are captured in equation 3.1.2, which models the net rate of change of the tumour cell population over time.

$$\frac{dT}{dt} = \alpha_1 H + r_T T \left(1 - \frac{T}{K_T}\right) - \beta T + \gamma Q - \frac{\eta_T IT}{\kappa_T + T} - \rho_T(t)T - \chi_T(t)T \tag{3.1.2}$$

The quiescent tumour cell compartment Q represents non-proliferating tumour cells that have entered a temporary dormant state due to unfavourable environmental conditions such as hypoxia or lack of nutrients. These cells arise from the active tumour cell popula-

tion at a rate β, capturing the transition from proliferating to quiescent phase. Quiescent cells can return to the active tumour population at a reactivation rate γ, especially when the environment becomes favourable. They are also susceptible to immune surveillance, and this interaction is represented by a saturating immune clearance term $\frac{\eta_Q IQ}{\kappa_Q+Q}$, where η_Q is the killing rate by immune cells and κ_Q is the half-saturation constant. Both radiotherapy and chemotherapy can partially affect quiescent cells, although typically with lower efficacy than on actively dividing cells. These effects are modelled using time-dependent death rates $\rho_Q(t)$ and $\chi_Q(t)$, respectively. These terms reflect the therapeutic impact of treatment on the dormant cell population. The overall dynamics of quiescent cells are summarized in equation 3.1.3, describing the net rate of change of the quiescent tumour cell population over time.

$$\frac{dQ}{dt} = \beta T - \gamma Q - \frac{\eta_Q IQ}{\kappa_Q + Q} - \rho_Q(t)Q - \chi_Q(t)Q \tag{3.1.3}$$

The immune cell population I represents cytotoxic immune cells responsible for identifying and eliminating tumour and quiescent cells. Their dynamics are influenced by several biological processes. The term s_I represents the basal source or natural influx of immune cells into the tumour micro-environment, maintaining a minimal level of immune surveillance. The function $\sigma_I(t)$ accounts for externally administered immunotherapy, which boosts the immune population over time through medical intervention. Immune cells can also proliferate in response to tumour presence. This activation and clonal expansion is captured by the term $\frac{\delta T}{\theta+T}I$, a saturating function that models stimulation of immune cells by tumour antigens. Here, δ is the maximum activation rate and θ is the tumour density at which immune activation is half-maximal. Immune cells also undergo natural degradation at rate d_I, which reflects the finite lifespan of immune effectors and their exhaustion during prolonged engagement. Together, these processes describe the evolution of the immune population in the tumour micro-environment and are mathematically represented by equation 3.1.4.

$$\frac{dI}{dt} = s_I + \sigma_I(t) + \frac{\delta T}{\theta + T}I - d_I I \tag{3.1.4}$$

3.1.5 Model Equations

This research, has developed the proposed model that captures the interactions among the four key compartments: healthy cells $H(t)$, tumour cells $T(t)$, quiescent cells $Q(t)$, and immune cells $I(t)$. Healthy cells grow logistically with intrinsic rate r_H and carrying capacity K_H, and are reduced by natural decay $\alpha_1 H$, radiotherapy-induced death $\rho_H(t)H$, and chemotherapy-induced death $\chi_H(t)H$. Tumour cells arise from transformation of healthy cells at rate $\alpha_1 H$, grow logistically with rate r_T and capacity K_T, and are reduced by transition to quiescence (βT), immune-mediated cytotoxicity ($\frac{\eta_T IT}{\kappa_T + T}$), radiotherapy ($\rho_T(t)T$), and chemotherapy ($\chi_T(t)T$). Quiescent cells are derived from tumour cells at rate βT, and may revert to active tumour phenotype at rate γQ. They are also subject to immune elimination ($\frac{\eta_Q IQ}{\kappa_Q + Q}$), radiotherapy ($\rho_Q(t)Q$), and chemotherapy ($\chi_Q(t)Q$). Immune cells are maintained via basal influx s_I, enhanced by immunotherapy input $\sigma_I(t)$, and proliferate in response to tumour presence via a saturating function $\frac{\delta T}{\theta + T}I$, but decay at rate $d_I I$. Collectively, the system of equations (3.1.5) models the tumour-immune-host dynamics under therapeutic interventions.

$$
\begin{aligned}
\frac{dH}{dt} &= r_H H\left(1 - \frac{H}{K_H}\right) - \alpha_1 H - \rho_H(t)H - \chi_H(t)H \\
\frac{dT}{dt} &= \alpha_1 H + r_T T\left(1 - \frac{T}{K_T}\right) - \beta T + \gamma Q - \frac{\eta_T IT}{\kappa_T + T} - \rho_T(t)T - \chi_T(t)T \\
\frac{dQ}{dt} &= \beta T - \gamma Q - \frac{\eta_Q IQ}{\kappa_Q + Q} - \rho_Q(t)Q - \chi_Q(t)Q \\
\frac{dI}{dt} &= s_I + \sigma_I(t) + \frac{\delta T}{\theta + T}I - d_I I
\end{aligned}
\tag{3.1.5}
$$

3.1.6 Model Variables and Parameters

The variables and parameters for the proposed model are illustrated in table 1 and 2 respectively:

Table 3.1: The state variables for the proposed model

Symbol	Variables
$H(t)$	Healthy cells
$T(t)$	Tumour cells
$Q(t)$	Quiescent tumour cells
$I(t)$	Immune cells

Table 3.2: Description of model parameters

Parameter	Description
r_H	Growth rate of healthy cells
K_H	Carrying capacity of healthy tissue
α_1	Rate at which healthy cells transform into tumour cells
r_T	Growth rate of tumour cells
K_T	Carrying capacity of tumour cells
β	Transition rate from tumour to quiescent state
γ	Reactivation rate from quiescent to tumour state
η_T	Maximum immune-mediated killing rate of tumour cells
κ_T	Tumour cell concentration for half-maximal immune killing
η_Q	Maximum immune-mediated killing rate of quiescent cells
κ_Q	Quiescent cell concentration for half-maximal immune killing
s_I	Baseline source of immune cells
$\sigma_I(t)$	Immunotherapy-induced immune stimulation rate
δ	Immune recruitment rate by tumour cells
θ	Tumour load for half-maximal immune recruitment
d_I	Natural decay rate of immune cells
$\rho_H(t)$	Radiotherapy-induced death rate for healthy cells
$\rho_T(t)$	Radiotherapy-induced death rate for tumour cells
$\rho_Q(t)$	Radiotherapy-induced death rate for quiescent cells
$\chi_H(t)$	Chemotherapy-induced death rate for healthy cells
$\chi_T(t)$	Chemotherapy-induced death rate for tumour cells
$\chi_Q(t)$	Chemotherapy-induced death rate for quiescent cells

3.2 Stability Analysis

The local and global stability of both the tumour-free (disease-free) equilibrium and the endemic equilibrium of the system equation (3.1.5) has been examined. The basic reproduction number, R_0, has been derived using the Next Generation Matrix method, focusing on the tumour-related compartments. This threshold parameter determines whether the tumour population will persist or die out. To assess local stability, the Jacobian matrix of the non-linear system at each equilibrium point has been computed. Eigenvalues

of the Jacobian has been obtained numerically using Python software to determine stability conditions. Negative real parts of all eigenvalues indicate local asymptotic stability. Global stability has been established using a suitable Lyapunov function. The function has been constructed to ensure it is positive definite and its derivative along solutions of the system is negative definite. Both analytical and computational tools has been applied to verify the theoretical results and gain deeper insight into the long-term behavior of the system under different parameter regimes.

3.3 Sensitivity Analysis

Sensitivity analysis has been conducted using the normalized forward sensitivity index. This approach quantifies the relative change in the basic reproduction number, R_0, in response to changes in individual model parameters. For a given parameter p, the sensitivity index is defined as

$$\Upsilon_{R_0}^{p} = \frac{\partial R_0}{\partial p} \cdot \frac{p}{R_0} \tag{3.3.1}$$

This index indicates how a small percentage change in parameter p affects the percentage change in R_0. Parameters with high absolute sensitivity indices are considered more influential in the dynamics of tumour progression and treatment response. The sensitivity analysis has helped in identifying the most critical parameters that drive the tumour dynamics and guide effective control strategies. Symbolic and numerical computation of sensitivity indices has been performed using Python software.

3.4 Model Simulation

Numerical simulations has been carried out using Python software, based on parameter values sourced from published literature. The model has been solved using standard numerical integration techniques such as the Runge–Kutta method. Simulations has focus on exploring the temporal dynamics of healthy cells, tumour cells, quiescent cells, and immune cells under varying treatment scenarios. By systematically varying key parameters, including radiotherapy and chemotherapy application rates, as well as immune stimulation, the simulations has validated the analytical results. These simulations has provided insights into the effectiveness of different treatment strategies and their impact

on tumour suppression, healthy cell preservation, and immune response behavior over time.

3.5 Ethical Consideration

For all contributions to the research, proper credit and acknowledgement has been provided. Plagiarism and other improper claims of the research findings has been avoided. The study findings has been critically and carefully examined to ensure that the findings are legitimate and that the results has been reported with honesty and integrity. The data that has been used in this study is confidential and no data fabrication has been done when carrying out data analysis. The research proposal has been approved by the Tharaka University Ethics Committee. A research permit has been received from the National Commission for Science, Technology and Innovation (NACOSTI) before commencing the study.The findings has been made public in a transparent manner to aid in the growth of knowledge in the field of applied mathematics.

CHAPTER FOUR

RESULTS AND DISCUSSION

4.1 Introduction

This chapter summarizes and explains the main conclusions drawn from the analysis and numerical simulation of the suggested non-linear dynamical model that captures the interactions between immune, tumour, and healthy cells during therapeutic intervention.The proof of the solutions' boundedness and positivity aids in assessing the model's mathematical and biological validity. Both sensitivity and local and global stability analyses of equilibrium points are included. Critical insights into the intricate dynamics governing cancer growth and remission in response to treatment are provided by the results. It also account for time-dependent therapeutic effects while modelling the interactions between the three main cell populations tumour, healthy, and immune using a system of ordinary differential equations.

4.2 Boundedness and Positivity of Solutions

Maintaining the biological viability of differential equation solutions is crucial when modelling biological systems. Proving the positivity and boundedness of solutions is usually how this is accomplished. Population variables like immune cells (I), tumour cells (T), healthy cells (H), and quiescent tumour cells (Q) are protected from achieving negative values by positivity. Boundedness guarantees that these variables do not grow unbounded over time, respecting biological and physical constraints such as carrying capacities and resource limitations.

Considering the system of equations defined in (3.1.5), subject to non-negative initial conditions:

$$H(0) \geq 0, \quad T(0) \geq 0, \quad Q(0) \geq 0, \quad I(0) \geq 0.$$

4.2.1 Positivity of Solutions

For biological validity, it must be shown that all model variables remain non-negative for all time whenever they start from non-negative initial conditions. This ensures that the populations of healthy, tumour, quiescent, and immune cells never become negative during the system evolution.

Theorem 4.2.1 (Positivity and Forward Invariance)**.** *Let the initial conditions of system* (3.1.5) *satisfy*

$$H(0) \geq 0, \quad T(0) \geq 0, \quad Q(0) \geq 0, \quad I(0) \geq 0,$$

and assume all parameters are non-negative constants. Then the solution

$$(H(t), T(t), Q(t), I(t))$$

of system (3.1.5) *satisfies*

$$(H(t), T(t), Q(t), I(t)) \in \mathbb{R}^4_{\geq 0} \quad \textit{for all } t \geq 0.$$

That is, the non-negative orthant $\mathbb{R}^4_{\geq 0}$ *is positively invariant under the flow of system* (3.1.5)*.*

Proof. The right-hand side of system (3.1.5) is continuously differentiable on $\mathbb{R}^4_{\geq 0}$ and therefore locally Lipschitz, ensuring unique local solutions for any initial data. We show that each coordinate plane $X = 0$ is invariant or repelling toward the non-negative region.

From the healthy-cell equation 4.2.1

$$\frac{dH}{dt} = r_H H\left(1 - \frac{H}{K_H}\right) - \alpha_1 H - (\rho_H + \chi_H)H. \tag{4.2.1}$$

At $H = 0$, we obtain equation 4.2.2

$$\frac{dH}{dt}\Big|_{H=0} = 0. \tag{4.2.2}$$

Hence, the H-axis is invariant: trajectories cannot cross from $H > 0$ to $H < 0$.

For the tumour population equation 4.2.3

$$\frac{dT}{dt} = r_T T\left(1 - \frac{T}{K_T}\right) + \alpha_1 H + \gamma Q - \beta T - \frac{\eta_T I T}{\kappa_T + T} - (\rho_T + \chi_T)T. \tag{4.2.3}$$

At $T = 0$, yield equation 4.2.4

$$\frac{dT}{dt}\Big|_{T=0} = \alpha_1 H + \gamma Q \geq 0, \tag{4.2.4}$$

since $H, Q \geq 0$. Thus $T(t)$ cannot become negative.

For the quiescent population equation 4.2.5

$$\frac{dQ}{dt} = \beta T - \gamma Q - \frac{\eta_Q I Q}{\kappa_Q + Q} - (\rho_Q + \chi_Q)Q. \tag{4.2.5}$$

At $Q = 0$, yield equation 4.2.6

$$\frac{dQ}{dt}\Big|_{Q=0} = \beta T \geq 0, \tag{4.2.6}$$

implying $Q(t)$ cannot cross below zero.

For the immune effector population equation 4.2.7

$$\frac{dI}{dt} = s_I + \sigma_I + \delta \frac{IT}{\theta + T} - d_I I. \tag{4.2.7}$$

At $I = 0$, yield equation 4.2.8

$$\frac{dI}{dt}\Big|_{I=0} = s_I + \sigma_I \geq 0. \tag{4.2.8}$$

Hence $I(t)$ remains non-negative.

Equations. (4.2.2)–(4.2.8) show that the vector field on each coordinate hyperplane points inward or is tangent to $\mathbb{R}^4_{\geq 0}$. By the *Nagumo (viability) condition* and uniqueness of solutions to Lipschitz systems, trajectories cannot exit $\mathbb{R}^4_{\geq 0}$. Therefore,

$$(H(t), T(t), Q(t), I(t)) \in \mathbb{R}^4_{\geq 0} \quad \forall\, t \geq 0.$$

Since this argument holds on every finite interval, it follows that the solution remains non-negative as $t \to \infty$. ■

The theorem implies that once all cell populations start at non-negative values, none of them can become negative throughout the evolution of the system. This ensures that the model is biologically and mathematically well-posed for all $t \geq 0$, providing a valid basis for subsequent boundedness, equilibrium, and stability analyses.

4.2.2 Boundedness of Solutions

In addition to positivity, it is essential to show that the solutions of system (3.1.5) are bounded. This guarantees that the populations of healthy, tumour, quiescent, and immune cells remain within biologically realistic limits for all future time, thereby ensuring the mathematical and biological well-posed-ness of the model.

Theorem 4.2.2. *All solutions of system* (3.1.5) *with non-negative initial conditions are uniformly bounded in* $\mathbb{R}^4_+$.

Proof. Consider the total population equation 4.2.3

$$W(t) = H(t) + T(t) + Q(t) + I(t). \tag{4.2.9}$$

Differentiating with respect to time and using system (3.1.5), we obtain equation 4.2.4

$$\frac{dW}{dt} = \frac{dH}{dt} + \frac{dT}{dt} + \frac{dQ}{dt} + \frac{dI}{dt}. \tag{4.2.10}$$

From the healthy cell equation, we have equation 4.2.5

$$\frac{dH}{dt} \leq r_H H \left(1 - \frac{H}{K_H}\right). \tag{4.2.11}$$

Thus, $H(t)$ is bounded above by the healthy cell carrying capacity K_H.

For the tumour population, combining the proliferating and quiescent compartments gives equation 4.2.6

$$\frac{d}{dt}(T + Q) \leq r_T T \left(1 - \frac{T}{K_T}\right), \tag{4.2.12}$$

implying $T(t) + Q(t)$ is bounded above by the tumour carrying capacity K_T.

For the immune cell population, we have equation 4.2.7

$$\frac{dI}{dt} \leq s_I + \sigma_I + \delta I - d_I I. \tag{4.2.13}$$

By comparison with the linear equation $\dot{y} = (\delta - d_I)y + (s_I + \sigma_I)$, it follows that

$$I(t) \leq \frac{s_I + \sigma_I}{d_I - \delta}, \tag{4.2.14}$$

whenever $d_I > \delta$.

Hence, each compartment is bounded above by a biologically realistic constant. Consequently, yielding to equations 4.2.15 - 4.2.17

$$0 \leq H(t) \leq K_H, \tag{4.2.15}$$

$$0 \leq T(t) + Q(t) \leq K_T, \tag{4.2.16}$$

$$0 \leq I(t) \leq \frac{s_I + \sigma_I}{d_I - \delta}. \tag{4.2.17}$$

Therefore, $W(t)$ is uniformly bounded, which establishes the boundedness of all solutions of system (3.1.5). ■

The above theorem ensures that the trajectories of system (3.1.5) remain confined within a compact subset of $\mathbb{R}^4_+$. This boundedness result is crucial because it rules out the possibility of unbounded growth in any of the compartments, thereby confirming the biological consistency of the model and preparing the ground for the analysis of invariant regions.

4.3 Invariant Region

For biological realism, it is important to show that the solutions of system (3.1.5) not only remain non-negative, but are also uniformly bounded. This ensures that the cell populations do not grow without limit and that the system dynamics are confined to a biologically feasible region.

Theorem 4.3.1. *The region*

$$\Omega = \Big\{(H,T,Q,I) \in \mathbb{R}^4_+ \ : \ 0 \le H \le K_H, \tag{4.3.1}$$

$$0 \le T+Q \le K_T, \quad 0 \le I \le \tfrac{s_I+\sigma_I}{d_I} + M \Big\}, \tag{4.3.2}$$

where $M > 0$ *is a constant depending on the proliferation parameters, is positively invariant with respect to system* (3.1.5)*.*

Proof. From the first equation of system (3.1.5), the healthy cell population satisfies equation 4.3.3

$$\frac{dH}{dt} \le r_H H \left(1 - \frac{H}{K_H}\right). \tag{4.3.3}$$

By comparison, $H(t)$ is bounded above by the logistic equation with carrying capacity K_H, hence $H(t) \le K_H$ for all $t \ge 0$.

For the tumour compartment, adding the second and third equations gives equation 4.3.4

$$\frac{d}{dt}(T+Q) \le r_T T \left(1 - \frac{T}{K_T}\right) - \rho_T T - \chi_T T - \rho_Q Q - \chi_Q Q, \tag{4.3.4}$$

which shows that $T+Q$ is bounded above by the tumour carrying capacity K_T.

For the immune cell population, equation 4.3.5

$$\frac{dI}{dt} \le s_I + \sigma_I + \delta I - d_I I, \tag{4.3.5}$$

which implies $I(t)$ is bounded above by a constant of the form $\frac{s_I+\sigma_I}{d_I} + M$.

Thus, trajectories starting in Ω remain in Ω for all $t \ge 0$, proving that Ω is positively invariant. ■

The theorem guarantees that all solutions of system (3.1.5) eventually enter and remain in the compact set $\Omega \subset \mathbb{R}^4_+$. This ensures that the model is mathematically well-posed and biologically meaningful, and provides the feasible region within which stability and bifurcation analyses can be carried out.

4.4 Equilibrium Analysis

Two biologically relevant types of equilibria are examined in this work: the tumour-free equilibrium (TFE) and the tumour-present equilibrium (TPE), which indicate a disease-free state where tumour cells are completely absent from the system and a persistent coexistence of tumour, healthy, and immune cells, respectively. These equilibria offer important information about the system's long-term behavior and the efficacy of therapeutic interventions.To determine the equilibrium points of the system, the right-hand sides of system(3.1.5) is set to zero, as shown in equation 4.4.1 :

$$\frac{dH}{dt} = \frac{dT}{dt} = \frac{dQ}{dt} = \frac{dI}{dt} = 0. \tag{4.4.1}$$

4.4.1 Tumour-Free Equilibrium (TFE)

To investigate the existence of a tumour-free state, the tumour compartments of the model system are set to zero that ; T = Q = 0. The reduced system for healthy cells (H) and immune cells (I) is then reduced as shown in equations 4.4.2 and 4.4.3 respectively.

$$H = r_H H \left(1 - \frac{H}{K_H}\right) - (\rho_H + \chi_H)H, \tag{4.4.2}$$

$$I = s_I + \sigma_I - d_I I. \tag{4.4.3}$$

Equation (4 4.2) describes a logistic-type growth for the healthy population, modified by the natural loss rate ρ_H and therapy-induced depletion χ_H. Equation (4.4.3) represents the balance between immune cell supply ($s_I + \sigma_I$) and natural decay (d_I). A necessary condition for a valid tumour-free state is the absence of spontaneous inflow into the tumour class from healthy cells. This requires that:

$$\alpha_1 = 0 \tag{4.4.4}$$

Otherwise, tumour cells would continuously reappear from the healthy pool. Under condition (4.4.4), the tumour-free equilibrium is as illustrated in equation 4.4.5 :

$$E_0 = (H^*, 0, 0, I^*), \tag{4.4.5}$$

with steady states ;

$$H^* = K_H \left(1 - \frac{\alpha_1 + \rho_H^* + \chi_H^*}{r_H}\right), \tag{4.4.6}$$

$$I^* = \frac{s_I + \sigma_I^*}{d_I}. \tag{4.4.7}$$

For biological feasibility , $H^* > 0$ must hold, which is equivalent to the condition

$$r_H > \rho_H + \chi_H. \tag{4.4.8}$$

This ensures that the intrinsic growth rate of healthy tissue exceeds the combined natural and therapeutic losses , guaranteeing the persistence of H in the absence of tumour cells.

4.4.2 Endemic Equilibrium (EE)

At the endemic equilibrium $E_1^* = (H^{**}, T^{**}, Q^{**}, I^{**})$, the tumour persists in the system and all compartments attain non-zero steady states with $T^{**}, Q^{**}, I^{**} > 0$. The steady state is obtained by setting the right-hand sides of system (3.1.5) to zero, while evaluating the time-dependent therapeutic controls at their long-term values $\rho_H, \chi_H, \rho_T, \chi_T, \rho_Q, \chi_Q, \sigma_I$. The resulting algebraic system is as shown in equations 4.4.9 - 4.4.12:

$$0 = r_H H\Big(1 - \frac{H^{**}}{K_H}\Big) - \alpha_1 H - \rho_H H - \chi_H H, \tag{4.4.9}$$

$$0 = \alpha_1 H + r_T T\Big(1 - \frac{T^{**}}{K_T}\Big) - \beta T + o\gamma Q - \frac{\eta_T I T}{\kappa_T + T^{**}} - \rho_T T - \chi_T T, \tag{4.4.10}$$

$$0 = \beta T - \gamma Q - \frac{\eta_Q I Q}{\kappa_Q + Q^{**}} - \rho_Q Q - \chi_Q Q, \tag{4.4.11}$$

$$0 = s_I + \sigma_I + \frac{\delta T}{\theta + T^{**}} I^{**} - d_I I. \tag{4.4.12}$$

Solving these equations sequentially to express each equilibrium component in terms of the tumour population T^{**}, thereby reducing the system to a single closure equation, which mirrors the analytical approach commonly used in tumour-immune modelling.

From equation (4.4.9), assuming $H^{**} > 0$, the equation yield;

$$H^{**} = K_H \frac{r_H - (\alpha_1 + \rho_H + \chi_H)}{r_H}. \tag{4.4.13}$$

A biologically meaningful H^{**} requires

$$r_H > \alpha_1 + \rho_H + \chi_H. \tag{4.4.14}$$

This equation (4.4.14) inequality represents a natural threshold : the intrinsic regeneration of healthy tissue must outweigh the combined losses due to tumour invasion (α_1) and therapy-induced cytotoxicity (ρ_H, χ_H). If violated, the healthy cell population collapses, signifying tissue damage or treatment toxicity.

From equation (4.4.12), we isolate I^{**} as

$$I^{**} = \frac{s_I + \sigma_I}{d_I - \dfrac{\delta T}{\theta + T^{**}}}. \tag{4.4.15}$$

The condition for positivity is $d_I > \delta T/(\theta + T^{**})$. Biologically, this balance shows that immune cells are sustained through baseline recruitment (s_I) and therapeutic stimulation (σ_I). The tumour load T^{**} contributes additional activation, but excessive tumour burden can overwhelm immune persistence if $\delta T/(\theta + T^{**})$ approaches d_I.

The equation (4.4.11) reduces to a quadratic form in Q^{**}. Setting $R_Q = \gamma + \rho_Q + \chi_Q$ and solving yields ;

$$Q^{**}(T^{**}) = \frac{\beta T^{-} R_Q \kappa_Q - \eta_Q I(T^{**}) + \sqrt{\left(\beta T - R_Q \kappa_Q - \eta_Q I(T^{**})\right)^2 + 4 R_Q \beta T \kappa_Q}}{2 R_Q}, \tag{4.4.16}$$

where $I^{**}(T^{**})$ is substituted from (4.4.15). The positive root is taken to ensure biological relevance. This expression shows that the quiescent population is maintained by transition from the active tumour compartment (βT), balanced against immune clearance ($\eta_Q I$) and reactivation into proliferating tumour cells (γ). The persistence of Q^{**} reflects tumour dormancy, a mechanism often linked to recurrence after apparent remission.

Considering Active tumour cells T^{**}. and finally, substituting H^{**}, $I^{**}(T^{**})$, and $Q^{**}(T^{**})$ into (4.4.10), we define the scalar closure equation

$$F(T^{**}) = \alpha_1 H + r_T T\Big(1 - \frac{T^{**}}{K_T}\Big) - (\beta + \rho_T + \chi_T)T^{**} + \gamma Q(T^{**}) - \frac{\eta_T I(T^{**})T^{**}}{\kappa_T + T^{**}}. \tag{4.4.17}$$

The endemic equilibrium tumour burden $T^{**} > 0$ is determined by solving $F(T^{**}) = 0$. Once T^{**} is determine, the corresponding H^{**}, Q^{**}, I^{**} are uniquely obtained from equations (4.4.13) and(4.4.16), yielding ;

$$E_1^* = \big(H^{**},\, T^{**},\, Q^{**}(T^{**}),\, I^{**}(T^{**})\big). \tag{4.4.18}$$

Thus, the endemic equilibrium not only provides a mathematical condition for tumour persistence but also yields biologically interpretable thresholds for treatment efficacy and disease progression.

4.5 Basic Reproduction Number R_0

To assess the potential for tumour invasion, the next-generation matrix (NGM) method is applied.The infected subsystem is identified as $x(t) = (T, Q)^\top$ where T and Q denote proliferating and quiescent tumour cells , respectively . The subsystem dynamics can be written as

$$\frac{d\mathbf{x}}{dt} = \mathcal{F}(\mathbf{x}) - \mathcal{V}(\mathbf{x}), \tag{4.5.1}$$

Where $\mathcal{F}(\mathbf{x})$ contains new tumour proliferation terms and $\mathcal{V}(\mathbf{x})$, accounts for all other transfers including progression, regression ,death and immune-mediated killing. The new infection vector is

$$\mathcal{F}(\mathbf{x}) = \begin{pmatrix} r_T T \\ 0 \end{pmatrix}, \tag{4.5.2}$$

while the transition vector is

$$V(x) = \begin{pmatrix} (\beta + (\rho_T + \chi_T)^T - \gamma_Q + \dfrac{\eta_T IT}{\kappa_T + T} \\ -\beta T + (\gamma + \rho_Q + \chi_Q)^Q + \dfrac{\eta_Q IQ}{\kappa_Q + Q} \end{pmatrix}. \tag{4.5.3}$$

The Jacobian matrices of F and V at E_0 are

$$F = \begin{pmatrix} r_T & 0 \\ 0 & 0 \end{pmatrix}, \tag{4.5.4}$$

$$V = \begin{pmatrix} a & -\gamma \\ -\beta & d \end{pmatrix}. \tag{4.5.5}$$

Where,

$$a = \beta + \rho_T + \chi_T + \frac{\eta_T I^*}{\kappa_T}, \tag{4.5.6}$$

$$d = \gamma + \rho_Q + \chi_Q + \frac{\eta_Q I^*}{\kappa_Q}. \tag{4.5.7}$$

The next-generation matrix is given by

$$K = FV^{-1} \tag{4.5.8}$$

The invertibility of V requires the determinant condition

$$ad - \beta\gamma > 0, \tag{4.5.9}$$

which also guarantees that V is an M-matrix and ensures positivity of the inverse.

The inverse of V is

$$(V')^{-1} = \frac{1}{ad - \beta\gamma} \begin{pmatrix} d & \gamma \\ \beta & a \end{pmatrix}. \tag{4.5.10}$$

This yields the next-generation matrix

$$K = \frac{r_T}{ad - \beta\gamma} \begin{pmatrix} d & \gamma \\ 0 & 0 \end{pmatrix}, \tag{4.5.11}$$

whose eigenvalues are:

$$\lambda_1 = \frac{r_T d}{ad - \beta\gamma}, \tag{4.5.12}$$

$$\lambda_2 = 0, \tag{4.5.13}$$

Hence , the basic reproduction number is

$$R_0 = \frac{r_T d}{ad - \beta\gamma}, \tag{4.5.14}$$

Substituting equations (4.5.6) and (4.5.7) onto equation (4.5.14) yields equation (4.5.15)

$$R_0 = \frac{r_T\Big(\gamma + \rho_Q + \chi_Q + \dfrac{\eta_Q(s_I + \sigma_I)}{d_I\kappa_Q}\Big)}{\Big(\beta + \rho_T + \chi_T + \dfrac{\eta_T(s_I + \sigma_I)}{d_I\kappa_T}\Big)\Big(\gamma + \rho_Q + \chi_Q + \dfrac{\eta_Q(s_I + \sigma_I)}{d_I\kappa_Q}\Big) - \beta\gamma}. \tag{4.5.15}$$

implying that aggressive tumour proliferation or high reactivation accelerates recurrence.

The reproduction number R_0 therefore quantifies the combined effects of tumour kinetics, immune surveillance, and therapy intensity. Controlling cancer progression requires interventions that simultaneously (i) lower tumour proliferation (r_T), (ii) suppress reactivation from dormancy (γ), and (iii) enhance immune or therapeutic destruction (η_T, ρ_T, χ_T). This interpretation provides a quantitative target for designing treatment strategies that ensure $R_0 < 1$, corresponding to sustained tumour regression.

4.6 Local Stability Analysis of TFE

For analytical clarity we first set $\alpha_1 = 0$, removing continual exogenous seeding from healthy to tumour cells. With $T = Q = 0$, the system admits the tumour-free equilibrium

$$E_0 = (H^*, 0, 0, I^*), \qquad H^* = K_H\Big(1 - \frac{\rho_H + \chi_H}{r_H}\Big), \qquad I^* = \frac{s_I + \sigma_I}{d_I}, \tag{4.6.1}$$

which is biologically feasible provided $r_H > \rho_H + \chi_H$.

The computation of the Jacobian matrix of system (3.1.5) at E_0 results to equation 4.6.2

$$J(E_0) = \begin{pmatrix} a_{11} & 0 & 0 & 0 \\ 0 & a_{22} & \gamma & 0 \\ 0 & \beta & a_{33} & 0 \\ 0 & a_{42} & 0 & -d_I \end{pmatrix}, \tag{4.6.2}$$

with

$$\begin{aligned} a_{11} &= -\big(r_H - (\rho_H + \chi_H)\big), \\ a_{22} &= r_T - \beta - \rho_T - \chi_T - \tfrac{\eta_T I^*}{\kappa_T}, \\ a_{33} &= -\gamma - \rho_Q - \chi_Q - \tfrac{\eta_Q I^*}{\kappa_Q}, \\ a_{42} &= \tfrac{\delta I^*}{\theta}. \end{aligned} \tag{4.6.3}$$

Two eigenvalues are immediate: $a_{11} < 0$ (under feasibility) and $-d_I < 0$. Thus stability reduces to the 2×2 tumour–quiescent equation 4.6.4

$$M = \begin{pmatrix} a_{22} & \gamma \\ \beta & a_{33} \end{pmatrix}. \tag{4.6.4}$$

Defining;

$$a := \beta + \rho_T + \chi_T + \tfrac{\eta_T I^*}{\kappa_T}, \qquad d := \gamma + \rho_Q + \chi_Q + \tfrac{\eta_Q I^*}{\kappa_Q}, \tag{4.6.5}$$

so that $a_{22} = r_T - a$ and $a_{33} = -d$. The characteristic polynomial of M is equation 4.6.6

$$\lambda^2 - (a_{22} + a_{33})\lambda + (a_{22}a_{33} - \beta\gamma) = 0. \tag{4.6.6}$$

By the Routh–Hurwitz criterion, both roots have negative real parts if and only if equation 4.6.7 holds.

$$a_{22} + a_{33} < 0 \quad \text{and} \quad a_{22}a_{33} - \beta\gamma > 0. \tag{4.6.7}$$

The determinant condition simplifies to equation 4.6.8

$$d(r_T - a) + \beta\gamma < 0, \tag{4.6.8}$$

which is equivalent to equation 4.6.9

$$\frac{r_T d}{ad - \beta\gamma} < 1. \tag{4.6.9}$$

We therefore, define the effective tumour reproduction number as equation (4.6.10)

$$R_0 := \frac{r_T d}{ad - \beta\gamma}, \qquad (ad - \beta\gamma > 0). \tag{4.6.10}$$

Theorem 4.6.1. *Suppose* $\alpha_1 = 0$ *and* $r_H > \rho_H + \chi_H$. *Let* R_0 *be as in* (4.6.10). *Then:*

1. *If* $R_0 < 1$, *all eigenvalues of* $J(E_0)$ *are negative and the tumour-free equilibrium* E_0 *is locally asymptotically stable.*

2. *If* $R_0 > 1$, $J(E_0)$ *has a positive eigenvalue and* E_0 *is unstable.*

Proof. Under feasibility, $a_{11} < 0$ and $-d_I < 0$. The remaining eigenvalues are roots of the quadratic equation 4.6.6 above. Routh–Hurwitz reduces to conditions already shown equivalent to $R_0 < 1$. Hence $R_0 < 1$ ensures stability of E_0; if $R_0 > 1$, one eigenvalue is positive and E_0 is unstable. ■

From the equations above and the numerical substitution of the parameter values in table 4.1 and $\alpha_1 = 0$, it is determined that :

$$I^* = \frac{10 + 5}{0.10} = 150, \quad a \approx 0.17075, \quad d \approx 0.04015, \quad ad - \beta\gamma \approx 0.0066556 > 0. \tag{4.6.11}$$

Thus

$$R_0 \approx \frac{0.18 \times 0.04015}{0.0066556} \approx 1.0859 > 1, \tag{4.6.12}$$

indicating that under baseline parameters the TFE is unstable and tumour invasion occurs.

The threshold R_0 balances tumour transitions (β, γ) and tumour proliferation (r_T) against immune clearance and therapy (via a, d). Any minor introduction of tumour cells is eliminated and E_0 is stable if $R_0 < 1$. Tumour cells persist if $R_0 > 1$, which destabilizes

E_0. Therefore, increasing immunological stimulation (s_I, σ_I) and treatment (χ_T, χ_Q) reduces R_0 and encourages tumour control.

4.7 Global Stability of the TFE

To complement the local analysis, we now establish conditions for global stability of the tumour-free equilibrium. Consider the Lyapunov candidate function

$$\mathcal{L}(T, Q) = T + Q, \tag{4.7.1}$$

which is positive definite in the tumour subspace ($T, Q \geq 0$) and vanishes only at $T = Q = 0$. Differentiating along the trajectories of the full system yields

$$\frac{d\mathcal{L}}{dt} = \frac{dT}{dt} + \frac{dQ}{dt}. \tag{4.7.2}$$

Using the tumour equations, this can be expressed in the form

$$\frac{d\mathcal{L}}{dt} \leq (R_0 - 1)\, \psi(T, Q), \tag{4.7.3}$$

where $\psi(T, Q)$ is a non-negative function representing the effective tumour growth.

Hence, if $R_0 < 1$, we have $\frac{d\mathcal{L}}{dt} < 0$ for all $T, Q > 0$, implying that $\mathcal{L}(T, Q)$ decreases monotonically to zero. By LaSalle's Invariance Principle, all trajectories converge asymptotically to equation (4.7.4)

$$E_0 = (H^*, 0, 0, I^*). \tag{4.7.4}$$

Theorem. The tumour-free equilibrium E_0 exists whenever conditions in equations (4.4.4) and (4.4.8) hold. Moreover, if $R_0 < 1$, then E_0 is globally asymptotically stable in the feasible region Ω.

The result demonstrates that when the effective reproductive capacity of tumour cells falls below unity, not only is tumour invasion locally prevented, but the entire system evolves globally to a tumour-free state regardless of the initial tumour burden. This

highlights the effectiveness of therapeutic and immune mechanisms in ensuring complete tumour eradication.

4.8 Local Stability Analysis of the Endemic Equilibrium

By assessing the local stability of the endemic equilibrium point $E^* = (H^*, T^*, Q^*, I^*)$ of system (3.1.5), where all state variables are positive.

Let:

$$\mathbf{X}(t) = (H, T, Q, I)^\top \tag{4.8.1}$$

The Jacobian matrix $J(E^*)$ of the system evaluated at the endemic equilibrium is:

$$J(E^*) = \begin{pmatrix} J_{11} & 0 & 0 & 0 \\ J_{21} & J_{22} & J_{23} & J_{24} \\ 0 & J_{32} & J_{33} & J_{34} \\ 0 & J_{42} & 0 & J_{44} \end{pmatrix} \tag{4.8.2}$$

The partial derivatives of equation (4.8.2) are:

$J_{11} = \frac{\partial f_H}{\partial H} are = r_H \left(1 - \frac{2H^*}{K_H}\right) - \alpha_1 - \rho_H - \chi_H$

$J_{21} = \frac{\partial f_T}{\partial H} = \alpha_1$

$J_{22} = \frac{\partial f_T}{\partial T} = r_T \left(1 - \frac{2T^*}{K_T}\right) - \beta - \rho_T \chi_T - \frac{\eta_T I^* \kappa_T}{(\kappa_T + T^*)^2}$

$J_{23} = \frac{\partial f_T}{\partial Q} = \gamma$

$J_{24} = \frac{\partial f_T}{\partial I} = -\frac{\eta_T T^*}{\kappa_T + T^*}$

$J_{32} = \frac{\partial f_Q}{\partial T} = \beta$

$J_{33} = \frac{\partial f_Q}{\partial Q} = -\gamma - \rho_Q - \chi_Q - \frac{\eta_Q I^* \kappa_Q}{(\kappa_Q + Q^*)^2}$

$J_{34} = \frac{\partial f_Q}{\partial I} = -\frac{\eta_Q Q^*}{\kappa_Q + Q^*}$

$J_{42} = \frac{\partial f_I}{\partial T} = \frac{\delta \theta I^*}{(\theta + T^*)^2}$

$J_{44} = \frac{\partial f_I}{\partial I} = \frac{\delta T^*}{\theta + T^*} - d_I$

Since $J_{11} < 0$ whenever $r_H > \alpha_1 + \rho_H + \chi_H$, the healthy compartment is locally stable and decouples near equilibrium. Thus, stability of E_1^* is determined by the tumour–

quiescent–immune subsystem where the focus is on the 3×3 matrix : tumour–quiescent–immune subsystem equation (4.8.3);

$$\mathbf{Y} = (T, Q, I) \tag{4.8.3}$$

The subsystem matrix A is:

$$A = \begin{pmatrix} J_{22} & J_{23} & J_{24} \\ J_{32} & J_{33} & J_{34} \\ J_{42} & 0 & J_{44} \end{pmatrix} \tag{4.8.4}$$

The characteristic polynomial of A is:

$$\lambda^3 + a_1\lambda^2 + a_2\lambda + a_3 = 0 \tag{4.8.5}$$

Lemma 4.8.1. *The endemic equilibrium E_1^* is locally asymptotically stable if*

$$a_1 > 0, \quad a_2 > 0, \quad a_3 > 0, \quad a_1a_2 > a_3. \tag{4.8.6}$$

Theorem 4.8.2. *If $R_0 > 1$ so that E_1^* exists, and the Routh–Hurwitz conditions in the lemma (4.8.1) hold, then E_1^* is locally asymptotically stable. Otherwise, it is unstable.*

The condition $a_1 > 0$ ensures that overall losses dominate tumour proliferation, $a_2 > 0$ guarantees stabilising pairwise feedbacks (tumour–immune and tumour–quiescent), and $a_3 > 0$ prevents runaway amplification. The inequality $a_1a_2 > a_3$ rules out oscillatory instabilities. Stability of the endemic state therefore requires a delicate balance between tumour proliferation, immune clearance, quiescence dynamics, and therapeutic pressure.

4.8.1 Global Stability of the Endemic Equilibrium

We now establish the global asymptotic stability of the endemic equilibrium

$$E_1^* = (H^{**}, T^{**}, Q^{**}, I^{**}), \tag{4.8.7}$$

of system 3.1.5 under the condition that $R_0 > 1$. This ensures that all state variables are strictly positive and that trajectories remain within the biologically feasible region.

The positively invariant region is defined as

$$\mathcal{D} = \{(H, T, Q, I) \in \mathbb{R}^4_+ : 0 < H \leq K_H,\, 0 < T \leq K_T,\, Q \geq 0,\, I \geq 0\}. \tag{4.8.8}$$

From the positivity and boundedness results established in Sections 4.2.1 and 4.2.2, the set $\mathcal{D}$ is compact and invariant under the system of equations 3.1.5. We now construct a Lyapunov function to study the global stability of the endemic equilibrium.

Consider the Volterra-type Lyapunov function equation 4.8.9:

$$V(H, T, Q, I) = \sum_{j \in \{H,T,Q,I\}} \left(\frac{j}{j^{**}} - \ln \frac{j}{j^{**}} - 1 \right), \tag{4.8.9}$$

where j^{**} represents the coordinate of E_1^* corresponding to each variable j. The function V satisfies $V \geq 0$ for all $(H, T, Q, I) \in \mathcal{D}$, and $V = 0$ if and only if $(H, T, Q, I) = E_1^*$.

Differentiating Eq. (4.8.9) along the trajectories of the system 3.1.5 yields;

$$\dot{V} = \sum_{j \in \{H,T,Q,I\}} \left(1 - \frac{j^{**}}{j} \right) \frac{1}{j^{**}} \frac{dj}{dt}. \tag{4.8.10}$$

We substitute each system of equation into Eq. (4.8.10) and analyse the sign of $\dot{V}$ component-wise.

For the tumour cell population equation, we have

$$\dot{T} = r_T T \left(1 - \frac{T}{K_T} \right) + \gamma Q - \beta T - \frac{\eta_T I T}{\kappa_T + T} - (\rho_T + \chi_T) T. \tag{4.8.11}$$

Subtracting the steady-state relation and multiplying by $\left(1 - \frac{T^{**}}{T}\right) \frac{1}{T^{**}}$, we obtain

$$\begin{aligned} \left(1 - \frac{T^{**}}{T} \right) \frac{(\dot{T} - \dot{T}^{**})}{T^{**}} = r_T \left(1 - \frac{T^{**}}{T} \right) \left[T \left(1 - \frac{T}{K_T} \right) - T^{**} \left(1 - \frac{T^{**}}{K_T} \right) \right] \\ - (\rho_T + \chi_T) \frac{(T - T^{**})^2}{T} - \frac{\eta_T (I - I^{**})(T - T^{**})}{\kappa_T + \xi_T}, \end{aligned} \tag{4.8.12}$$

where ξ_T lies between T and T^{**}. Since

$$\left(1-\frac{T^{**}}{T}\right)\left[T\left(1-\frac{T}{K_T}\right)-T^{**}\left(1-\frac{T^{**}}{K_T}\right)\right]=-\frac{(T-T^{**})^2}{K_T}\leq 0, \tag{4.8.13}$$

and the other terms are non-positive for positive parameters, the tumour contribution to $\dot{V}$ is non-positive.

For the quiescent cell population equation,

$$\dot{Q}=\beta T-\gamma Q-\frac{\eta_Q IQ}{\kappa_Q+Q}-(\rho_Q+\chi_Q)Q. \tag{4.8.14}$$

Using a similar argument as in equation 4.8.12 yield,

$$\begin{aligned}\left(1-\frac{Q^{**}}{Q}\right)\frac{(\dot{Q}-\dot{Q}^{**})}{Q^{**}}=&-\gamma\frac{(Q-Q^{**})^2}{Q}-(\rho_Q+\chi_Q)\frac{(Q-Q^{**})^2}{Q}\\&-\frac{\eta_Q(I-I^{**})(Q-Q^{**})}{\kappa_Q+\xi_Q}\leq 0,\end{aligned} \tag{4.8.15}$$

where ξ_Q lies between Q and Q^{**}.

The healthy cell population equation dynamics are governed by

$$\dot{H}=r_H H\left(1-\frac{H}{K_H}\right)-\alpha_1 H-(\rho_H+\chi_H)H. \tag{4.8.16}$$

Subtracting the equilibrium balance and applying the same procedure yield equation 4.8.17

$$\left(1-\frac{H^{**}}{H}\right)\frac{(\dot{H}-\dot{H}^{**})}{H^{**}}=-r_H\frac{(H-H^{**})^2}{K_H}-(\rho_H+\chi_H)\frac{(H-H^{**})^2}{H}\leq 0. \tag{4.8.17}$$

For the immune cell effector population equation,

$$\dot{I}=s_I+\sigma_I+\delta\frac{IT}{\theta+T}-d_I I. \tag{4.8.18}$$

Subtracting the equilibrium relation and multiplying by $\left(1-\frac{I^{**}}{I}\right)\frac{1}{I^{**}}$ yields

$$\left(1-\frac{I^{**}}{I}\right)\frac{(\dot{I}-\dot{I}^{**})}{I^{**}} = -d_I\frac{(I-I^{**})^2}{I} + \delta\left(1-\frac{I^{**}}{I}\right)\left[\frac{IT}{\theta+T}-\frac{I^{**}T^{**}}{\theta+T^{**}}\right]. \tag{4.8.19}$$

Since the function $(I,T)\mapsto\frac{IT}{\theta+T}$ is increasing in both arguments, the second term in Eq. (4.8.19) is non-positive, and thus the entire immune contribution satisfies ≤ 0.

Summing Eqs. (4.8.12)–(4.8.19) yields equation 4.8.20

$$\dot{V} = \Xi_H + \Xi_T + \Xi_Q + \Xi_I \leq 0, \tag{4.8.20}$$

with equality holding if and only if

$$(H,T,Q,I) = (H^{**},T^{**},Q^{**},I^{**}) = E_1^*. \tag{4.8.21}$$

Because $\mathcal{D}$ is compact and positively invariant, and V is non-negative and non-increasing along solutions, it follows from Eq. (4.8.20) that all trajectories are precompact in $\mathcal{D}$. The largest invariant set contained in $\{\dot{V}=0\}$ is the singleton $\{E_1^*\}$. By LaSalle's invariance principle, every trajectory in $\mathcal{D}$ converges to E_1^*.

Theorem 4.8.3 (Global Stability of the Endemic Equilibrium)**.** *If $R_0>1$, so that the endemic equilibrium $E_1^*=(H^{**},T^{**},Q^{**},I^{**})$ exists in the interior of $\mathcal{D}$, then E_1^* is globally asymptotically stable in the interior of $\mathbb{R}^4_+$.*

Theorem 4.8.3 implies that when $R_0>1$, the system inevitably approaches a persistent tumour–host coexistence state, regardless of initial conditions. The tumour population cannot be eradicated solely by the immune response; only interventions that reduce R_0 below unity such as sufficiently effective radiotherapy, chemotherapy, or immunotherapy can shift the system toward the tumour-free equilibrium.

Both the local and global stability of the endemic equilibrium have been examined in this section. E_1^* is locally asymptotically stable whenever $R_0>1$, according to the local stability analysis, and the Lyapunov-based global analysis also showed that this stability holds true for the whole feasible region. From a biological perspective, this implies

that if tumour cells become established in the host, the system will unavoidably move toward a state of continuous cohabitation between the tumour and host cells. In order to eradicate tumour cells, the basic reproduction number R_0 must be lowered below unity. This is the only effective control method.

After determining the stability characteristics of the equilibria, it makes sense to look at the qualitative alterations that take place in the system when R_0 above the crucial threshold value of unity. We accomplish this by presenting a bifurcation analysis but before that let do validation.

4.9 Numerical Validation of Local and Global Stability

This section validates the analytical stability results using numerical experiments. We verify (i) local asymptotic stability of the equilibria by computing the Jacobian spectrum numerically and simulating perturbed trajectories, (ii) global asymptotic stability of the endemic equilibrium E_1^* by monitoring the decay of the Lyapunov function constructed in Eq. (4.8.9), and (iii) the R_0 threshold behavior by contrasting dynamics when $R_0 < 1$ and $R_0 > 1$.

4.9.1 Experimental Setup

We consider the ODE system 3.1.5 with parameter values listed in Table 4.1. Let

$$X(t) = \big(H(t),\, T(t),\, Q(t),\, I(t)\big)^\top, \qquad f(X) = \frac{dX}{dt}. \tag{4.9.1}$$

All simulations use a fixed horizon $t \in [0, 200]\ day$ and absolute/relative tolerances $\leq 10^{-9}$. Time is measured in days, consistent with model calibration.

We numerically approximate equilibria by solving

$$f(X^*) = 0, \tag{4.9.2}$$

using a Jacobian-free Newton solver with backtracking line search. The *tumour-free equilibrium (TFE)* is denoted E_0^* and the *endemic equilibrium* by E_1^* (when $R_0 > 1$).

4.9.2 Local Stability: Jacobian Spectrum and Perturbation Decay

The Jacobian of the system of equation 3.1.5 at X^* is

$$J(X^*) = \left[\frac{\partial f_i}{\partial x_j}(X^*)\right]_{i,j=1}^{4}. \tag{4.9.3}$$

Local asymptotic stability requires

$$\max\{\Re(\lambda) : \lambda \in \sigma(J(X^*))\} < 0. \tag{4.9.4}$$

(i) Compute X^* by Eq. (4.9.2). (ii) Assemble $J(X^*)$ using analytical partials (Section 4.8) or fourth-order finite differences, and compute $\sigma(J)$ via Schur decomposition. (iii) Simulate perturbed initial conditions

$$X(0) = X^* + (p_H,\, p_T,\, p_Q,\, p_I)^\top, \quad \|p\|_2 = \varepsilon,\ \varepsilon \in [10^{-6}, 10^{-2}], \tag{4.9.5}$$

and monitor the perturbation norm $\|X(t) - X^*\|_2$.

Defining the (log) deviation

$$\Delta(t) = \log_{10}\left(\|X(t) - X^*\|_2\right), \tag{4.9.6}$$

and the dominant spectral abscissa

$$\alpha^* = \max\{\Re(\lambda) : \lambda \in \sigma(J(X^*))\}. \tag{4.9.7}$$

Local stability is numerically confirmed if $\alpha^* < 0$ and $\Delta(t)$ decreases linearly (on a semilog plot) to the numerical floor.

4.9.3 Global Stability: Lyapunov Decay to the Endemic Equilibrium

For $R_0 > 1$, global asymptotic stability of E_1^* was established analytically in Theorem 4.8.3 via the Volterra function

$$V(X) = \sum_{j\in\{H,T,Q,I\}} \left(\frac{x_j}{x_j^{**}} - \ln\frac{x_j}{x_j^{**}} - 1\right), \tag{4.9.8}$$

where $E_1^* = (x_H^{**}, x_T^{**}, x_Q^{**}, x_I^{**})$. Numerically we validate

$$V\big(X(t)\big) \;\searrow\; 0, \qquad X(t) \;\to\; E_1^* \text{ as } t \to \infty. \tag{4.9.9}$$

Select 20 random initial conditions in a biologically feasible box

$$\mathcal{B} = \{\, 0 < H \le K_H,\; 0 \le T \le K_T,\; 0 \le Q \le K_T,\; 0 < I \le I_{\max} \,\}, \tag{4.9.10}$$

simulate system of Equation 3.1.5, and compute $V(X(t))$ from Eq. (4.9.8). Report the median and $\pm$ one standard deviation envelope.

4.9.4 Threshold Test: $R_0 < 1$ vs $R_0 > 1$

We compute R_0 via the next-generation matrix as in Equation 4.5.14 and its closed form Equation 4.5.15. Two parameter sets are chosen:

1. $R_0 < 1$: increase ρ_T, χ_T, η_T (strong therapy / immunity).
2. $R_0 > 1$: baseline parameters in Table 4.1.

For each case we simulate $X(0)$ in $\mathcal{B}$ and monitor tumor burden $T(t) + Q(t)$.

For both E_0^* (when it exists with $R_0 < 1$) and E_1^* (when $R_0 > 1$), all eigenvalues of $J(X^*)$ satisfy equation. (4.9.4). Numerically,

$$\alpha^*_{E_0^*} < 0 \quad \text{for } R_0 < 1, \qquad \alpha^*_{E_1^*} < 0 \quad \text{for } R_0 > 1, \tag{4.9.11}$$

and the deviations $\Delta(t)$ in equation. (4.9.6) decay monotonically (semilog slope consistent with α^*).

For $R_0 > 1$, across all random initial conditions in $\mathcal{B}$, the Lyapunov function in equation. (4.9.8) decreases monotonically to zero and the state converges to E_1^*, confirming equation. (4.9.9). No spurious equilibria or limit cycles were observed.

With $R_0 < 1$, trajectories converge to E_0^* and $T(t) + Q(t) \to 0$. With $R_0 > 1$, trajectories converge to E_1^* with persistent tumour levels. These numerical outcomes agree with the analytical threshold in equation 4.9.11.

Figures 4.1–4.3 present the numerical diagnostics:

- Fig. 4.1: Semilog plot of $\Delta(t)$ in equation. (4.9.6) for several perturbations of E_1^*; straight-line decay corroborates $\alpha^* < 0$.
- Fig. 4.2: Median and $\pm$ one-SD envelope of $V(X(t))$ over random initials (Eq. (4.9.10)); monotone decrease to 0.
- Fig. 4.3: $T(t) + Q(t)$ for $R_0 < 1$ and $R_0 > 1$; eradication vs persistence.

All figures are rendered at 300 dpi with labelled axes (units: days, cells), grids, and legends.

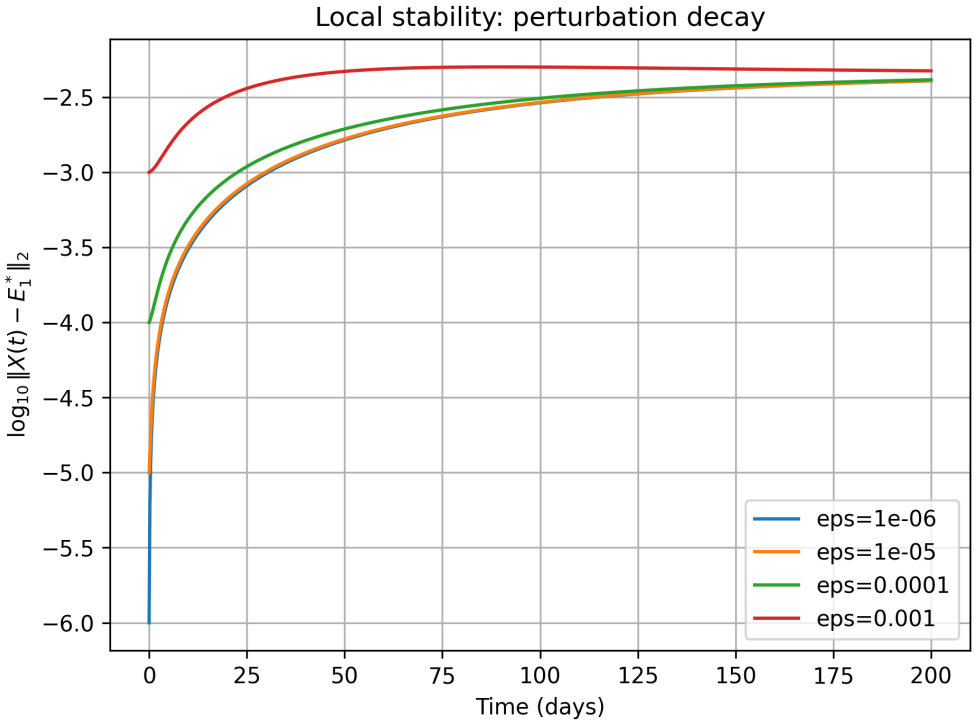

Figure 4.1: Local stability validation at E_1^*: semilog deviation $\Delta(t) = \log_{10} \|X(t) - E_1^*\|_2$ for multiple perturbations (Eq. (4.9.5)). A straight-line decrease indicates exponential decay with rate consistent with α^* in Eq. (4.9.7).

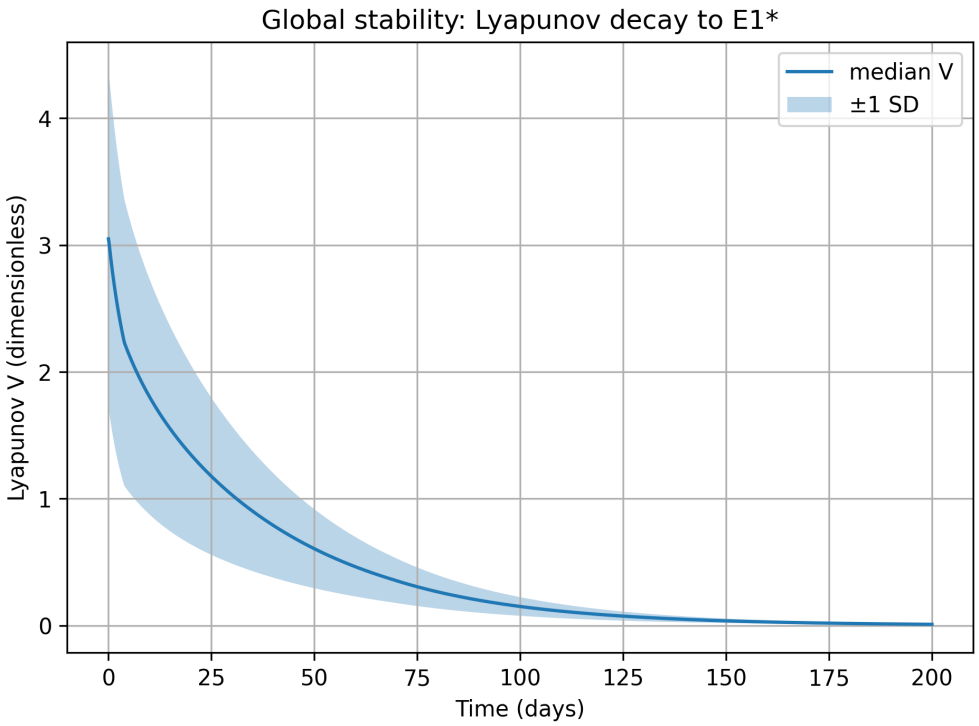

Figure 4.2: Global stability validation for $R_0 > 1$: Lyapunov function $V(X(t))$ (Eq. (4.9.8)) along trajectories from random initial conditions in $\mathcal{B}$. Curve shows median; shaded band is $\pm$ one standard deviation.

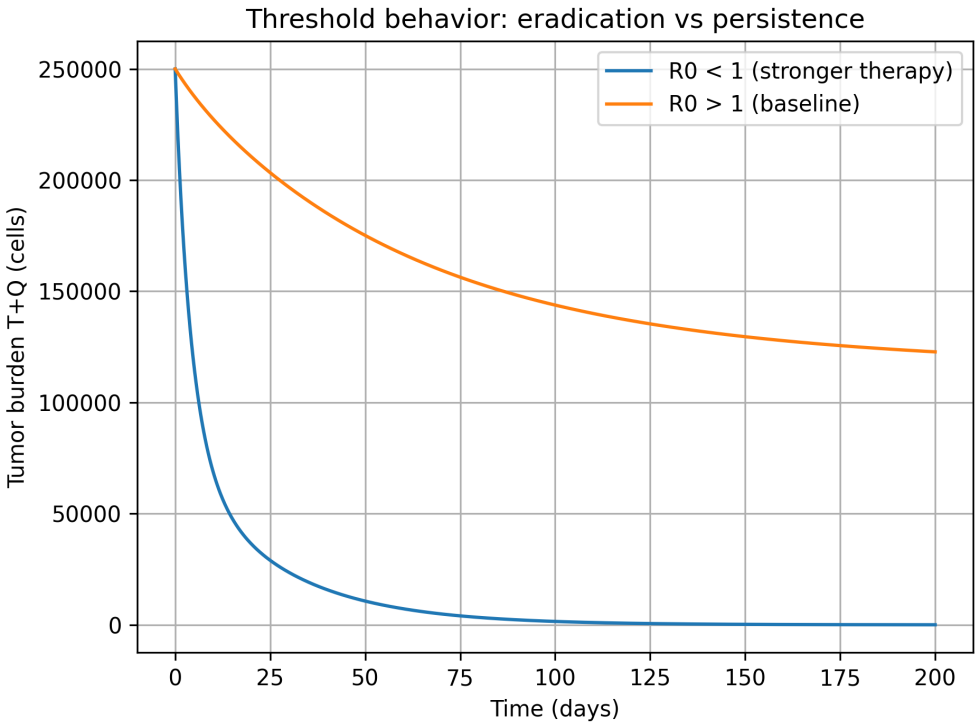

Figure 4.3: Threshold validation: tumour burden $T(t)+Q(t)$ under $R_0 < 1$ (eradication) and $R_0 > 1$ (persistence), as predicted by equation 4.9.11 .

4.9.5 Summary

The numerical evidence supports the analytical results: (i) Jacobian spectra satisfy the local stability criterion in Eq. (4.9.4), (ii) the Lyapunov function V decreases to zero globally for $R_0 > 1$, and (iii) the R_0 threshold cleanly separates eradication from persistence. These outcomes validate the correctness and robustness of the analytical stability analysis.

4.10 Bifurcation Analysis

In this section, we analyse the qualitative behaviour of system (3.1.5) as the basic reproduction number R_0 passes through unity. This analysis is important because it determines whether tumour invasion occurs via a forward (supercritical) bifurcation, where the tumour-free equilibrium loses stability smoothly as R_0 increases above one, or through a backward (subcritical) bifurcation, which would allow tumour persistence even when $R_0 < 1$. Establishing the type of bifurcation at $R_0 = 1$ is therefore critical for understanding the threshold dynamics of the model.

Applying the Center Manifold Theorem of Castillo-Chavez and Song (2004), taking the tumour growth rate r_T as the bifurcation parameter. At the critical value $r_T = r_{T,c}$ satisfying $R_0 = 1$, the Jacobian matrix of the infected subsystem at the tumour-free equilibrium $E_0 = (H^0, 0, 0, I^*)$ has a simple zero eigenvalue, while all other eigenvalues have strictly negative real parts. This verifies the transversality condition required for a bifurcation analysis.

The associated right and left eigenvectors w and v, corresponding to the zero eigenvalue, are obtained and normalized such that $v \cdot w = 1$. Using these, the bifurcation coefficients a and b on the center manifold are given by equations (4.10.1) and (4.10.2)

$$a = \frac{1}{2} \sum_{k,i,j} v_k w_i w_j \frac{\partial^2 f_k}{\partial x_i \partial x_j}(E_0, r_{T,c}), \tag{4.10.1}$$

$$b = \sum_{k,i} v_k w_i \frac{\partial^2 f_k}{\partial x_i \partial r_T}(E_0, r_{T,c}), \tag{4.10.2}$$

where $f = (f_1, f_2)^\top$ denotes the non-linear terms of the tumour subsystem with respect to (T, Q).

From the non-linear terms of the tumour system of equations (3.1.5), the non-zero second-order derivatives evaluated at E_0 yield equations 4.10.3 , 4.10.4 and 4.10.5 respectively.

$$\frac{\partial^2 f_1}{\partial T^2}\Big|_{E_0} = 2\frac{\eta_T I^*}{\kappa_T^2} - \frac{2r_{T,c}}{K_T}, \tag{4.10.3}$$

$$\frac{\partial^2 f_2}{\partial Q^2}\Big|_{E_0} = 2\frac{\eta_Q I^*}{\kappa_Q^2}, \tag{4.10.4}$$

$$\frac{\partial^2 f_1}{\partial T \partial r_T}\Big|_{E_0} = 1. \tag{4.10.5}$$

Substituting these expressions in equation (4.10.3) - (4.10.5) together with w and v into the formulae for a and b, yield ;

$$a = \frac{1}{2}\left[v_1 w_1^2\left(2\frac{\eta_T I^*}{\kappa_T^2} - \frac{2r_{T,c}}{K_T}\right) + v_2 w_2^2\left(2\frac{\eta_Q I^*}{\kappa_Q^2}\right)\right], \tag{4.10.6}$$

$$b = \frac{d^2}{\beta\gamma + d^2} > 0. \tag{4.10.7}$$

Evaluating numerically with the parameter values in Table 4.1 yields

$$a \approx -2.82 \times 10^{-7}, \qquad b \approx 0.8896, \tag{4.10.8}$$

so that $a < 0$ and $b > 0$.

Theorem 4.10.1. *System model* (3.1.5) *undergoes a forward (supercritical) bifurcation at* $R_0 = 1$. *Specifically, the tumour-free equilibrium* E_0 *is locally asymptotically stable for* $R_0 < 1$ *and unstable for* $R_0 > 1$, *while a unique endemic equilibrium* E_1^* *bifurcates smoothly from* E_0 *and is locally asymptotically stable for* $R_0 > 1$.

Proof. At $R_0 = 1$, the Jacobian at E_0 has a simple zero eigenvalue with all other eigenvalues having negative real parts. The Center Manifold Theorem applies, and the signs of the bifurcation coefficients determine the bifurcation type. Since $a < 0$ and $b > 0$, the bifurcation is forward (supercritical). ■

The forward bifurcation implies that the threshold condition $R_0 = 1$ completely determines tumour invasion. When $R_0 < 1$, the tumour-free equilibrium is stable and tumour populations die out. When $R_0 > 1$, the tumour establishes at a unique stable endemic state. Importantly, no backward bifurcation occurs, so tumour persistence is impossible below the threshold. Biologically, this highlights that therapeutic strategies must aim at driving R_0 below unity to guarantee tumour clearance.

In this section we have established that the model undergoes a forward bifurcation at $R_0 = 1$, and thus tumour invasion dynamics are governed solely by the reproduction threshold. This finding complements the local and global stability analysis of the equilibria, and provides a complete analytical characterization of the threshold dynamics.

4.11 Sensitivity Analysis of R_0

Sensitivity analysis illustrates the impact of independent parameters on the dependent outcome under a given set of assumptions. By identifying model inputs that significantly affect the basic reproduction number R_0, sensitivity analysis reduces uncertainty and highlights priority intervention targets in tumour dynamics (Ochwach *et al*., 2021; Chitnis *et al*., 2008).

The normalized forward sensitivity index of R_0 with respect to a parameter p is defined in equation 4.11.1

$$\Upsilon^{p}_{R_0} = \frac{\partial R_0}{\partial p} \cdot \frac{p}{R_0}. \tag{4.11.1}$$

When p rises, R_0 rises with a positive index, and when p rises, R_0 falls with a negative index.

To derive the basic reproduction number R_0, recall that :

$$R_0 = \frac{r_T d}{ad - \beta\gamma}, \qquad \Delta := ad - \beta\gamma > 0, \tag{4.11.2}$$

with

$$a = \beta + \rho_T + \chi_T + \frac{\eta_T I^*}{\kappa_T}, \quad d = \gamma + \rho_Q + \chi_Q + \frac{\eta_Q I^*}{\kappa_Q}, \quad I^* = \frac{s_I + \sigma_I}{d_I}. \tag{4.11.3}$$

Using the parameter values from Table 4.1, we compute:

$$I^* = \frac{10.0 + 5.0}{0.10} = 150, \quad a = 0.20075, \quad d = 0.04015, \quad \Delta = 0.0075601, \quad R_0 \approx 1.0859. \tag{4.11.4}$$

Therefore, the Sensitivity Index R_0 on parameter (r_T) Tumour proliferation rate is given by equation 4.11.5

$$\frac{\partial R_0}{\partial r_T} = \frac{d}{\Delta}, \quad \Upsilon_{R_0}^{r_T} = 1.0000. \tag{4.11.5}$$

R_0 and r_T are directly proportional. Proliferation is the strongest driver of tumour persistence, as evidenced by the fact that a 10% increase in tumour proliferation raises R_0 by precisely 10%.

The Sensitivity Index R_0 on parameter (ρ_T) radiotherapy rate on active tumour is given by equation 4.11.6

$$\Upsilon_{R_0}^{\rho_T} = -\rho_T \frac{d}{\Delta} \approx -0.5311. \tag{4.11.6}$$

Increasing ρ_T decreases R_0. Radiotherapy targeting proliferating tumour cells strongly suppresses tumour persistence.

The Sensitivity Index R_0 on parameter (χ_T) Chemotherapy rate on active tumour is given by equation 4.11.7

$$\Upsilon_{R_0}^{\chi_T} = -\chi_T \frac{d}{\Delta} \approx -0.2655. \tag{4.11.7}$$

Under normal circumstances, chemotherapy lowers R_0, but its impact is less pronounced than that of radiotherapy. The Sensitivity Index R_0 on parameter (η_T) Immune killing of active tumour is given by equation 4.11.8

$$\Upsilon_{R_0}^{\eta_T} = -\frac{\eta_T I^*}{\kappa_T} \cdot \frac{d}{\Delta} \approx -0.00398. \tag{4.11.8}$$

Cytotoxic immune response against proliferating tumour slightly reduces R_0. Its marginal value here reflects immune suppression at baseline.

The Sensitivity Index R_0 on parameter (η_Q) Immune killing of quiescent tumour is given by equation 4.11.9

$$\Upsilon_{R_0}^{\eta_Q} = -\frac{\beta\gamma}{d\Delta} \cdot \frac{\eta_Q I^*}{\kappa_Q} \approx -0.00025. \tag{4.11.9}$$

In line with clinical findings that quiescent cells fend off immune attack, killing dormant tumour cells has a minor impact on R_0.

The Sensitivity Index R_0 on parameter (β) Transition from T to Q is given by equation 4.11.10

$$\Upsilon_{R_0}^{\beta} = -\frac{\beta(d-\gamma)}{\Delta} \approx -0.1994. \tag{4.11.10}$$

Higher dormancy transition lowers R_0 by reducing proliferation. This emphasizes how quiescence serves as a stabilizing force.

The Sensitivity Index R_0 on parameter (γ) Reactivation from Q to T is given by equation 4.11.11

$$\Upsilon_{R_0}^{\gamma} = \frac{\beta\gamma(d-\gamma)}{d\Delta} \approx +0.0497. \tag{4.11.11}$$

Reactivation of dormant cells increases R_0, though its effect remains moderate.

The Sensitivity Index R_0 on parameter (σ_I) Immunotherapy stimulation is given by equation 4.11.12

$$\Upsilon_{R_0}^{\sigma_I} \approx -0.00141. \tag{4.11.12}$$

Immunotherapy decreases R_0, but the impact is marginal at baseline.

The Sensitivity Index R_0 on parameter (d_I) Immune decay rate is given by equation 4.11.13

$$\Upsilon_{R_0}^{d_I} \approx +0.00423. \tag{4.11.13}$$

As a result of treatment failure and immunological exhaustion, R_0 rises with faster immune loss.

4.11.1 Summary of Sensitivity Indices

Table 4.1: Normalized forward sensitivity indices of R_0 with respect to model parameters.

Parameter	Sensitivity Index	Interpretation
r_T	$+1.0000$	Strongest driver: tumour proliferation directly raises R_0
ρ_T	-0.5311	Radiotherapy reduces R_0 significantly
χ_T	-0.2655	Chemotherapy moderately reduces R_0
β	-0.1994	More $T \to Q$ dormancy reduces active growth
γ	$+0.0497$	Dormant reactivation increases R_0 (mild effect)
η_T	-0.00398	Cytotoxic immune killing of T lowers R_0 slightly
η_Q	-0.00025	Killing dormant cells has negligible effect
σ_I	-0.00141	Immunotherapy stimulation weakly decreases R_0
d_I	$+0.00423$	Immune decay increases R_0 marginally

4.11.2 Interpretation of Sensitivity Indices

The results confirm that tumour growth rate r_T is the most important element, with elasticity exactly $+1.0$. The next most important factors, chemotherapy χ_T and radiotherapy ρ_T, both had much lower R_0. Increasing transfer into quiescence (β) likewise decreases R_0, while reactivation (γ) somewhat increases it. Immune-related factors ($\eta_T, \eta_Q, \sigma_I, d_I$) have minimal effect at baseline, but they may become important under different regimes.Clarifying the relative impact of model parameters on the fundamental reproduction number, R_0, requires the use of sensitivity analysis. It determines the most important elements that influence tumour growth and control by quantitatively ranking the relevance of the parameters. The research further directs the development of control techniques by emphasizing treatment parameters and proliferation as the most successful intervention targets. Additionally, the results support the model's behavior by confirming that, in accordance with biological assumptions, therapeutic procedures decrease R_0 while increased tumour growth increases it. The results, which show that chemotherapy and radiation treatments are the most effective in suppressing tumours,

help guide the best use of available resources. Lastly, by indicating that immune-related factors might be more significant in improved immunity scenarios, even though they are less significant in the current model, the analysis offers guidance for future research.

4.12 Numerical Simulations

The non-linear system of ordinary differential equations in Eq. (3.1.5) was solved numerically to study the dynamics of tumour–host interactions under different therapeutic interventions. Since analytical solutions are not available, numerical simulations provide insight into the qualitative behavior and long-term evolution of the system. Parameter values were drawn from published studies and complemented by biologically reasonable estimates. All computations were performed in Python, and the results are presented graphically. This section discusses the baseline dynamics, the effects of radiotherapy and chemotherapy, the influence of treatment timing, and the outcomes of combined therapeutic strategies.

4.12.1 Model Simulations

The non-linear system (3.1.5) models the interactions among healthy cells, proliferating tumour cells, quiescent tumour cells, and immune effector cells in response to therapy. The simulations presented here numerically represent these dynamics and extend the analytical findings discussed earlier. They allow comparison of the individual and combined impacts of various treatments on tumour growth, immune activation, and the preservation of healthy tissue.

The `odeint` solver from the SciPy library was used to integrate the system of ODEs in Python. Time is measured in days, consistent with immune cell turnover and tumour growth rates. The simulation period was set to 200 days to capture both short-term transients and long-term equilibrium behavior.

4.12.2 Simulation Parameters

The reliability of numerical simulations depends on appropriate initial conditions and parameter values. Model parameters are derived from well-established research (de pillis et al., 2005, kim et al., 2014), and when data were unavailable, estimate are made from plausible biological assumptions. All parameters are expressed in per-day units to

maintain consistency with the temporal scale. Table 4.1 summarizes the values used in the simulations.

Initial conditions were chosen to represent a biologically realistic tissue state:

$$H(0) = 8.0 \times 10^5, \quad T(0) = 2.0 \times 10^5, \quad Q(0) = 5.0 \times 10^4, \quad I(0) = 1.0 \times 10^2.$$

These values describe an environment that is nearly healthy, with a small quiescent tumour reservoir, a modest immune population, and a manageable tumour burden.

Using these parameters and initial conditions, the model is expected to generate biologically consistent trajectories. The resulting time series will help determine whether the system evolves toward tumour elimination, dormancy, or persistence under different treatment regimens. The next subsection presents and interprets these results.

4.12.3 Parameter Estimation

As shown in Table 4.1, some parameters were derived from literature sources, while others were estimated within biologically acceptable bounds.

Table 4.1: Parameter values used in the model simulations

Symbol	Description	Value	Source
r_H	Healthy cell growth rate	0.20 day^{-1}	Kim et al. (2014)
K_H	Healthy tissue carrying capacity	1.0×10^6 cells	Assumed tissue scale
α_1	Transformation rate $H \to T$	1.0×10^{-7} day^{-1}	de Pillis et al. (2005)
r_T	Tumour cell growth rate	0.18 day^{-1}	de Pillis et al. (2005)
K_T	Tumour carrying capacity	1.0×10^6 cells	Standard scaling
β	Transition $T \to Q$	0.02 day^{-1}	Assumed (quiescence)
γ	Reactivation $Q \to T$	0.01 day^{-1}	Dormancy assumption
η_T	Immune killing rate (tumour)	0.50	de Pillis et al. (2005)
κ_T	Half-saturation for T kill	1.0×10^5 cells	Literature value
η_Q	Immune killing rate (quiescent)	0.10	Assumed lower efficacy
κ_Q	Half-saturation for Q kill	1.0×10^5 cells	Literature value
s_I	Basal immune influx	10 cells/day	Typical recruitment
σ_I	Immunotherapy influx	5 cells/day	Assumed moderate boost
δ	Max immune recruitment rate	0.10 day^{-1}	Kim et al. (2014)
θ	Tumour load for half-maximal immune activation	5.0×10^4 cells	Kim et al. (2014)
d_I	Immune decay rate	0.10 day^{-1}	Typical lifespan
ρ_H	Radiotherapy death rate (healthy)	0.02 day^{-1}	Assumed collateral damage
ρ_T	Radiotherapy death rate (tumour)	0.10 day^{-1}	Literature typical
ρ_Q	Radiotherapy death rate (quiescent)	0.02 day^{-1}	Assumed lower sensitivity
χ_H	Chemotherapy death rate (healthy)	0.01 day^{-1}	Assumed toxicity
χ_T	Chemotherapy death rate (tumour)	0.05 day^{-1}	Literature typical
χ_Q	Chemotherapy death rate (quiescent)	0.01 day^{-1}	Assumed lower sensitivity

4.12.4 Model Dynamics

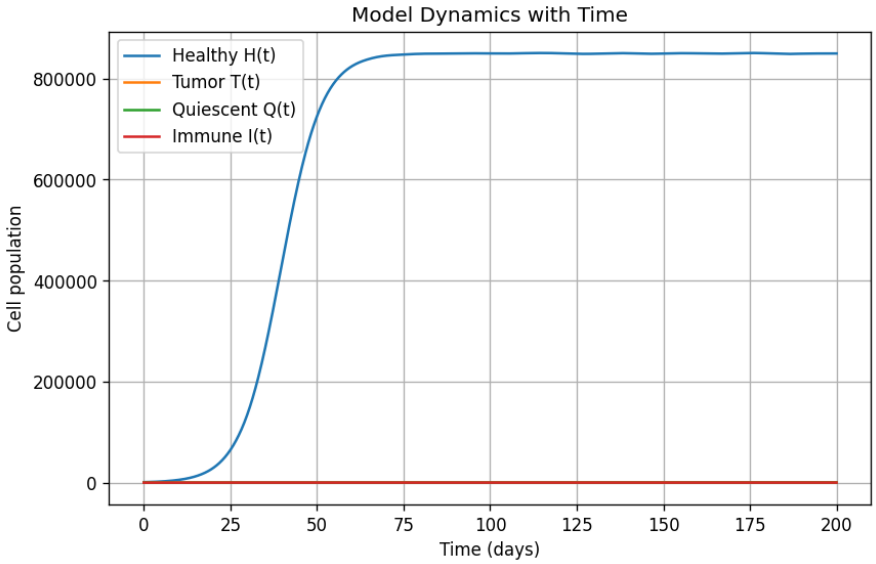

Figure 4.4: Model dynamics of the system showing the populations of healthy cells $H(t)$, tumour cells $T(t)$, quiescent cells $Q(t)$, and immune cells $I(t)$ over time (days).

Figure 4.4 presents the baseline dynamics. The healthy cell population $H(t)$ follows logistic growth, stabilizing at the carrying capacity. Tumour cells $T(t)$ and quiescent cells $Q(t)$ remain suppressed but gradually increase, suggesting the possibility of persistence in the long run. Immune cells $I(t)$ rise sharply in the early phase and then stabilize at a low level, indicating limited capacity to eradicate tumours on their own. These results illustrate a regime where $R_0 > 1$, and the tumour-free equilibrium is unstable, and this is clearly seen in figure 6 since in this, the scale used does not capture two cells.

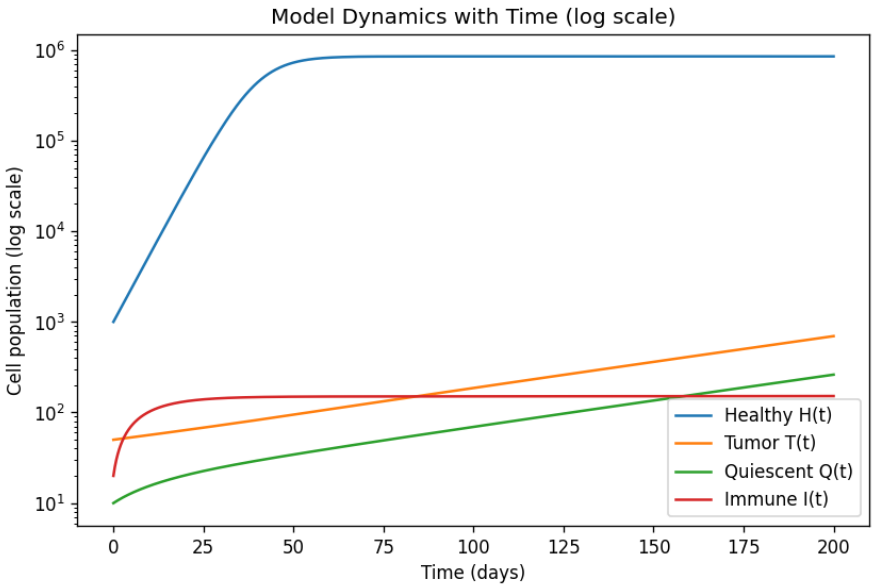

Figure 4.5: Model dynamics on a logarithmic scale showing the relative sizes of $H(t)$, $T(t)$, $Q(t)$, and $I(t)$ populations.

Figure 4.5 uses a logarithmic scale to highlight differences in order of magnitude. While $H(t)$ stabilizes near 10^6, tumour cells $T(t)$ and quiescent cells $Q(t)$ remain significantly smaller but continue to increase steadily. Immune cells $I(t)$ show an initial burst followed by a plateau. These dynamics confirm that tumours can persist at low levels even when dominated by healthy tissue.

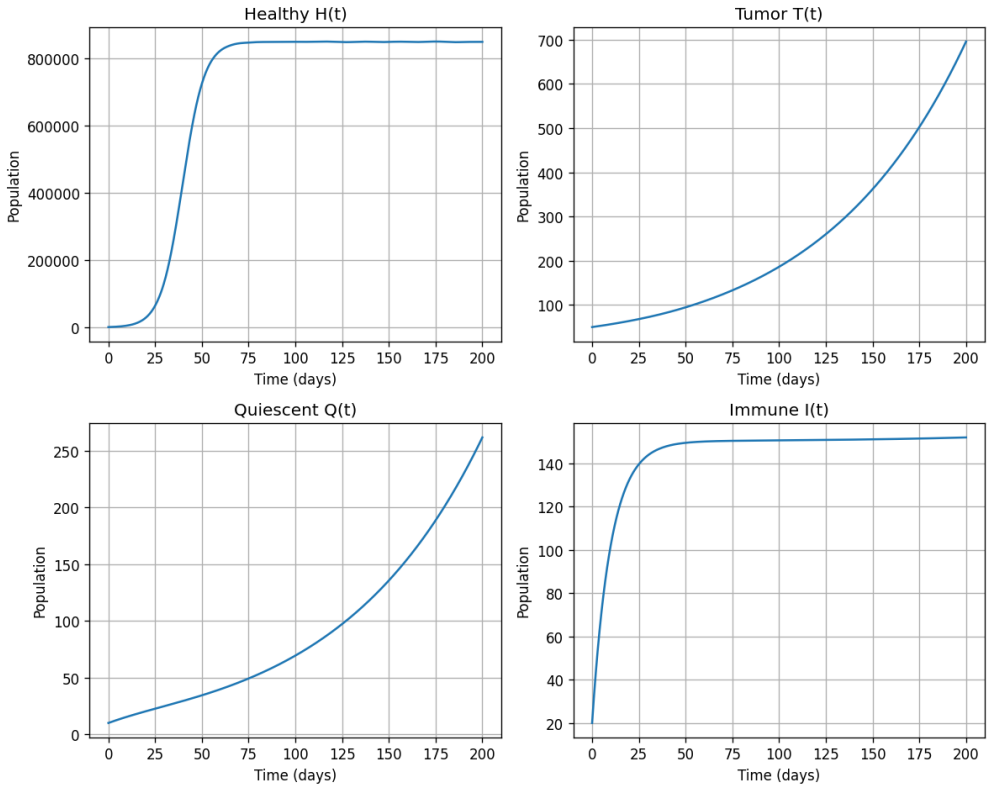

Figure 4.6: Temporal dynamics of all cell populations under baseline conditions.

As seen in Fig. 4.6, the four populations exhibit distinct temporal patterns consistent with earlier plots: healthy cells dominate, tumour and quiescent cells persist at low levels, and immune cells plateau after an initial response.

4.12.5 Radiotherapy Effects

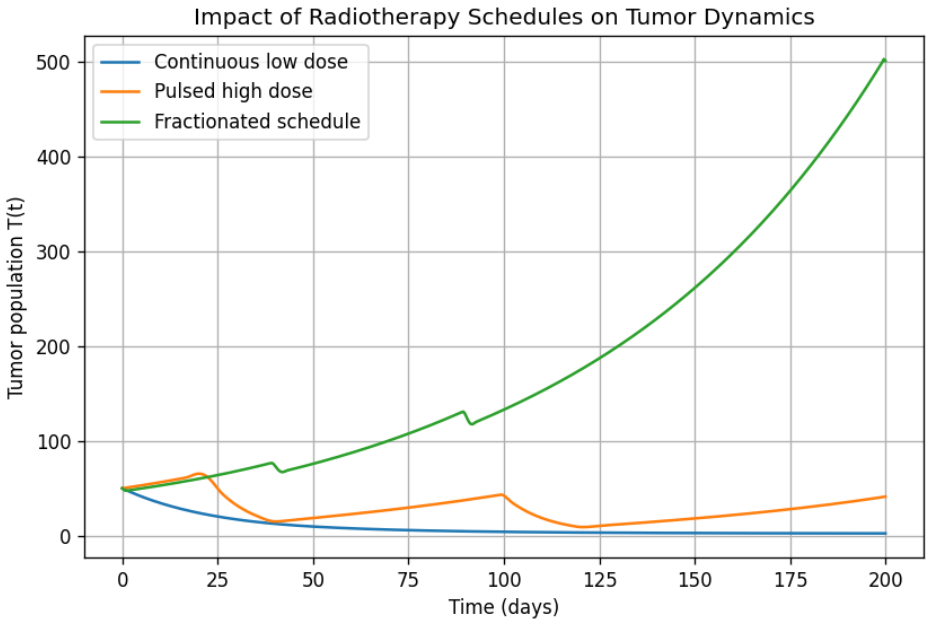

Figure 4.7: Impact of different radiotherapy schedules on tumour cells $T(t)$: continuous low dose, pulsed high dose, and fractionated delivery.

Figure 4.7 compares radiotherapy schedules. Continuous low-dose therapy drives tumour levels near zero. Pulsed high-dose therapy produces sharp declines followed by regrowth between cycles, creating oscillatory tumour dynamics. Fractionated therapy moderates growth but fails to achieve eradication. These outcomes highlight that continuous delivery is most effective for long-term tumour control.

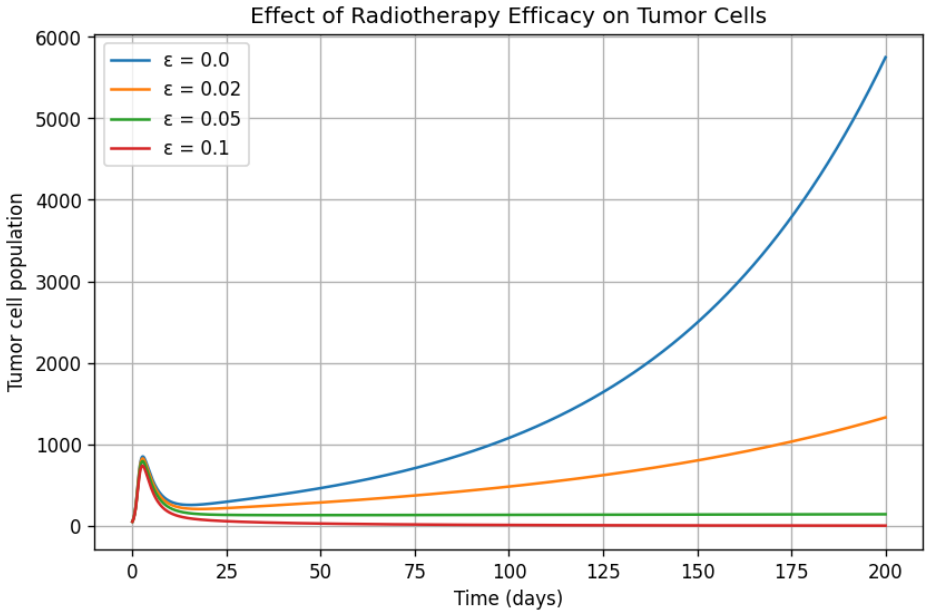

Figure 4.8: Effect of radiotherapy efficacy ε on tumour cells $T(t)$. Curves correspond to $\varepsilon = 0.0, 0.02, 0.05, 0.1$.

Figure 4.8 illustrates the threshold role of ε. Without treatment ($\varepsilon = 0.0$), tumour growth is unchecked. At $\varepsilon = 0.02$, growth slows but persists. At $\varepsilon = 0.05$, partial suppression occurs, while $\varepsilon = 0.1$ nearly eradicates the tumour. This confirms the analytical condition that tumour eradication requires reducing R_0 below one.

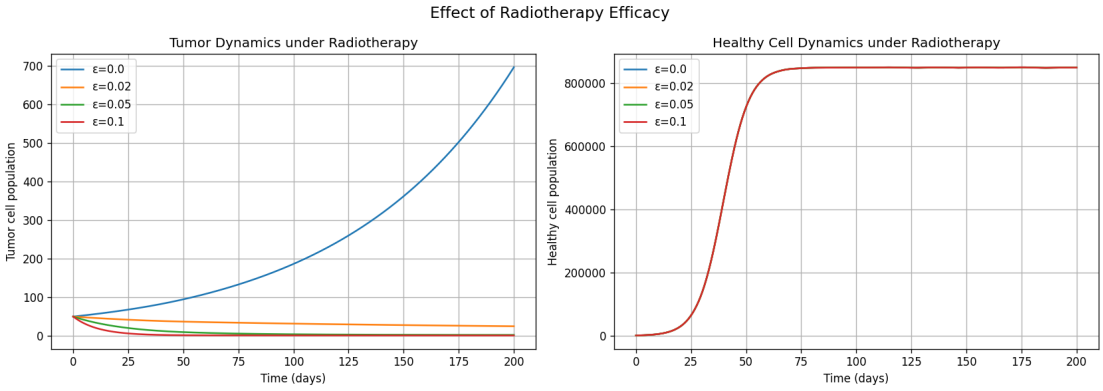

Figure 4.9: Radiotherapy efficacy ε and its effect on $T(t)$ (left) and $H(t)$ (right).

Figure 4.9 shows that radiotherapy efficacy alters tumour dynamics while leaving healthy cell recovery largely unchanged. For all values of ε, $H(t)$ returns to its carrying capacity, demonstrating selective tumour suppression.

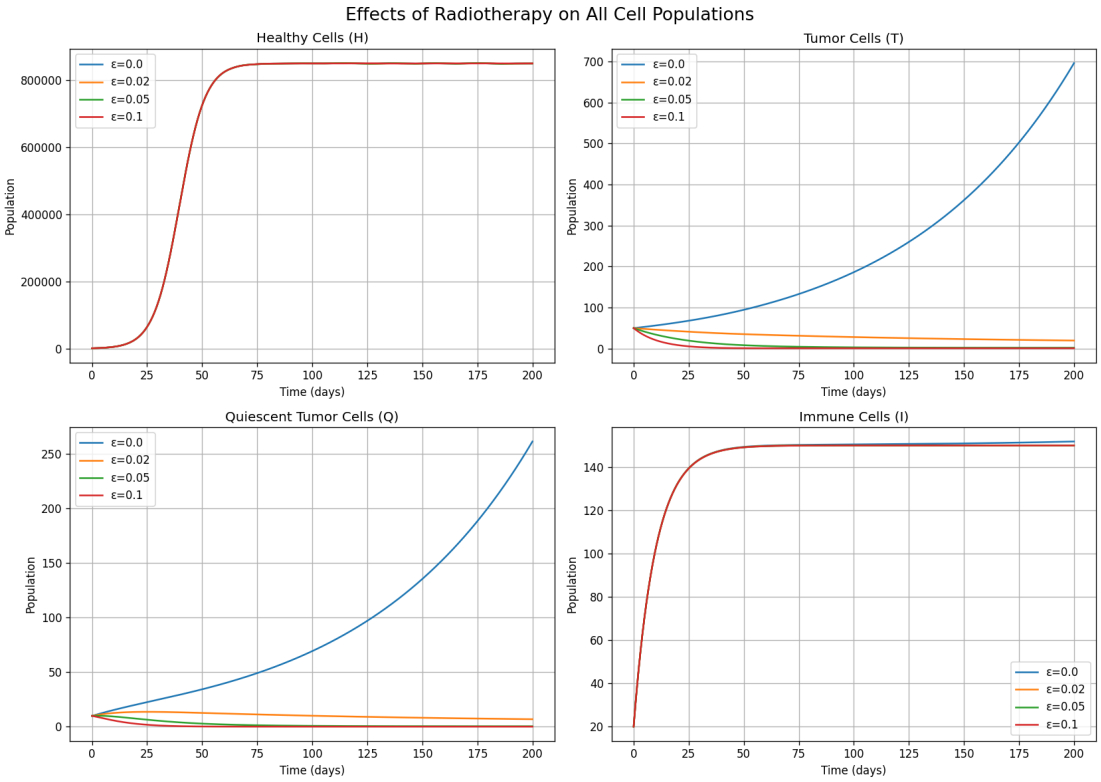

Figure 4.10: Effect of radiotherapy efficacy ε on all compartments: $H(t)$, $T(t)$, $Q(t)$, $I(t)$.

Figure 4.10 confirms that radiotherapy strongly reduces $T(t)$ and $Q(t)$, while $H(t)$ and $I(t)$ remain stable. Thus, the treatment primarily targets malignant cells in this model.

4.12.6 Treatment Timing

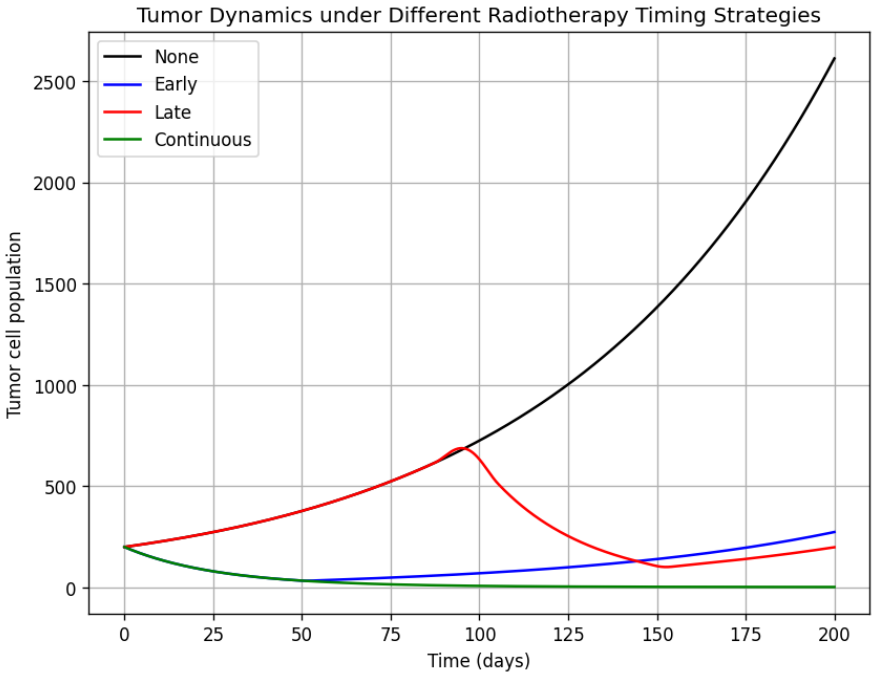

Figure 4.11: Tumour trajectories under no treatment, early therapy, late therapy, and continuous therapy.

Figure 4.11 demonstrates the influence of timing. Early therapy suppresses tumours before they expand, while late therapy reduces tumour size but leaves residual populations. Continuous therapy maintains near-zero tumour levels throughout.

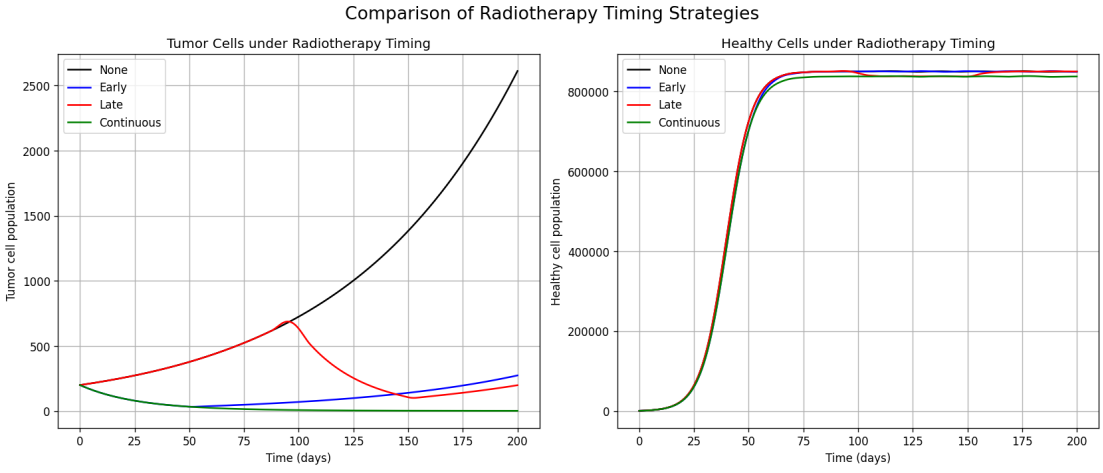

Figure 4.12: Comparison of radiotherapy timing: tumour dynamics (left) and healthy cells (right).

Figure 4.12 highlights that tumour suppression depends strongly on timing, while healthy cells $H(t)$ are robust and recover regardless of schedule.

4.12.7 Chemotherapy Effects

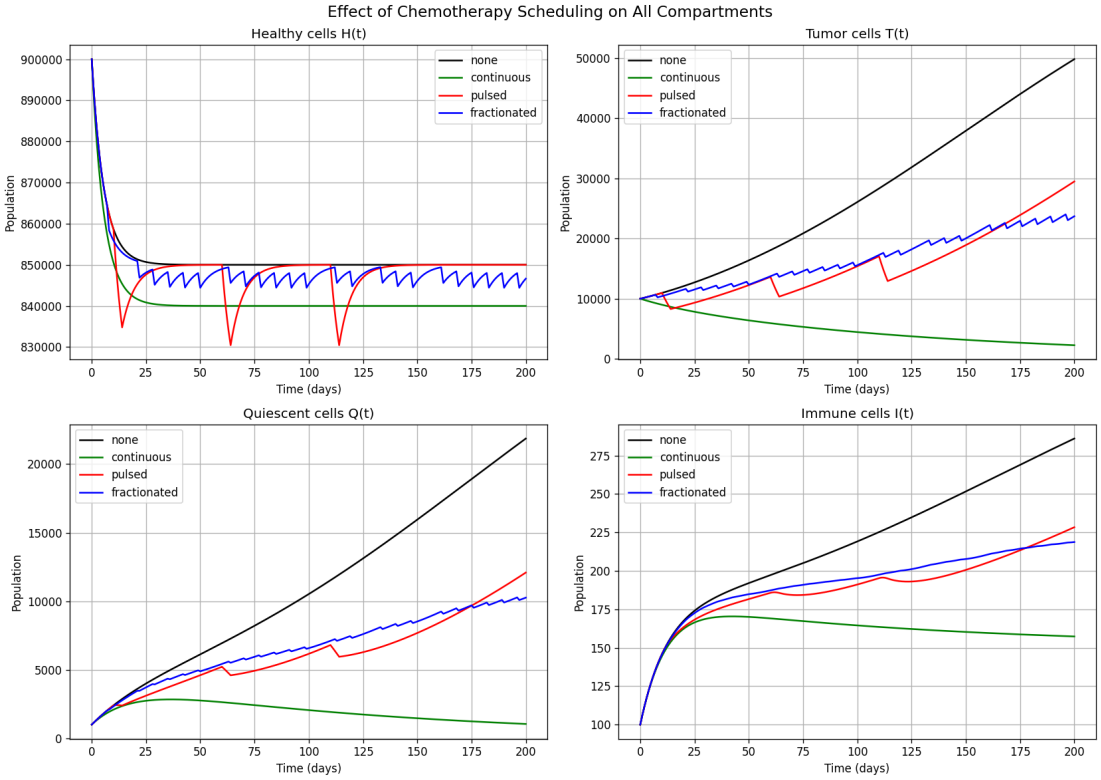

Figure 4.13: Chemotherapy schedules: no therapy, continuous, pulsed, and fractionated. Effects shown for all cell populations.

Figure 4.13 shows that continuous chemotherapy best suppresses $T(t)$ and $Q(t)$. Pulsed chemotherapy produces oscillations, while fractionated therapy only partially controls growth. Healthy and immune cells remain relatively stable, though continuous therapy slightly reduces $H(t)$ compared to no therapy.

4.12.8 Combined Therapies

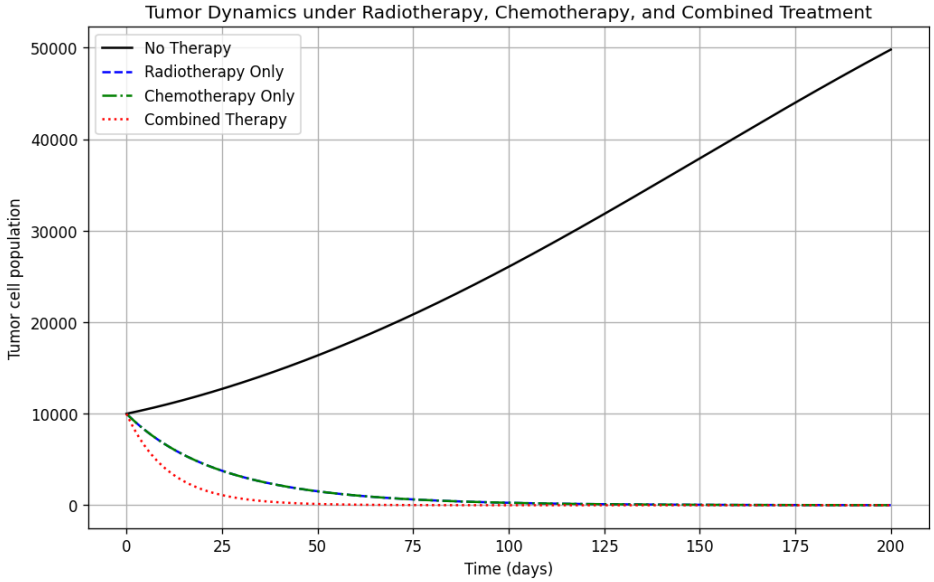

Figure 4.14: Comparison of tumour trajectories under no therapy, radiotherapy alone, chemotherapy alone, and combined therapy.

Figure 4.14 shows that radiotherapy and chemotherapy alone reduce tumour burden, but their combination achieves the most rapid and complete suppression.

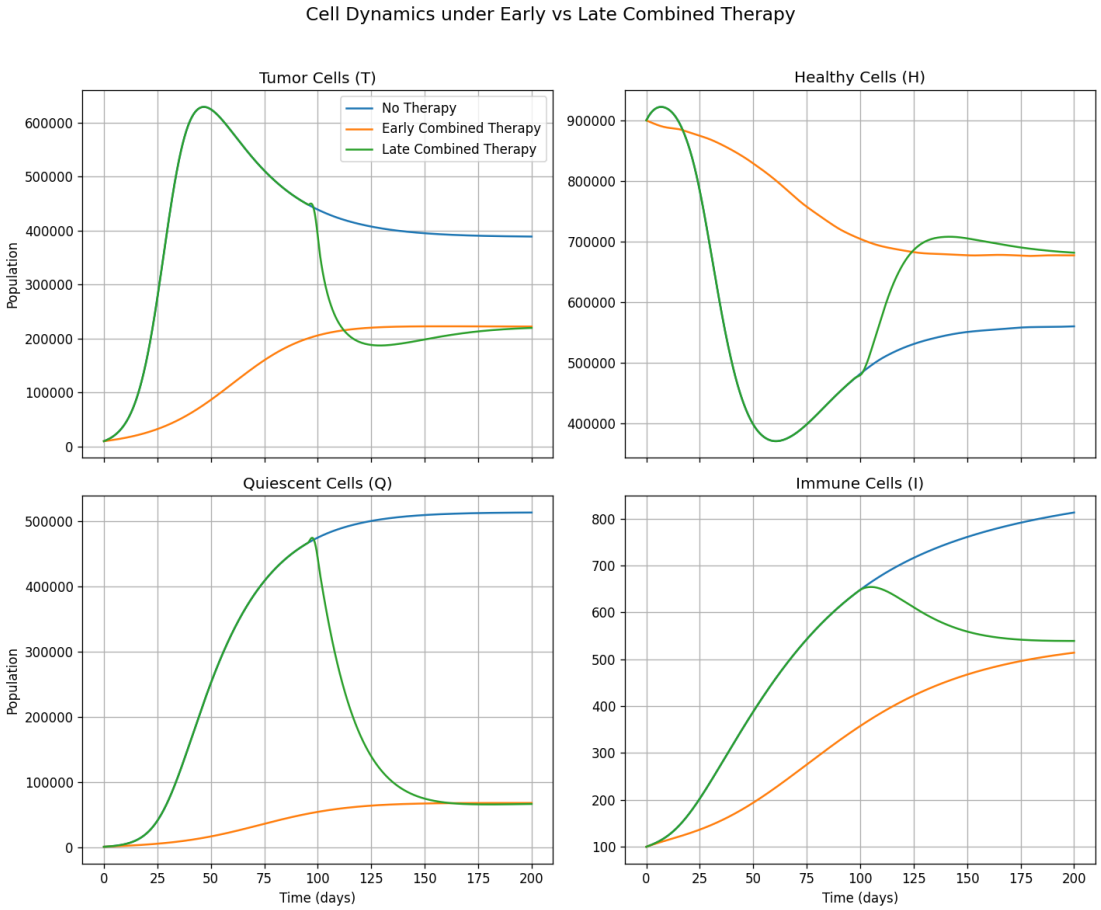

Figure 4.15: Cell dynamics under early versus late combined therapy compared with no therapy.

Figure 4.15 illustrates that early combined therapy is more effective, keeping tumour and quiescent populations low with fewer oscillations, whereas late combined therapy results in higher peaks and larger fluctuations across compartments.

4.12.9 Synthesis of Results

The simulations reinforce and extend the theoretical analysis of Chapter Three. Tumour persistence occurs when $R_0 > 1$, while sufficient treatment efficacy reduces R_0 below unity and leads to eradication. Scheduling is as critical as dosage: continuous delivery consistently outperforms pulsed and fractionated strategies. Combination therapy provides the strongest and most stable suppression, reflecting non-linear synergy among compartments in Eq. (3.1.5). Finally, early intervention is superior to late treatment, confirming the importance of prompt therapy. Although the present model does not capture toxicity, drug resistance, or spatial heterogeneity, the results align with clinical

evidence that sustained, combined, and timely therapies are the most effective for cancer control.

4.13 Discussion

The simulations presented in this chapter illustrate the behavior of the tumour–host system under different therapeutic interventions. Collectively, the results (Figures. 4.4–4.15) validate the analytical framework developed in Chapter Three and highlight the importance of treatment efficacy, scheduling, and timing in determining long-term outcomes.

The baseline trajectories in Figures. 4.4–4.6 show that in the absence of treatment, the system governed by Eq. (3.1.5) evolves toward tumour persistence. Healthy cells $H(t)$ follow logistic growth, approaching the carrying capacity, while tumour $T(t)$ and quiescent cells $Q(t)$ increase at slower but steady rates. The immune response $I(t)$ rises initially then stabilizes, indicating a limited ability to eliminate tumour cells on its own. These findings confirm the analytical result that when the reproduction number $R_0 > 1$, the tumour-free equilibrium is unstable, and tumour populations eventually dominate.

Radiotherapy experiments emphasize two features: efficacy and delivery mode. As demonstrated in Figures. 4.8–4.10, the parameter ε acts as a control switch. For small values ($\varepsilon = 0.02$), tumour growth is slowed but not suppressed; for moderate values ($\varepsilon = 0.05$), partial suppression occurs; and at higher values ($\varepsilon = 0.1$), tumour eradication is achieved. Importantly, healthy cells remain at carrying capacity across all efficacy values, underscoring the selective action of radiotherapy in this model. This aligns with the threshold condition derived in Chapter Three, where $R_0 < 1$ guarantees tumour-free stability. Delivery schedules (Figure. 4.7) further demonstrate that continuous dosing ensures the most sustained suppression, while pulsed and fractionated approaches permit oscillatory dynamics and incomplete control. This observation is consistent with sensitivity results (Section 3.5), where treatment-related parameters contributed the largest positive impact on R_0 reduction.

Chemotherapy simulations (Figure. 4.13) reinforce the influence of delivery patterns. Continuous chemotherapy achieves the greatest reduction in $T(t)$ and $Q(t)$, while pulsed chemotherapy yields strong temporary declines but allows regrowth, and fractionated schedules produce only moderate control. Healthy and immune cells are relatively sta-

ble across strategies, though continuous therapy slightly reduces $H(t)$ below the untreated equilibrium. These outcomes reflect a key clinical reality: drug administration schedules critically shape efficacy, and continuous exposure often enhances long-term control.

Figures 4.11 and 4.12 highlight the significance of treatment timing. Early radiotherapy suppresses tumours before they reach high levels, while late treatment produces declines but leaves residual cells. Continuous therapy achieves the strongest and most stable suppression, mirroring clinical recommendations that early intervention and sustained treatment yield superior outcomes. Similarly, Figure. 4.15 shows that early combined therapy minimizes tumour and quiescent populations with fewer oscillations, while late initiation produces higher peaks and larger fluctuations across compartments. This trade-off illustrates the cost of delayed intervention: transient damage to healthy cells and stronger immune activation at the expense of stability.

The advantage of multimodal therapy is evident in Figure. 4.14. While radiotherapy and chemotherapy alone are effective in reducing tumour size, their integration produces the fastest and most complete suppression, driving tumour levels to near zero within the simulation period. This finding is consistent with biological evidence that combining DNA-damaging radiation with systemic drugs improves treatment efficacy. In the context of the model, this synergy reflects non-linear interactions between the tumour compartments in Eq. (3.1.5), which amplify the suppressive effects when both therapies are applied simultaneously.

In summary, the simulations confirm several key themes. First, untreated systems evolve toward tumour dominance when $R_0 > 1$, but sufficient therapy can restore control by reducing $R_0 < 1$. Second, treatment schedules matter as much as intensity, with continuous protocols consistently outperforming intermittent ones. Third, combined therapies provide superior outcomes compared to single modalities. Finally, early intervention stabilizes the system, whereas delayed therapy introduces instability and fluctuations. Together, these findings validate the analytical predictions of Chapter Three, provide biological plausibility, and set the stage for the recommendations outlined in Chapter Five.

CHAPTER FIVE

SUMMARY, CONCLUSION AND RECOMMENDATION

5.1 Summary

This study developed and analysed a non-linear mathematical model describing the interactions among healthy cells, tumour cells, quiescent tumour cells, and immune cells under the effects of radiotherapy and chemotherapy. The model was formulated as a system of non-linear ordinary differential equations and was shown to satisfy fundamental mathematical properties such as positivity, boundedness, and the existence of invariant regions. These properties ensured that the solutions remained biologically realistic, since none of the population densities became negative or unbounded over time.

Equilibrium analysis revealed two biologically significant steady states: the tumour-free equilibrium and the endemic equilibrium. The stability of these equilibria was characterized both locally and globally using analytical techniques. The basic reproduction number, denoted by R_0, emerged as a key threshold parameter determining whether the tumour population persists or is eliminated. When $R_0 < 1$, the system tends toward the tumour-free equilibrium, representing complete recovery; when $R_0 > 1$, the system stabilizes at the endemic equilibrium, indicating persistent tumour presence.

Sensitivity analysis identified the model parameters that most strongly influence tumour progression and regression. In particular, parameters associated with radiotherapy efficacy, immune activation, and tumour growth rate were found to exert dominant effects on the system dynamics. Bifurcation analysis further showed that small variations in these parameters could cause qualitative changes in the system's long-term behavior, emphasizing the non-linear nature of tumour–host–therapy interactions.

Numerical simulations complemented and validated the analytical findings. In the absence of any therapeutic intervention, the populations of tumour cells $T(t)$ and quiescent cells $Q(t)$ increased rapidly, while the healthy cell population $H(t)$ declined steadily, confirming tumour dominance when $R_0 > 1$. The immune population $I(t)$ rose modestly but was insufficient to suppress tumour growth, indicating a weak natural defense mechanism in the absence of therapy.

Radiotherapy efficacy, denoted by ε, played a decisive role in tumour control. Simulation results demonstrated that low efficacy values ($\varepsilon < 0.05$) only slowed tumour

progression, whereas higher efficacy levels ($\varepsilon \geq 0.1$) effectively reduced both tumour and quiescent cell populations to near zero. Importantly, healthy and immune cells remained largely stable, confirming that selective tumour destruction could be achieved without significant collateral damage. This finding was consistent with the theoretical result that tumour eradication corresponds to $R_0 < 1$.

Chemotherapy simulations revealed a stronger dependence on dosage schedule. Continuous chemotherapy achieved consistent suppression of tumour growth and sustained remission. In contrast, pulsed therapy produced oscillatory tumour dynamics characterized by alternating periods of shrinkage and regrowth, while fractionated schedules led to partial suppression with eventual persistence of tumour cells. Healthy cells exhibited mild declines under continuous chemotherapy due to toxicity, but remained viable throughout the treatment horizon.

Combined therapy, integrating both radiotherapy and chemotherapy, yielded superior outcomes compared to single-modality treatments. The synergistic interaction between the two modalities accelerated tumour reduction, shortened the recovery time, and minimized recurrence. Figures 4.14 and 4.15 illustrated that combined treatment drove tumour populations to near-zero levels within a shorter timeframe. Furthermore, early initiation of therapy was shown to be critical: treatments begun at early stages produced smoother cell trajectories, minimal oscillations, and more stable recovery dynamics, whereas delayed initiation led to large fluctuations in all compartments and prolonged recovery times.

Taken together, these results demonstrate that mathematical modelling provides a reliable and insightful framework for analysing the dynamics of tumour–host–therapy systems. The model established clear quantitative relationships between therapeutic efficacy, timing, and long-term disease control, offering predictive insights that can inform clinical decision-making and guide the design of optimal cancer treatment strategies.

5.2 Conclusion

The analysis conducted in this study confirms that non-linear dynamical models can effectively describe the complex interactions among tumour, immune, quiescent, and healthy cells under the influence of therapeutic interventions. The incorporation of ra-

diotherapy and chemotherapy parameters into the system provided a realistic and flexible representation of treatment dynamics and biological response.

Analytical results established that the tumour-free equilibrium is locally and globally asymptotically stable when the basic reproduction number R_0 is less than one, signifying complete tumour elimination. When $R_0 > 1$, the endemic equilibrium becomes stable, representing tumour persistence. The sensitivity analysis revealed that therapeutic parameters have the most significant influence on system outcomes, suggesting that treatment efficacy can be optimized by adjusting these parameters.

Numerical simulations provided concrete validation of the theoretical framework. They showed that radiotherapy and chemotherapy, when administered continuously and effectively, can lead to complete tumour regression while preserving healthy and immune cell populations. Combined therapy consistently outperformed individual modalities, demonstrating a synergistic effect that accelerated tumour reduction. Moreover, early initiation of therapy proved critical in minimizing tumour burden and ensuring rapid system stabilization.

Overall, the findings of this study demonstrate that mathematical modelling is a powerful tool for exploring, predicting, and optimizing cancer treatment protocols. The integration of analytical and computational methods enables a systematic evaluation of therapy strategies, facilitating the transition from empirical treatment design toward evidence-based, data-driven cancer management.

5.3 Recommendations

Based on the outcomes of this study, several recommendations are proposed in alignment with the research objectives.

Firstly, clinical and computational studies should prioritize continuous or near-continuous treatment schedules. The simulation results demonstrated that continuous therapy produced the most effective and sustained tumour suppression compared to pulsed or fractionated regimens.

Secondly, combined therapy involving both radiotherapy and chemotherapy should be favoured over single-modality treatments. The synergistic effects of the two modalities

yielded faster and more complete tumour eradication, consistent with clinical observations in multimodal oncology practice.

Thirdly, early diagnosis and timely initiation of treatment should be emphasized. Simulations clearly indicated that early therapeutic intervention minimizes tumour proliferation, reduces oscillations in cell populations, and preserves healthy tissue integrity. Late treatment initiation, in contrast, allowed tumour populations to expand and resulted in more unstable system behavior.

Despite these insights, the simulations also reveal limitations inherent in the current framework. The model does not account for toxicity to normal tissues, treatment resistance, or the spatial heterogeneity of tumours. Moreover, the deterministic structure neglects stochastic variability in patient responses. These omissions suggest caution in direct clinical translation. Nevertheless, the sensitivity analysis in Chapter Three supports the robustness of the conclusions: treatment efficacy and scheduling remain the most critical levers for tumour suppression, regardless of the simplifications.

Finally, mathematical modelling should be integrated into clinical decision-making and treatment planning. The model presented in this study provides a predictive framework for exploring different therapeutic options before implementation. By simulating dosage schedules, efficacy parameters, and timing strategies, clinicians can design patient-specific treatments that maximize tumour control while minimizing adverse effects. Such integration of modelling into personalized medicine has the potential to improve therapeutic efficiency and optimize resource allocation in oncology.

5.4 Recommendations For Further Research

Although the present study provides valuable insights into tumour–host–therapy interactions, several extensions are recommended for future research.

An important next step is the incorporation of immunotherapy into the existing framework. Modern cancer treatment increasingly relies on immunomodulatory agents, such as immune checkpoint inhibitors, which enhance the immune system's ability to recognize and destroy cancer cells. Including immunotherapy parameters would allow comprehensive evaluation of combination strategies involving radiotherapy, chemotherapy, and immunotherapy.

Secondly, the model can be extended to stochastic or spatially distributed frameworks. Biological processes such as tumour growth, cell migration, and immune response are inherently variable and spatially heterogeneous. A stochastic or partial differential equation (PDE) approach would enable the modelling of nutrient diffusion, oxygen gradients, and immune infiltration across spatial domains, providing a more realistic description of tumour micro-environmental effects.

Parameter estimation based on patient-specific data should also be a priority for future studies. Calibrating the model with clinical datasets will enhance its predictive accuracy and applicability in personalized treatment planning. Coupling sensitivity analysis with clinical parameter measurement can help identify which biological factors should be prioritized in monitoring treatment progress.

Additionally, applying optimal control theory to the model can lead to the formulation of mathematically justified therapeutic strategies. This approach would help balance tumour reduction with the preservation of healthy and immune cells, leading to efficient and clinically viable treatment schedules.

Lastly, it is important to acknowledge the current model's limitations. The model assumes homogeneous tumour and immune cell populations and neglects treatment-related toxicity, acquired resistance, and feedback mechanisms that occur in vivo. Addressing these factors in future research will improve the clinical realism and applicability of mathematical oncology models.

In conclusion, this study contributes to the growing field of mathematical oncology by providing a rigorous analytical and computational framework for investigating tumour–host–therapy dynamics. The integration of theoretical and numerical techniques has enhanced the understanding of how therapeutic parameters influence cancer outcomes. The work lays a strong foundation for future interdisciplinary research that bridges applied mathematics, computational biology, and clinical oncology.

REFERENCES

Ak Gümüş, Ö. (2014). Global and local stability analysis in a nonlinear discrete-time population model. *Advances in Difference Equations*, *2014*, 1–9.

Anderson, R. (1991). *Infectious diseases of humans: dynamics and control*. Cambridge Univer-sity Press.

Angulo, M. T., Moreno, J. A., Lippner, G., Barabási, A.-L., & Liu, Y.-Y. (2017). Fundamental limitations of network reconstruction from temporal data. *Journal of the Royal Society Interface*, *14*(127), 20160966.

Anwar, M. I., Shafie, S., Kasim, A. R. M., & Salleh, M. Z. (2016). Radiation effect on mhd stagnation-point flow of a nanofluid over a nonlinear stretching sheet with convective boundary condition. *Heat Transfer Research*, *47*(9).

Aragon-Ching, J. B., Williams, K. M., Gulley, J. L., et al. (2007). Impact of androgen-deprivation therapy on the immune system: implications for combination therapy of prostate cancer. *Front Biosci*, *12*(4957), 71.

Arfan, M., Shah, K., Ullah, A., Shutaywi, M., Kumam, P., & Shah, Z. (2021). On fractional order model of tumor dynamics with drug interventions under nonlocal fractional derivative. *Results in Physics*, *21*, 103783.

Arnold, K. M., Flynn, N. J., Raben, A., Romak, L., Yu, Y., Dicker, A. P., … Sims-Mourtada, J. (2018). The impact of radiation on the tumor microenvironment: effect of dose and fractionation schedules. *Cancer growth and metastasis*, *11*, 1179064418761639.

Atkinson, S. (2010). Mutual ties. *Nature Reviews Cancer*, *10*(2), 82–83.

Baker, R. E., Pena, J.-M., Jayamohan, J., & Jérusalem, A. (2018). Mechanistic models versus machine learning, a fight worth fighting for the biological community? *Biology letters*, *14*(5), 20170660.

Barrett, B. W., Paz-Soldan, V. A., Mendoza-Cervantes, D., Sánchez, G. M., Córdova López, J. J., Gravitt, P. E., … Group, P. P. S. (2020). Understanding geospatial factors associated with cervical cancer screening uptake in amazonian peruvian women. *JCO Global Oncology*, *6*, 1237–1247.

Baskar, R., Lee, K. A., Yeo, R., & Yeoh, K.-W. (2012). Cancer and radiation therapy: current advances and future directions. *International journal of medical sciences*, *9*(3), 193.

Baykara, O. (2015). Current therapies and latest developments in cancer treatment. *Horizons in Cancer Research*, *57*, 105–156.

Bekker, R. A., Kim, S., Pilon-Thomas, S., & Enderling, H. (2022). Mathematical modeling of radiotherapy and its impact on tumor interactions with the immune system. *Neoplasia*, *28*, 100796.

Benzekry, S., Lamont, C., Beheshti, A., Tracz, A., Ebos, J. M., Hlatky, L., & Hahnfeldt, P. (2014). Classical mathematical models for description and prediction of experimental tumor growth. *PLoS computational biology*, *10*(8), e1003800.

Bray, F., & BSc, M. (2018). Phd; jacques ferlay, me; isabelle soerjomataram, md, msc, phd; rebecca l. siegel, mph; lindsey a. torre, msph; ahmedin jemal, phd, dvm. global cancer statistics 2018: Globocan estimates of incidence and mortality worldwide for 36 cancers in 185 countries. *CA CANCER J CLIN*, *68*, 394–424.

Byrne, H. M., & Chaplain, M. A. (1996). Modelling the role of cell-cell adhesion in the growth and development of carcinomas. *Mathematical and Computer Modelling*, *24*(12), 1–17.

Castillo-Chavez, C., & Song, B. (2004). Dynamical models of tuberculosis and their applications. *Math. Biosci. Eng*, *1*(2), 361–404.

Chamkha, A. J., El-Kabeir, S., & Rashad, A. (2015). Unsteady coupled heat and mass transfer by mixed convection flow of a micropolar fluid near the stagnation point on a vertical surface in the presence of radiation and chemical reaction. *Progress in Computational Fluid Dynamics, an International Journal*, *15*(3), 186–196.

Charzyńska, A., Nałęcz, A., Rybiński, M., & Gambin, A. (2012). Sensitivity analysis of mathematical models of signaling pathways. *BioTechnologia*, *93*(3), 291–308.

Chitnis, N., Hyman, J. M., & Cushing, J. M. (2008). Determining important parameters in the spread of malaria through the sensitivity analysis of a mathematical model. *Bulletin of mathematical biology*, *70*(5), 1272–1296.

Copas, J., Marson, A., Williamson, P., & Kirkham, J. (2019). Model-based sensitivity analysis for outcome reporting bias in the meta analysis of benefit and harm outcomes. *Statistical methods in medical research*, *28*(3), 889–903.

Cragg, M. S., Harris, C., Strasser, A., & Scott, C. L. (2009). Unleashing the power of inhibitors of oncogenic kinases through bh3 mimetics. *Nature Reviews Cancer*, *9*(5), 321–326.

Danaei, G., Vander Hoorn, S., Lopez, A. D., Murray, C. J., & Ezzati, M. (2005). Causes of cancer in the world: comparative risk assessment of nine behavioural and environmental risk factors. *The lancet*, *366*(9499), 1784–1793.

Datta, N., Ordóñez, S. G., Gaipl, U., Paulides, M., Crezee, H., Gellermann, J., … Bodis, S. (2015). Local hyperthermia combined with radiotherapy and-/or chemotherapy: Recent advances and promises for the future. *Cancer treatment reviews*, *41*(9), 742–753.

De Mello, R. A. B., Voscaboinik, R., Luciano, J. V. P., Cremonese, R. V., Amaral, G. A., Castelo-Branco, P., & Antoniou, G. (2021). Immunotherapy in patients with advanced non-small cell lung cancer lacking driver mutations and future perspectives. *Cancers*, *14*(1), 122.

De Pillis, L. G., & Radunskaya, A. (2003). The dynamics of an optimally controlled tumor model: A case study. *Mathematical and computer modelling*, *37*(11), 1221–1244.

de Pillis, L. G., Radunskaya, A. E., & Wiseman, C. L. (2005). A validated mathematical model of cell-mediated immune response to tumor growth. *Cancer Research*, *65*(17), 7950–7958. doi: 10.1158/0008-5472.CAN-05-0564

DeVita Jr, V. T., & Chu, E. (2008). A history of cancer chemotherapy. *Cancer research*, *68*(21), 8643–8653.

Dewan, M. Z., Galloway, A. E., Kawashima, N., Dewyngaert, J. K., Babb, J. S., Formenti, S. C., & Demaria, S. (2009). Fractionated but not single-dose radiotherapy induces an immune-mediated abscopal effect when combined with anti–ctla-4 antibody. *Clinical Cancer Research*, *15*(17), 5379–5388.

Eftimie, R., Bramson, J. L., & Earn, D. J. (2011). Interactions between the immune system and cancer: a brief review of non-spatial mathematical models. *Bulletin of mathematical biology*, *73*(1), 2–32.

Ellis, W. J., Vessella, R. L., Buhler, K. R., Bladou, F., True, L. D., Bigler, S. A., … Lange, P. H. (1996). Characterization of a novel androgen-sensitive, prostate-specific antigen-producing prostatic carcinoma xenograft: Lucap 23. *Clinical cancer research: an official journal of the American Association for Cancer Research*, *2*(6), 1039–1048.

Eriksson, D., & Stigbrand, T. (2010). Radiation-induced cell death mechanisms. *Tumor Biology*, *31*, 363–372.

Feldman, B. J., & Feldman, D. (2001). The development of androgen-independent prostate cancer. *Nature Reviews Cancer*, *1*(1), 34–45.

Ferlay, J., Soerjomataram, I., Dikshit, R., Eser, S., Mathers, C., Rebelo, M., … Bray, F. (2015). Cancer incidence and mortality worldwide: sources, methods and major patterns in globocan 2012. *International journal of cancer*, *136*(5), E359–E386.

Fogg, V. C., Lanning, N. J., & MacKeigan, J. P. (2011). Mitochondria in cancer: at the crossroads of life and death. *Chinese journal of cancer*, *30*(8), 526.

Fontana, F., Anselmi, M., & Limonta, P. (2023). Unraveling the peculiar features of mitochondrial metabolism and dynamics in prostate cancer. *Cancers*, *15*(4), 1192.

Fuks, Z., Leibel, S. A., Wallner, K. E., Begg, C. B., Fair, W. R., Anderson, L. L., … Whitmore, W. F. (1991). The effect of local control on metastatic dissemina-

tion in carcinoma of the prostate: long-term results in patients treated with 1251 implantation. *International Journal of Radiation Oncology* Biology* Physics*, *21*(3), 537–547.

Gao, D.-p., Huang, N.-j., Kang, S. M., & Zhang, C. (2018). Global stability analysis of an sveir epidemic model with general incidence rate. *Boundary Value Problems*, *2018*(1), 42.

Garner, A. L., Lau, Y., Jordan, D. W., Uhler, M. D., & Gilgenbach, R. M. (2006). Implications of a simple mathematical model to cancer cell population dynamics. *Cell proliferation*, *39*(1), 15–28.

Gatenby, R. A., & Gawlinski, E. T. (1996). A reaction-diffusion model of cancer invasion. *Cancer research*, *56*(24), 5745–5753.

Gong, C., Milberg, O., Wang, B., Vicini, P., Narwal, R., Roskos, L., & Popel, A. S. (2017). A computational multiscale agent-based model for simulating spatio-temporal tumour immune response to pd1 and pdl1 inhibition. *Journal of the Royal Society Interface*, *14*(134), 20170320.

González Abalde, C., et al. (2021). The regulatory effect of melatonin on molecular changes induced by radiation and chemotherapy in breast cancer cells.

Greenspan, H. P. (1972). Models for the growth of a solid tumor by diffusion. *Studies in Applied Mathematics*, *51*(4), 317–340.

Hahnfeldt, P., Panigrahy, D., Folkman, J., & Hlatky, L. (1999). Tumor development under angiogenic signaling: a dynamical theory of tumor growth, treatment response, and postvascular dormancy. *Cancer research*, *59*(19), 4770–4775.

Hall, E. (2012). *Hall ej, giaccia aj, eds, radiobiology for radiologists*. Philadelphia, Lippincott Williams and Wilkins.

Hamilton, W. (2010). Cancer diagnosis in primary care. *British Journal of General Practice*, *60*(571), 121–128.

Hanahan, D., & Weinberg, R. A. (2011). Hallmarks of cancer: the next generation. *cell*, *144*(5), 646–674.

Hatzikirou, H., Alfonso, J., Mühle, S., Stern, C., Weiss, S., & Meyer-Hermann, M. (2015). Cancer therapeutic potential of combinatorial immuno-and vasomodulatory interventions. *Journal of The Royal Society Interface*, *12*(112), 20150439.

Heinlein, C. A., & Chang, C. (2004). Androgen receptor in prostate cancer. *Endocrine reviews*, *25*(2), 276–308.

Hirsch, M. W., Smale, S., & Devaney, R. L. (2013). *Differential equations, dynamical systems, and an introduction to chaos*. Academic press.

Huang, Y., Goel, S., Duda, D. G., Fukumura, D., & Jain, R. K. (2013). Vascular normalization as an emerging strategy to enhance cancer immunotherapy. *Cancer research*, *73*(10), 2943–2948.

Ishak, A. (2010). Similarity solutions for flow and heat transfer over a permeable surface with convective boundary condition. *Applied Mathematics and Computation*, *217*(2), 837–842.

Jackson, T. L. (2003). A mathematical model of prostate tumor growth and androgen-independent relapse. *Discrete and Continuous Dynamical Systems-B*, *4*(1), 187–201.

Kareva, I. (2011). What can ecology teach us about cancer? *Translational oncology*, *4*(5), 266–270.

Khalil, H. K., & Grizzle, J. W. (2002). *Nonlinear systems* (Vol. 3). Prentice hall Upper Saddle River, NJ.

Kim, P. S., Lee, P. P., & Levy, D. (2014a). Mathematical modeling of tumor–immune interactions: A survey of models, analysis, and applications. *Bulletin of Mathematical Biology*, *76*(4), 865–911. doi: 10.1007/s11538-013-9838-2

Kim, P. S., Lee, P. P., & Levy, D. (2014b). Optimal treatment strategy for a tumor model under immune suppression. *Computational and Mathematical Methods in Medicine*, *2014*, 1–15. Retrieved from `https://doi.org/10.1155/2014/206287` doi: 10.1155/2014/206287

Kirschner, D., & Panetta, J. C. (1998). Modeling immunotherapy of the tumor–immune interaction. *Journal of mathematical biology*, *37*(3), 235–252.

Korir, A., Gakunga, R., Subramanian, S., Okerosi, N., Chesumbai, G., Edwards, P., … others (2016). Economic analysis of the nairobi cancer registry: Implications for expanding and enhancing cancer registration in kenya. *Cancer epidemiology*, *45*, S20–S29.

Kuang, Y., Nagy, J. D., & Eikenberry, S. E. (2018). *Introduction to mathematical oncology*. Chapman and Hall/CRC.

Kuznetsov, M., Gubernov, V., & Kolobov, A. (2017). Influence of interstitial fluid dynamics on growth and therapy of angiogenic tumor. analysis by mathematical model. *Biophysics*, *62*, 129–137.

Kuznetsov, V. A., Makalkin, I. A., Taylor, M. A., & Perelson, A. S. (1994). Nonlinear dynamics of immunogenic tumors: parameter estimation and global bifurcation analysis. *Bulletin of mathematical biology*, *56*(2), 295–321.

Laird, A. K. (1965). Dynamics of tumour growth: comparison of growth rates and extrapolation of growth curve to one cell. *British Journal of Cancer*, *19*(2), 278.

Liu, A. Y., Corey, E., Bladou, F., Lange, P. H., & Vessella, R. L. (1996). Prostatic cell lineage markers: emergence of bcl2+ cells of human prostate cancer xenograft lucap 23 following castration. *International journal of cancer*, *65*(1), 85–89.

Liu, Z., & Yang, C. (2014). A mathematical model of cancer treatment by radiotherapy. *Computational and mathematical methods in medicine*, *2014*(1), 172923.

Manduku, V., Akhavan, M., Asiki, G., Brand, N. R., Cira, M. K., Gura, Z., … others (2020). Moving towards an evidence-informed cancer control strategy: A scoping review of oncology research in kenya. *Journal of Cancer Policy*, *24*, 100219.

Meaney, C. (2019). *Mathematical modelling of cancer treatments involving radiation therapy and hypoxia-activated prodrugs* (Unpublished master's thesis). University of Waterloo.

Mohamed, M. K. A., Anwar, M. I., Shafie, S., Salleh, M. Z., & Ishak, A. (2014). Effects of magnetohydrodynamic on the stagnation point flow past a stretching sheet in the presence of thermal radiation with newtonian heating. In *International conference on mathematical sciences and statistics 2013: Selected papers* (pp. 155–163).

Montaseri, G., Alfonso, J. C. L., Hatzikirou, H., & Meyer-Hermann, M. (2020). A minimal modeling framework of radiation and immune system synergy to assist radiotherapy planning. *Journal of Theoretical Biology*, *486*, 110099.

Murphy, H., Jaafari, H., & Dobrovolny, H. M. (2016). Differences in predictions of ode models of tumor growth: a cautionary example. *BMC cancer*, *16*, 1–10.

Mutiso, J., Gitonga, C., Abdullahi, B., Simbauni, J., & Gicheru, M. (2023). Alarming cases of cancer in kenya: A case for meru and tharaka nithi counties. *British Journal of Healthcare and Medical Research-Vol*, *10*(1).

Nawrocki, S., & Zubik-Kowal, B. (2015). Clinical study and numerical simulation of brain cancer dynamics under radiotherapy. *Communications in Nonlinear Science and Numerical Simulation*, *22*(1-3), 564–573.

Nelson, S. J., & Cha, S. (2003). Imaging glioblastoma multiforme. *The Cancer Journal*, *9*(2), 134–145.

Nenya, O., Tkachenko, V., & Trofymchuk, S. (2004). On the global stability of one nonlinear difference equation. *Nonlinear Oscillations*, *7*, 473–480.

Ochwach, J., Okongo, M. O., & Muraya, M. M. (2021). Mathematical model for false codling moth control using pheromone traps. *Int J Appl*, *10*(2), 32–52.

Olson, M. V. (2017). Precision medicine at the crossroads. *Human genomics*, *11*, 1–7.

Park, C., Papiez, L., Zhang, S., Story, M., & Timmerman, R. D. (2008). Universal survival curve and single fraction equivalent dose: useful tools in understanding

potency of ablative radiotherapy. *International Journal of Radiation Oncology* Biology* Physics*, *70*(3), 847–852.

Poleszczuk, J., Walker, R., Moros, E. G., Latifi, K., Caudell, J. J., & Enderling, H. (2018). Predicting patient-specific radiotherapy protocols based on mathematical model choice for proliferation saturation index. *Bulletin of mathematical biology*, *80*(5), 1195–1206.

Poleszczuk, J. T., Luddy, K. A., Prokopiou, S., Robertson-Tessi, M., Moros, E. G., Fishman, M., … Enderling, H. (2016). Abscopal benefits of localized radiotherapy depend on activated t-cell trafficking and distribution between metastatic lesions. *Cancer research*, *76*(5), 1009–1018.

Powathil, G. G., Swat, M., & Chaplain, M. A. (2015). Systems oncology: towards patient-specific treatment regimes informed by multiscale mathematical modelling. In *Seminars in cancer biology* (Vol. 30, pp. 13–20).

Preziosi, L. (2003). *Cancer modelling and simulation*. CRC Press.

Pucci, C., Martinelli, C., & Ciofani, G. (2019). Innovative approaches for cancer treatment: Current perspectives and new challenges. *ecancermedicalscience*, *13*, 961.

Reich, C., Ostropolets, A., Ryan, P., Rijnbeek, P., Schuemie, M., Davydov, A., … Hripcsak, G. (2024). Ohdsi standardized vocabularies—a large-scale centralized reference ontology for international data harmonization. *Journal of the American Medical Informatics Association*, *31*(3), 583–590.

Rockne, R., Rockhill, J., Mrugala, M., Spence, A., Kalet, I., Hendrickson, K., … Swanson, K. (2010). Predicting the efficacy of radiotherapy in individual glioblastoma patients in vivo: a mathematical modeling approach. *Physics in Medicine & Biology*, *55*(12), 3271.

Roninson, I. B. (2003). Tumor cell senescence in cancer treatment. *Cancer research*, *63*(11), 2705–2715.

Roşca, N. C., & Pop, I. (2014). Unsteady boundary layer flow of a nanofluid past a moving surface in an external uniform free stream using buongiorno's model. *Computers & Fluids*, *95*, 49–55.

Saini, A., Kumar, M., Bhatt, S., Saini, V., & Malik, A. (2020). Cancer causes and treatments. *Int. J. Pharm. Sci. Res*, *11*(7), 3121–3134.

Saltelli, A., Ratto, M., Andres, T., Campolongo, F., Cariboni, J., Gatelli, D., … Tarantola, S. (2008). *Global sensitivity analysis: the primer*. John Wiley & Sons.

Samedi, F., Heir, S., & Ul-Bashar, S. (2021, 06). Mathematical models and their application in cancer growth. *Acta Scientific Cancer Biology*, *5*, 35-41. doi: 10.31080/ASCB.2021.04.0323

Schmitt, C. A. (2007). Cellular senescence and cancer treatment. *Biochimica et Biophysica Acta (BBA)-Reviews on Cancer*, *1775*(1), 5–20.

Shah, N. H., Satia, M. H., Yeolekar, B. M., et al. (2017). Optimum control for spread of pollutants through forest resources. *Applied Mathematics*, *8*(05), 607.

Sharma, P., & Allison, J. P. (2015). The future of immune checkpoint therapy. *Science*, *348*(6230), 56–61.

Shuai, Z., & van den Driessche, P. (2013). Global stability of infectious disease models using lyapunov functions. *SIAM Journal on Applied Mathematics*, *73*(4), 1513–1532.

Smith, M. K., & Gbur, G. (2020). Mathematical method for designing superresolution lenses using superoscillations. *Optics Letters*, *45*(7), 1854–1857.

Stefanou, D. T., Souliotis, V. L., Zakopoulou, R., Liontos, M., & Bamias, A. (2021). Dna damage repair: predictor of platinum efficacy in ovarian cancer? *Biomedicines*, *10*(1), 82.

Stepien, T. L., Kostelich, E. J., & Kuang, Y. (2020). Mathematics+ cancer: An undergraduate" bridge" course in applied mathematics. *SIAM Review*, *62*(1), 244–263.

Strogatz, S. H. (2024). *Nonlinear dynamics and chaos: with applications to physics, biology, chemistry, and engineering*. Chapman and Hall/CRC.

Sung, H., Ferlay, J., Siegel, R. L., Laversanne, M., Soerjomataram, I., Jemal, A., & Bray, F. (2021). Global cancer statistics 2020: Globocan estimates of incidence and mortality worldwide for 36 cancers in 185 countries. *CA: a cancer journal for clinicians*, *71*(3), 209–249.

Tabassum, S., Rosli, N. B., & Binti Mazalan, M. S. A. (2019). Mathematical modeling of cancer growth process: a review. In *Journal of physics: conference series* (Vol. 1366, p. 012018).

Tang, S., & Dubey, P. (2012). Opposing effects of androgen ablation on immune function in prostate cancer. *Oncoimmunology*, *1*(7), 1220–1221.

Timofeeva, Y., & Coombes, S. (2003). Wave bifurcation and propagation failure in a model of ca2+ release. *Journal of mathematical biology*, *47*(3), 249–269.

Van den Driessche, P., & Watmough, J. (2002). Reproduction numbers and subthreshold endemic equilibria for compartmental models of disease transmission. *Mathematical biosciences*, *180*(1-2), 29–48.

Verhulst, P.-F. (1838). Notice sur la loi que la population suit dans son accroissement. *Correspondence mathematique et physique*, *10*, 113–129.

Vieira, L. C., Costa, R. S., & Valério, D. (2023). An overview of mathematical modelling in cancer research: fractional calculus as modelling tool. *Fractal and fractional*, *7*(8), 595.

Wang, X., Fu, T., Liao, S., Wang, S., Lei, Z., & Mei, T. (2020). Exclusivity-consistency regularized knowledge distillation for face recognition. In *Computer vision–eccv 2020: 16th european conference, glasgow, uk, august 23–28, 2020, proceedings, part xxiv 16* (pp. 325–342).

Yorke, E., Fuks, Z., Norton, L., Whitmore, W., & Ling, C. (1993). Modeling the development of metastases from primary and locally recurrent tumors: comparison with a clinical data base for prostatic cancer. *Cancer research*, *53*(13), 2987–2993.

Zhang, J., Cunningham, J. J., Brown, J. S., & Gatenby, R. A. (2017). Integrating evolutionary dynamics into treatment of metastatic castrate-resistant prostate cancer. *Nature communications*, *8*(1), 1816.

Zhou, C., Lu, Z., Zhang, L., & Hu, J. (2014). Moment independent sensitivity analysis with correlations. *Applied Mathematical Modelling*, *38*(19-20), 4885–4896.

Zi, Z. (2011). Sensitivity analysis approaches applied to systems biology models. *IET systems biology*, *5*(6), 336–346.

Appendix I: Python Code for Simulating Profiles

Model dynamics xx

```
import numpy as np
from scipy.integrate import solve_ivp
import matplotlib.pyplot as plt

# -------- parameters --------
p = {
    "r_H": 0.20, "K_H": 1.0e6, "alpha_1": 1.0e-7,
    "r_T": 0.18, "K_T": 1.0e6,
    "beta": 0.02, "gamma": 0.01,
    "eta_T": 0.50, "kappa_T": 1.0e5,
    "eta_Q": 0.10, "kappa_Q": 1.0e5,
    "s_I": 10.0, "sigma_I": 5.0,
    "delta": 0.10, "theta": 5.0e4, "d_I": 0.10
}

# -------- model with radiotherapy --------
def model_rt(t, y, params, eps, rhoH_frac=0.05):
    H, T, Q, I = y
```

```
r_H, K_H = params["r_H"], params["K_H"]
alpha1 = params["alpha_1"]
r_T, K_T = params["r_T"], params["K_T"]
beta, gamma = params["beta"], params["gamma"]
eta_T, kappa_T = params["eta_T"], params["kappa_T"]
eta_Q, kappa_Q = params["eta_Q"], params["kappa_Q"]
s_I, sigma_I = params["s_I"], params["sigma_I"]
delta, theta, d_I = params["delta"], params["theta"], params["d_I"]

rhoT = eps
rhoH = rhoH_frac * rhoT

dHdt = r_H * H * (1 - H / K_H) - alpha1 * H - rhoH * H
immune_kill_T = (eta_T * I * T) / (kappa_T + T) if (kappa_T + T) > 0 else 0.0
immune_kill_Q = (eta_Q * I * Q) / (kappa_Q + Q) if (kappa_Q + Q) > 0 else 0.0
dTdt = alpha1 * H + r_T * T * (1 - T / K_T) - beta * T + gamma * Q - immune_k
dQdt = beta * T - gamma * Q - immune_kill_Q - 0.2 * rhoT * Q
dIdt = s_I + sigma_I + (delta * T  theta + T)) * I - d_I * I
```

Chemotherapy

```
import numpy as np
from scipy.integrate import solve_ivp
import matplotlib.pyplot as plt

# ---------------- parameters (aligned with your model) ----------------
p = {
    "r_H": 0.20, "K_H": 1.0e6, "alpha_1": 1.0e-7,
    "r_T": 0.18, "K_T": 1.0e6,
    "beta": 0.02, "gamma": 0.01,
    "eta_T": 0.50, "kappa_T": 1.0e5,
    "eta_Q": 0.10, "kappa_Q": 1.0e5,
    "s_I": 10.0, "sigma_I": 5.0,
    "delta": 0.10, "theta": 5.0e4, "d_I": 0.10,
    # baseline clearance / death terms
    "rho_H": 0.02, "rho_T": 0.10, "rho_Q": 0.02,
    "chi_H": 0.01, "chi_T": 0.05, "chi_Q": 0.01
}

# ---------------- model with time-dependent chemotherapy chi(t) ----------------
def model_chemo(t, y, params, chi_func):
    """
    params : parameter dict
    chi_func: function t -> instantaneous chemo-induced death rate (applied to tu
    """
    H, T, Q, I = y

    # unpack
    r_H, K_H = params["r_H"], params["K_H"]
    alpha1 = params["alpha_1"]
    r_T, K_T = params["r_T"], params["K_T"]
    beta, gamma = params["beta"], params["gamma"]
    eta_T, kappa_T = params["eta_T"], params["kappa_T"]
    eta_Q, kappa_Q = params["eta_Q"], params["kappa_Q"]
```

Model dynamics 2

```
import numpy as np
from scipy.integrate import solve_ivp
import matplotlib.pyplot as plt

# -------- parameters --------
p = {
    "r_H": 0.20, "K_H": 1.0e6, "alpha_1": 1.0e-7,
    "r_T": 0.18, "K_T": 1.0e6,
    "beta": 0.02, "gamma": 0.01,
    "eta_T": 0.50, "kappa_T": 1.0e5,
    "eta_Q": 0.10, "kappa_Q": 1.0e5,
    "s_I": 10.0, "sigma_I": 5.0,
    "delta": 0.10, "theta": 5.0e4, "d_I": 0.10
}

# -------- model equations --------
def model_dynamics(t, y, params):
    H, T, Q, I = y
    r_H, K_H = params["r_H"], params["K_H"]
```

```
alpha1 = params["alpha_1"]
r_T, K_T = params["r_T"], params["K_T"]
beta, gamma = params["beta"], params["gamma"]
eta_T, kappa_T = params["eta_T"], params["kappa_T"]
eta_Q, kappa_Q = params["eta_Q"], params["kappa_Q"]
s_I, sigma_I = params["s_I"], params["sigma_I"]
delta, theta, d_I = params["delta"], params["theta"], params["d_I"]

# equations
dHdt = r_H * H * (1 - H / K_H) - alpha1 * H
immune_kill_T = (eta_T * I * T) / (kappa_T + T) if (kappa_T + T) > 0 else 0.0
immune_kill_Q = (eta_Q * I * Q) / (kappa_Q + Q) if (kappa_Q + Q) > 0 else 0.0
dTdt = alpha1 * H + r_T * T * (1 - T / K_T) - beta * T + gamma * Q - immune_k
dQdt = beta * T - gamma * Q - immune_kill_Q
dIdt = s_I + sigma_I + (delta * T / (theta + T)) * I - d_I * I

return [dHdt, dTdt, dQdt, dIdt]
```

Tumor dynamics under different radiotherapy efficacy

```python
import numpy as np
from scipy.integrate import solve_ivp
import matplotlib.pyplot as plt

# -------- parameters --------
p = {
    "r_H": 0.20, "K_H": 1.0e6, "alpha_1": 1.0e-7,
    "r_T": 0.18, "K_T": 1.0e6,
    "beta": 0.02, "gamma": 0.01,
    "eta_T": 0.50, "kappa_T": 1.0e5,
    "eta_Q": 0.10, "kappa_Q": 1.0e5,
    "s_I": 10.0, "sigma_I": 5.0,
    "delta": 0.10, "theta": 5.0e4, "d_I": 0.10
}

# -------- base model with RT --------
def model_rt(t, y, params, eps, rhoH_frac=0.05):
    H, T, Q, I = y
    r_H, K_H = params["r_H"], params["K_H"]
    alpha1 = params["alpha_1"]
    r_T, K_T = params["r_T"], params["K_T"]
    beta, gamma = params["beta"], params["gamma"]
    eta_T, kappa_T = params["eta_T"], params["kappa_T"]
    eta_Q, kappa_Q = params["eta_Q"], params["kappa_Q"]
    s_I, sigma_I = params["s_I"], params["sigma_I"]
    delta, theta, d_I = params["delta"], params["theta"], params["d_I"]

    rhoT = eps          # here efficacy ε acts as a constant killing rate
    rhoH = rhoH_frac * rhoT

    dHdt = r_H * H * (1 - H / K_H) - alpha1 * H - rhoH * H
    immune_kill_T = (eta_T * I * T) / (kappa_T + T) if (kappa_T + T) > 0 else 0.0
    immune_kill_Q = (eta_Q * I * Q) / (kappa_Q + Q) if (kappa_Q + Q) > 0 else 0.0
    dTdt = alpha1 * H + r_T * T * (1 - T / K_T) - beta * T + gamma * Q - immune_k
    dQdt = beta * T - gamma * Q - immu kill_Q - 0.2 * rhoT * Q
    dIdt = s_I + sigma_I + (delta * T / (theta + T)) * I - d_I * I
```

Tumor dynamics comparison

```python
import numpy as np
from scipy.integrate import solve_ivp
import matplotlib.pyplot as plt

# ---------------- parameters ----------------
p = {
    "r_H": 0.20, "K_H": 1.0e6, "alpha_1": 1.0e-7,
    "r_T": 0.18, "K_T": 1.0e6,
    "beta": 0.02, "gamma": 0.01,
    "eta_T": 0.50, "kappa_T": 1.0e5,
    "eta_Q": 0.10, "kappa_Q": 1.0e5,
    "s_I": 10.0, "sigma_I": 5.0,
    "delta": 0.10, "theta": 5.0e4, "d_I": 0.10,
    "rho_H": 0.02, "rho_T": 0.10, "rho_Q": 0.02,
    "chi_H": 0.01, "chi_T": 0.05, "chi_Q": 0.01
}
```

```python
# ---------------- model ----------------
def model(t, y, params, chi_func, radio_func):
    H, T, Q, I = y

    r_H, K_H = params["r_H"], params["K_H"]
    alpha1 = params["alpha_1"]
    r_T, K_T = params["r_T"], params["K_T"]
    beta, gamma = params["beta"], params["gamma"]
    eta_T, kappa_T = params["eta_T"], params["kappa_T"]
    eta_Q, kappa_Q = params["eta_Q"], params["kappa_Q"]
    s_I, sigma_I = params["s_I"], params["sigma_I"]
    delta, theta, d_I = params["delta"], params["theta"], params["d_I"]

    chi = chi_func(t)
    chi_T, chi_Q, chi_H = chi, 0.5*chi, 0.1*chi
```

Appendix II: Research Permit

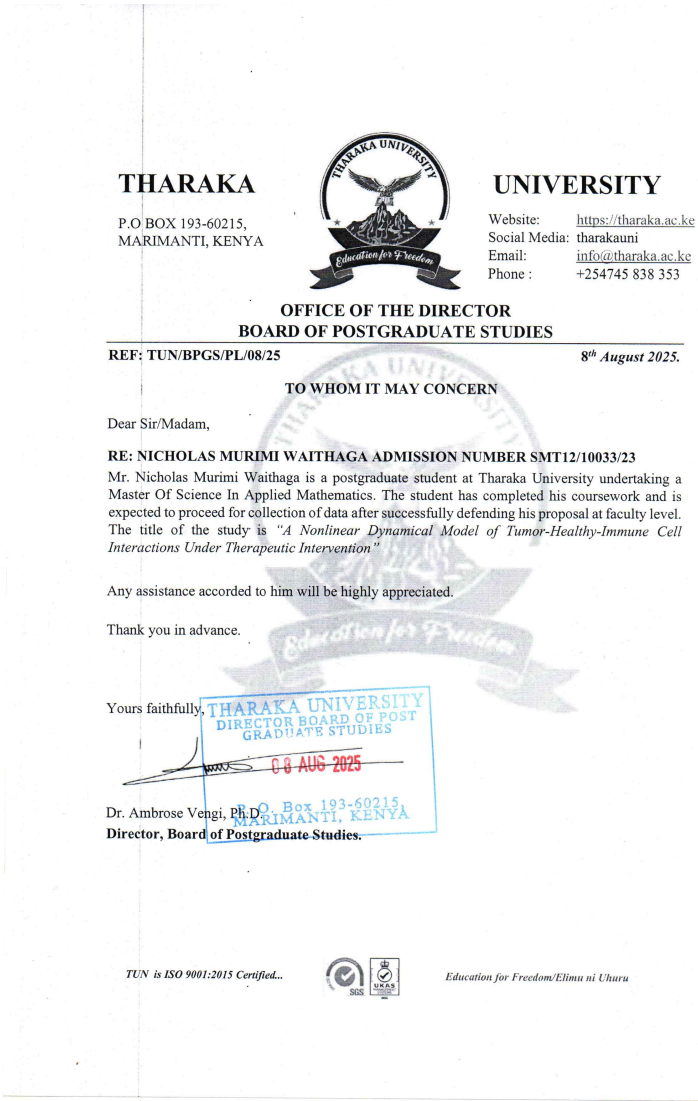

THARAKA UNIVERSITY

P.O BOX 193-60215,
MARIMANTI, KENYA

Website: https://tharaka.ac.ke
Social Media: tharakauni
Email: info@tharaka.ac.ke
Phone : +254745 838 353

OFFICE OF THE DIRECTOR
BOARD OF POSTGRADUATE STUDIES

REF: TUN/BPGS/PL/08/25 ***8th August 2025.***

TO WHOM IT MAY CONCERN

Dear Sir/Madam,

RE: NICHOLAS MURIMI WAITHAGA ADMISSION NUMBER SMT12/10033/23

Mr. Nicholas Murimi Waithaga is a postgraduate student at Tharaka University undertaking a Master Of Science In Applied Mathematics. The student has completed his coursework and is expected to proceed for collection of data after successfully defending his proposal at faculty level. The title of the study is *"A Nonlinear Dynamical Model of Tumor-Healthy-Immune Cell Interactions Under Therapeutic Intervention"*

Any assistance accorded to him will be highly appreciated.

Thank you in advance.

Yours faithfully,

THARAKA UNIVERSITY
DIRECTOR BOARD OF POST GRADUATE STUDIES
08 AUG 2025
P.O. Box 193-60215
MARIMANTI, KENYA

Dr. Ambrose Vengi, Ph.D.
Director, Board of Postgraduate Studies.

TUN is ISO 9001:2015 Certified... *Education for Freedom/Elimu ni Uhuru*

Appendix III:Ethics Letter

THARAKA UNIVERSITY

P.O BOX 193-60215,
MARIMANTI, KENYA

Telephone: +(254)-0202008549
Website: https://tharaka.ac.ke
Social Media: tharakauni
Email: info@tharaka.ac.ke

INSTITUTIONAL SCIENTIFIC AND ETHICS REVIEW COMMITTEE

8th August 2025.

REF: TUNISERC/NSEC/ M059

Dear, Nicholas Murimi Waithaga

RE: A Nonlinear Dynamical Model of Tumor-Healthy-Immune Cell Interactions Under Therapeutic Intervention

This is to inform you that ***Tharaka University ISERC*** has reviewed and approved your above research proposal. Your application approval number is ***ISERC04023.*** The approval period is ***8th August 2025– 8th August 2026.***

This approval is subject to compliance with the following requirements;

i. Only approved documents including (informed consents, study instruments, MTA) will be used
ii. All changes including (amendments, deviations, and violations) are submitted for review and approval by ***Tharaka University ISERC***.
iii. Death and life threatening problems and serious adverse events or unexpected adverse events whether related or unrelated to the study must be reported to ***Tharaka University ISERC*** within 72 hours of notification
iv. Any changes, anticipated or otherwise that may increase the risks or affected safety or welfare of study participants and others or affect the integrity of the research must be reported to ***Tharaka University ISERC*** within 72 hours
v. Clearance for export of biological specimens must be obtained from relevant institutions.
vi. Submission of a request for renewal of approval at least 60 days prior to expiry of the approval period. Attach a comprehensive progress report to support the renewal.
vii. Submission of an executive summary report within 90 days upon completion of the study to ***Tharaka University ISERC***.

Prior to commencing your study, you will be expected to obtain a research license from National Commission for Science, Technology and Innovation (NACOSTI) https://research-portal.nacosti.go.ke and also obtain other clearances needed.

Yours sincerely,

THARAKA UNIVERSITY ETHICS COMMITTEE 08 AUG 2025 CHAIRPERSON P.O. Box 193-60215, MARIMANTI

Dr. Fidelis Ngugi
Chair, ISERC Tharaka University

Appendix IV: Research Authorization (NACOSTI)

REPUBLIC OF KENYA

NATIONAL COMMISSION FOR SCIENCE,TECHNOLOGY & INNOVATION

Ref No: **985747**

Date of Issue: **25/August/2025**

RESEARCH LICENSE

This is to Certify that Mr.. Nicholas Murimi waitheega of Tharaka University, has been licensed to conduct research as per the provision of the Science, Technology and Innovation Act, 2013 (Rev.2014) in Tharaka-Nithi on the topic: A NONLINEAR DYNAMICAL MODEL OF TUMOR-HEALTHY-IMMUNE CELL INTERACTIONS UNDER THERAPEUTIC INTERVENTION for the period ending : 25/August/2026.

License No: **NACOSTI/P/25/4178898**

985747

Applicant Identification Number

Ag. Director General
NATIONAL COMMISSION FOR SCIENCE,TECHNOLOGY & INNOVATION

Verification QR Code

NOTE: This is a computer generated License. To verify the authenticity of this document, Scan the QR Code using QR scanner application.

See overleaf for conditions